REPUBLIC OF TÜRKİYE
YILDIZ TECHNICAL UNIVERSITY
GRADUATE SCHOOL OF SCIENCE AND ENGINEERING

STABILITY OF BREAKWATER ROUNDHEADS WITH A SINGLE LAYER OF HIGH DENSITY CUBE ARMOR UNITS

Baran POLAT

MASTER OF SCIENCE THESIS

Department of Civil Engineering

Program of Coastal and Port Engineering

Supervisor

Prof. Dr. Yalçın YÜKSEL

November, 2024

REPUBLIC OF TÜRKİYE

YILDIZ TECHNICAL UNIVERSITY

GRADUATE SCHOOL OF SCIENCE AND ENGINEERING

STABILITY OF BREAKWATER ROUNDHEADS WITH A SINGLE LAYER OF HIGH DENSITY CUBE ARMOR UNITS

A thesis submitted by Baran POLAT in partial fulfillment of the requirements for the degree of **MASTER OF SCIENCE** is approved by the committee on 14.11.2024 in Department of Civil Engineering, Program of Coastal and Port Engineering.

Prof. Dr. Yalçın YÜKSEL
Yildiz Technical University
Supervisor

Approved By the Examining Committee

Prof. Dr. Yalçın YÜKSEL, Supervisor
Yildiz Technical University _____

Prof. Dr. Esin ÇEVİK, Member
Yildiz Technical University _____

Assoc. Prof. Dilek Eren AKYÜZ, Member
Istanbul University-Cerrahpasa _____

I hereby declare that I have obtained the required legal permissions during data collection and exploitation procedures, that I have made the in-text citations and cited the references properly, that I haven't falsified and/or fabricated research data and results of the study and that I have abided by the principles of the scientific research and ethics during my Thesis Study under the title of "Stability of Breakwater Roundheads with a Single Layer of High Density Cube Armor Units" supervised by my supervisor, Prof. Dr. Yalçın YÜKSEL. In the case of a discovery of false statement, I am to acknowledge any legal consequence.

Baran POLAT

Signature

This work was supported by the the project no “FBG-2022-4935 of YTU Coordinator ship of Scientific Research Projects’’

To my dear family, whose unwavering

dedication and support have never faltered…

ACKNOWLEDGEMENTS

In this study, the stability of a breakwater roundhead with a single layer of regularly placed high-density cube armor units was investigated. I would like to extend my sincere gratitude to my advisor, Prof. Dr. Yalçın YÜKSEL, who guided me to this study and shared his extensive knowledge and experience with me throughout the process. I also thank Prof. Dr. Esin ÇEVİK and Assoc. Prof. Dr. Cihan ŞAHİN for their support in this study.

I am grateful to my colleague Chingiz MUSTAFAZADE and Muhammed Burak REHBER, who accompanied me on this journey, and to our valuable laboratory officer, Muhammed ULUÇAY, who provided great support with his solutions to every problem encountered during the experimental study.

I would like to express my deepest gratitude to my dear father, Cahit POLAT, and my dear mother, Hatice POLAT, for their unwavering support in all circumstances, who have always supported me in every aspect and stood behind me with patience throughout this process.

Baran POLAT

TABLE OF CONTENTS

LIST OF SYMBOLS

P_r	Actual Porosity
A_i	Area of the sector i
B	Area width
M_{armor}	Armor unit mass
V_b	Block volume
D_{crit}	Damage level in the critical sector
$D_{\%crit}$	Damage value in the critical sector
S_{0m}	Deep water mean wave steepness
S_{0p}	Deep water peak wave steepness
$T_{m-1,0}$	Deep water spectral wave period
H_d	Diffracted wave height
K_d	Diffraction coefficient
R_n	Dimensionless head radius
X	Distance along the direction of the breakwater
Y	Distance perpendicular to the direction of the breakwater
A, B, C	Experimental Coefficient
P_{crit}	fraction of displaced units in the critical sector
g	Gravitational acceleration
H_i	Incoming wave height
P_{0i}	Initial porosity in the sector
ξ	Irrıbaren Parameter
ν	Kinematic viscosity
k_Δ	Layer thickness coefficient
L	Length of the area measured for each experiment on the slope
N_{PBL}	Maximum block volume per layer corresponding to one face
T_m	Mean wave period
L_m	Mean wavelength
$M_{50,\ core}$	Median mass of core material

P_r	Movement percentage
D_n	Nominal diameter
$D_{n,\ armor}$	Nominal diameter of the armor units
$D_{n50,\ core}$	Nominal diameter of the median core material
D_{n50}	Nominal diameter of the median grain size
N_i	Number of Cubipods in the test i
n_r	Number of moving units
N_{BL}	Number of placed blocks
Ψ_s	Packing density
T_p	Peak wave period
L_p	Peak wavelength
D_1	Primary displacement
M_1	Primary movement
R	Radius of roundhead
K_r	Reflection coefficient
N_0, N_{0d}	Relative Damage
Δ	Relative specific gravity
R_e	Reynolds number
D_2	Secondary displacement
M_2	Secondary movement
H_s	Significant wave height
K	Size coefficient
α	Slope angle
a	Slope angle of structure
m	Slope of the structure
ρ_r	Specific mass of stone
ρ_w	Specific mass of water
H_{m0}	Spectral significant wave height
T_{m-1}	Spectral wave period
N_s	Stability number
ξ_{0p}	Surf parameter
t	Thickness of armour layer

t_1	Time 1
t_2	Time 2
t_3	Time 3
D_T	Total displacement
M_T	Total movement
U	Velocity
V	Volume
D_i	Volumetric Damage
d	Water depth
R_u	Wave run-up
L	Wavelength
W	Weight

LIST OF ABBREVIATIONS

CEM	Coastal engineering manual
CERC	Coastal Engineering Research Center
CIRIA	Construction Industry Research and Information Association
D	Displacement
HD	High density
JONSWAP	Joint North Sea Wave Project
LCW	Long crested waves
M	Movement
ND	Normal density
PDF	Probability Density Function
S1	Sector 1
S2	Sector 2
S3	Sector 3
S4	Sector 4
SCW	Short crested waves
SWL	Still water level
SW	Swell wave
WS	Without structure
WW	Wind wave

LIST OF FIGURES

LIST OF TABLES

ABSTRACT

Stability of Breakwater Roundheads with a Single Layer of High Density Cube Armor Units

Baran POLAT

Department of Civil Engineering
Program of Coastal and Port Engineering
Master of Science Thesis

Supervisor: Prof. Dr. Yalçın YÜKSEL

Breakwaters are high-cost and complex marine structures to construct. If they sustain damage, port operations may cease, leading to significant financial losses. When designed as protective structures, they can result in irreplaceable losses for residential areas or strategic investments. Although there are numerous studies on the design of the bodies of rubble mound breakwaters, the number of studies on the roundheads is very limited due to the challenges of experimentation, and thus, the behavior of the roundhead is not well understood. Moreover, during the design of breakwater roundheads, the need to implement new design methods to reduce costs has arisen.

In this study, the focus will be on the single-layer regular placement of cube armor units in the protective layer, a method that has started to be studied in recent years, and it will be applied to the roundhead section. Besides using cubes with normal concrete density (24 kN/m³), high-density concrete cubes (31.5 kN/m³) were also employed. The use of high-density cube blocks is a very new research topic and has not been studied in the roundhead section until now.

In this study, the stability of high-density cube blocks was investigated under the influence of wind and swell waves by setting up a three-dimensional physical model of a breakwater roundhead in the wave basin at YTU Hydrodynamic Research Laboratory. It was observed that single-layer cube blocks with normal density

experienced displacement damage, whereas such damage did not occur in the high-density cube model blocks of the same size. When examining the movement rates, this type of damage was found to be significantly lower in the high-density blocks. Consequently, high-density concrete blocks can be used to design more robust breakwater roundheads, making these breakwaters economically feasible and easier to construct with the same mold and equipment.

Keywords: Rubble mound breakwaters, breakwater roundhead stability, concrete blocks, climate change, sustainable design.

ÖZET

Tek Sıra Yüksek Yoğunluklu Küp Koruma Tabakasına Sahip Dalgakıranın Kafasında Stabilite

Baran POLAT

İnşaat Mühendisliği Anabilim Dalı
Kıyı ve Liman Mühendisliği Programı
Yüksek Lisan Tezi

Danışman: Prof. Dr. Yalçın YÜKSEL

Dalgakıranlar maliyeti yüksek ve imalatı oldukça zor olan deniz yapılarıdır. Hasar görmeleri durumunda limanların işletmeleri durabilir ve ciddi maddi kayıplara yol açar. Koruma yapısı olarak planlanmaları durumunda ise yerleşim bölgeleri ya da stratejik yatırımlarda telafisi mümkün olmayan kayıplara yol açar. Özellikle taş dolgu dalgakıranların gövdelerinin tasarımı hakkında çok sayıda çalışma olmasına karşın kafa kesitlerindeki araştırma sayısı deneylerindeki zorluklardan dolayı oldukça azdır ve dolayısıyla kafa kesitinin davranışı yeterince bilinmemektedir. Bunun yanı sıra dalgakıran kafalarının tasarımları sırasında maliyetin düşürülmesi amacıyla yeni tasarım yöntemlerinin uygulanması ihtiyacı da ortaya çıkmıştır.

Bu çalışmada son yıllarda çalışılmaya başlanan koruma tabakasında tek sıra düzenli küp blok yerleşimi dikkate alınacaktır ve kafa kesitinde uygulanacaktır. Normal beton yoğunluğuna sahip (24kN/m^3) küplerin yanı sıra yüksek yoğunluklu beton küpler (31.5kN/m^3) kullanılmıştır. Yüksek yoğunluklu küp blok kullanımı çok yeni bir araştırma konusudur ve kafa kesitinde bugüne kadar çalışılmamıştır.

Bu çalışmada YTÜ Hidrodinamik Araştırma Laboratuvarında bulunan dalga baseninde üç boyutlu dalgakıran kafası fiziksel modeli kurularak rüzgar ve soluğan dalgaları etkisinde yüksek yoğunluklu küp blokların stabilitesi araştırılmıştır. Tek sıra yerleştirilmiş küp blokların normal yoğunluklu olmaları durumunda yer değiştirme hasarı gözlenirken yüksek yoğunluklu aynı boyuttaki küp model

bloklarda böyle bir hasar meydana gelmemiştir. Hareket etme oranlarına da bakıldığında yüksek yoğunluklu bloklarda bu hasar tipinde hareket yüzdesi oldukça düşük bulunmuştur. Sonuç olarak, yüksek yoğunluklu beton bloklar ile dayanımı yüksek dalgakıran kafaları tasarlanabilecek olup aynı kalıp ile ekipman açısından da yapımı kolay olacaktır.

Anahtar Kelimeler: Taş dolgu dalgakıranlar, dalgakıran kafasında stabilite, beton blok, iklim değişikliği, sürdürülebilir tasarım.

1
INTRODUCTION

1.1 Motivation

The motivation for this study is determined by the limited research in the literature on breakwater roundhead stability, the economic problems caused by the increase in the size of breakwater armor units due to rising wave heights with climate change, and the inherent instability of roundheads compared to the trunk section of a breakwater. The roundhead of a breakwater is less stable than the trunk section. The reasons for this include the roundhead geometry, which causes the armor units to be less stable, and the problems posed by increasing wave heights for roundhead stability. In this context, conducted studies are detailed in the following sections.

1.2 Hypothesis

In coastal engineering, breakwaters play a critical role in protecting harbors, beaches, and marinas from wave action. While conventional breakwater designs have been extensively studied, there is a need for further research on the stability of breakwater roundheads using innovative materials and configurations. This study focuses on the use of a single layer of high-density cube armor units in breakwater roundheads, an area where existing research is limited.

The primary aim of this study is to evaluate the stability of breakwater roundheads when subjected to different wave conditions, specifically wind waves and swell waves, tested separately. The hypothesis posits that a single layer of high-density cubes can provide enhanced stability compared to traditional armor layers, particularly in complex wave environments. The research will explore the effectiveness of these cubes in mitigating wave forces and preventing structural displacement, with the expectation that their application could lead to more economical, environmentally friendly, and durable coastal protection structures.

Given the scarcity of studies in this area, this experimental investigation is expected to fill a critical gap in the literature. By systematically testing the performance of these armor units under varying wave conditions, this study aims to provide new

insights into the design and optimization of breakwaters, ultimately contributing to the development of more resilient coastal infrastructure.

1.3 Literature Review

Roundhead section is the most critical part of the rubble mound breakwaters in terms of stability. This is because refraction, diffraction and shoaling effects increase the energy release at roundhead, however mostly because of the less support from neighboring armor units and high current velocities. Armor units at roundheads are less interlocked. If the units are displaced, they tend to move the rear side of roundhead and causing structure to be less stable at this section. Over the past years, many physical studies providing great knowledge about effects of hydraulic and structural parameters on roundhead stability. Experiments have been conducted to investigate the relationship between wave steepness and Iribarren number with the occurrence of damage. Researches made to determine the damage at roundhead in which sector.

Jensen (1984) stated that, by placing the armor units with interlocking, more stable roundhead can be achieved, Burcharth et al. (2003) suggested that, increasing densities provide more effective way to achieve stability.

Vidal et al. (1989, 1991) used concrete block to conduct experimental studies. In this study, they obtained that, wave steepness does not have any effect on the initiation of the damage but influences the damage propagation. Same results are also observed in Madrigal and Lorenzo (1992), Berenguer and Baonza (1999). Carver and Heimbaugh (1989) stated that, for rock and dolos; minimum stability occurs at a certain value of Iribarren number. Matsumi et al. (1996) reported that the magnitude of the velocity around the roundhead has a stronger spatial correlation in long waves than in short waves. Burcharth et al. (2003) showed that, damage can be characterized by a parameter using the combination of H_s, T_m and D_n. Jensen (1984), Vidal et al. (1991), Madrigal and Lozano (1992), Berenguer and Baonza (1999), Matsumi et al. (2000), Burcharth et al. (2003) have observed the effect of incident wave angle and demonstrated that, most critical part is the 90^0 and 150^0 degree from mean angle.

Burcharth et al. (2003) investigated the stability of cube units at roundhead with density of 2.34 and 2.73 t/m^3. In this research, wave steepness and surf parameters are determined as s_{0p}=0.02-0.03 and ξ_{0p}=2.9 – 3.6 respectively. Roundhead includes 16 sectors, 1811 cubes used for irregular placement and 1940 cubes used for regular placement. Initially for irregularly placed normal density cubes, test series are conducted for 2 water level and 2 wave direction. For each sea state, damage location and damage propagation is determined. Test series with damaged part is replaced with high density cube units are also done with 2 water level and 2 wave angles. Research shows that for normal density cube units, damage is starting earlier in irregular placement than the regular placement. For high density cube units, results are vice versa, which means irregular placement is more stable. Visually, damage is more brittle in regular placement, because cube units at upper rows suddenly slide over the lower rows. In addition, stability capacity that remains after damage for regular placement seems lower. Macineira and Burcharth (2008) stated that, most critical sector is between 90^0 to 135^0 degree for cube armored roundheads. However, they observed the same damage at 45^0 to 90^0 and 90^0 to 135^0 degree with waves steepness of 0.04. They observed, with roundhead radius less than $12D_{n,}$ damage difference is lower between these sectors.

Matsumi et al. (1994, 1996, 1998, 2000) showed that wave loads on armor layer increased with directional spreading of the waves. Madrigal and Lorenzo (1992) have observed that there is no difference for roundhead stability by using different types of accropodes and parallelpipedic armor layer. Berenguer and Baonza (1999) has compared antifer, cube and hollowed cube. They developed a formula, by analyzing the roundhead, armored with cubes and antifer blocks. Jensen (1984) found that interlocking units are more stable than the gravity type armor units. Burcharth et al. (2003) stated that, increasing the density of armor units is a way to contribute to stability. Jensen (1984) has determined that, increasing the R roundhead radius at still water level increases the stability. Again Vidal et al. (1989) and Losada (1990) stated that, R/L is the suitable parameter for diffraction and refraction effects. Macineira and Burcharth (2007) found that decreasing the radius at the head causes a non-linear reduction between the initiation of damage and failure, whereas this behavior is reversed for short period waves and steep slopes. Stability expression for roundheads assumed the damage is homogeneous but more

damage occurs in critical sectors. (Macineira and Burcharth, 2007 and Berenguer and Baonza, 1999). Berenguer and Baonza (1999) has produced an expression for cube and antifer cube with slope angle of 1/2. Macineira and Burcharth (2007) has developed this expression slopes with 1/1.5 and 1/2, waves with non-directional and directional. In stability studies, Berenguer and Baonza (1999) divided the head into three sectors (0°-30°, 30°-90°, 90°-150°), whereas Macineira and Burcharth (2007) divided it into four sectors (0°-45°, 45°-90°, 90°-135°, 135°-180°).

Researches of Comola et al. (2014) stated that armor layer dimensions at roundhead should be bigger than the trunk section. The reason is, increasing wave energy due to wave transformations and decreased support from neighboring units at roundhead. In addition, less interlocking mechanism at roundhead section causes armor units to move leeward side of the breakwater.

Comola et al. (2014) examined the damage to the breakwater head under different wave angles in shallow water conditions with a single head radius and a single slope angle under wind, swell, and complex wave conditions. Their study demonstrated that the peak wave period is the most influential factor on the most damaged sectors. It was determined that with increasing wave period, the most damaged sector shifted to the back of the head. However, the wave period had no effect on the initiation of damage. The progression of damage was found to be faster for swell waves. It was noted that the displacement of stones behind the breakwater did not occur due to wave overtopping.

Comola, et al., (2014) carried out total of 12 test series, with waves being sent in multiple directions and the JONSWAP spectrum being used (JONSWAP spectrum parameters: peak period (T_p), peak factor (γ), and directional spreading parameter (s)). In each test series, a certain number of tests were performed with increasing H_s until the filter layer became exposed over an area larger than D_{n50}. In each test, H_s was increased by 10%, and 1000 waves were generated in each test. In each test series, T_p was kept constant while H_s was variable, resulting in changes to the wave steepness S_{0p}. This approach differs from the study by Maciñeira and Burcharth (2007), where S_{0p} was kept constant

Although breakwater roundheads have been researched for many years, there is limited literature available on this topic. In this study, the stability of a single layer

regularly arranged breakwater roundhead was investigated. The studies related to breakwater roundheads are presented in Table 1.1. Researchers have used both quarry stones and concrete cube blocks, and the increased use of cube blocks in recent years indicates the growing interest and demand for such practical and easy-to-implement units. With the rise in wave heights due to global climate change, there is a need to increase the size of the armor units. However, this size increase presents challenges in terms of cost and mold workmanship. At this point, increasing the density of cube blocks offers a practical solution, and in this study, the stability of high-density cubes on breakwater roundheads was investigated. The cube blocks were placed in a single-layer regular arrangement, subjected separately to both wind and swell waves, and their stability was examined accordingly. Parameters for Table 1.1 are given below. Table 1.1 presents the studies arranged in chronological order, along with the limit conditions and the circumstances under which they were conducted. Additionally, the type of armor units used, and the slope gradients are provided. Parameters in Table 1.1 explained below.

Table 1.1 Previous studies on the stability of breakwater roundheads

Author	Formula		Experimental Conditions
Burcharth et al. (2016)	Scw (Short-crested waves)	$N_s = Z.[\,0.56.e^{0.07.\frac{R}{D_n}}.\cot a^{0.71}.D_{\%}^{0.19}.s^{0.44} + 2.07.s^{0.15}K_{size}^{scw}\,]$	cot α=1.5 to 2.0, Armor: Cube Units Wave Steepness (s_{0p}) =0.026 to 0.065 $K_{D\,(\%5)}$ =3.7 to 4.5
	Lcw (Long-crested waves)	$N_s = Z.[\,0.44.e^{0.07\frac{R}{D_n}}.\cot a^{0.71}.D_{\%}^{0.25}.s^{0.44} + 4.06.s^{0.32}.K_{size}^{lcw}\,]$	cot α=1.5 to 2.0, Armor: Cube Wave Steepness (s_{0p}) =0.031 to 0.066 $K_{D\,(\%5)}$ =4.0 to 7.0
J.Sande et al. (2016)	To calculate the damage： $D_i = \frac{N_i D_n^2}{A_i(1-P_{oi})}100$		cot α=1.5, Armor: Cubipod Wave Steepness (s_p) =0.02 to 0.06
Comola et al. (2014)	$N_s = 0.94 + 0.41.\left(\frac{D_{\%cs}}{P_{crit}}\right)^{0.42}.S_{0p}^{0.23}$		cot α=1.5, Armor: Quarry Stone Wave Steepness (s_{0p}) =0.004 to 0.041 Ns=1.1 to 2.0
Burcharth et al. (2010)	$N_s = \frac{H_s}{\Delta D_{n50}}$		cot α=1.5, Armor: Cubipod and Cubes Wave Steepness (s_{0p})=0.02 to 0.05, Ns=3.4 (Max.)

Table 1.1 Previous studies on the stability of breakwater roundheads (cont.)

Burcharth et al. (2010)	$N_s = \frac{H_s}{\Delta D_{n50}}$	cot α=1.5, Armor: Cubipod and Cubes Wave Steepness (s_{0p})=0.02 to 0.05, Ns=3.4 (Max.)
Maciñeira and Burcharth (2007)	$N_s = 0.57.\exp(0.07.R_n).\cot a^{0.71}.D_{\%crit}^{0.2}.S_{0p}^{0.4} + 2.08.S_{0p}^{0.4} - 0.17$	cot α=1.5 to 2.0, Armor: Cube Units Wave Steepness (s_{0p}) =0.02 to 0.06
Burcharth et al. (2003)	$N_s = \frac{H_s}{\Delta D_{n50}}$	cot α=2.0, Armor: Cube Units Wave Steepness (s0p) =0.02 to 0.03 $K_{D\ (\%5)}$ =2.6
Berenguer and Baonza (1999)	$N_s = 1.8 + 2.3\ D_{crit}^{0.4}\ S_{0m}^{0.5}$	cot α=2.0, Armor: Halowed cubes antifer
Jorgen Juhl et al. (1996)	-	cot α=1.5, Armor: Quarry Stone Wave Steepness (s_m) =0.03 to 0.05, Ns=2.0 to 4.0

Table 1.1 Previous studies on the stability of breakwater roundheads (cont.)

Cesar Vidal et al. (1991)	-	cot α=2.0, Armor: Cube Units Wave Steepness (s_0) =0.0693 to 0.0484
Carver and Heimbaugh (1989)	$N_s = A\xi_p^2 + B\xi_p + C_c$	cot α=1.5 to 2.0, Armor: Quarry Stone
Hudson (1959)	$N_s = \frac{H_s}{\Delta D_n} = (K_D.\cot a)^{\frac{1}{3}}$	cot α=1.5 to 3.0, Armor: Quarry Stone $K_{D\ (\%5)}$ =1.3 to 3.2

2
STABILITY OF BREAKWATER ROUNDHEADS

2.1 Roundhead Stability

The breakwater roundhead is often curved or rounded section of a breakwater structure, extending into the sea. It serves to dissipate wave energy, thereby protecting coastal infrastructure such as ports, marinas, and beaches. The design of the roundhead is crucial in minimizing wave-induced forces and subsequent structural damage. Unlike the trunk section of a breakwater, the roundhead experiences unique wave-structure interactions due to its geometry and location, making its design and analysis particularly challenging.

The roundhead is characterized by its curved geometry, which leads to variable wave impacts as waves approach from different angles. This curvature causes wave breaking, diffraction, and reflection, resulting in complex wave dynamics that are distinct from those affecting the straight trunk section of the breakwater. The roundhead is subjected to higher wave energy and the generation of three-dimensional currents, which must be carefully considered during the design process.

The wave diffraction at the roundhead leads to three-dimensional currents, which can significantly affect the stability of the armor units placed on the roundhead. This complex interaction between waves and the structure can cause displacement of the armor units, particularly under high wave energy conditions, potentially leading to structural damage.

Given that the roundhead is the most exposed part of the breakwater, its stability is of utmost importance. According to the Rock Manual (2007), achieving stability often requires the use of larger and denser armor units, such as rock or concrete blocks, on the roundhead. Additionally, the slope of the roundhead must be carefully designed to effectively dissipate wave energy and protect the structure. Ensuring the stability of the roundhead requires careful selection of materials, precise geometric design, and extensive testing through three-dimensional wave models. By adhering to the guidelines provided in the Rock Manual (2007) and conducting

appropriate testing, engineers can optimize the design of breakwater roundheads, thereby enhancing the overall performance and durability of coastal protection structures.

A typical example of the layout of a roundhead armored with concrete armor units is shown in Figure 2.1. The center point of the roundhead section is shifted to the leeward side, resulting in a circular shape as shown in Figure 2.1. Also the degree of this shift depends upon the radius that has to be applied: $R = nH_{s,d}$, where n depends on the armor unit (CIRIA, 2007).

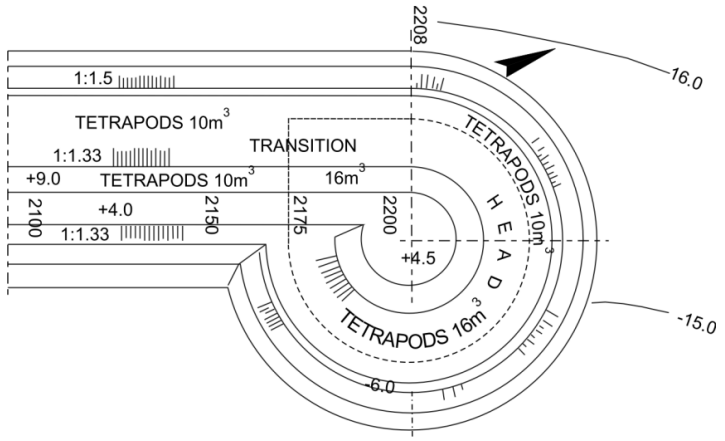

Figure 2.1 Typical roundhead layout with tetrapods (CIRIA, 2007)

The stability in the critical area of the roundhead might be improved by increasing the head diameter or adding a tail as shown in Figure 2.2.

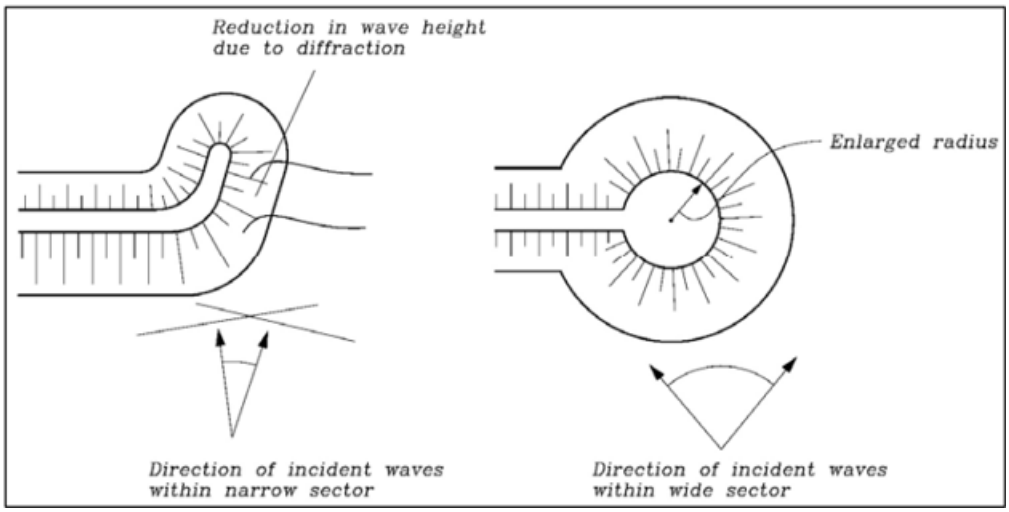

Figure 2.2 Tailed and enlarged roundheads (Burchart, 1993)

In addition, the corner section of the breakwater is exposed to waves more than trunk section and these sections are treated like roundhead sections. Since structures built in deep water increase the cost, the convex and corner parts of the structure usually follow the seabed elevation curves. Refraction sometimes can increase the wave heights, as shown in Figure 2.3a. This will increase the wave run-up and wave overtopping values.

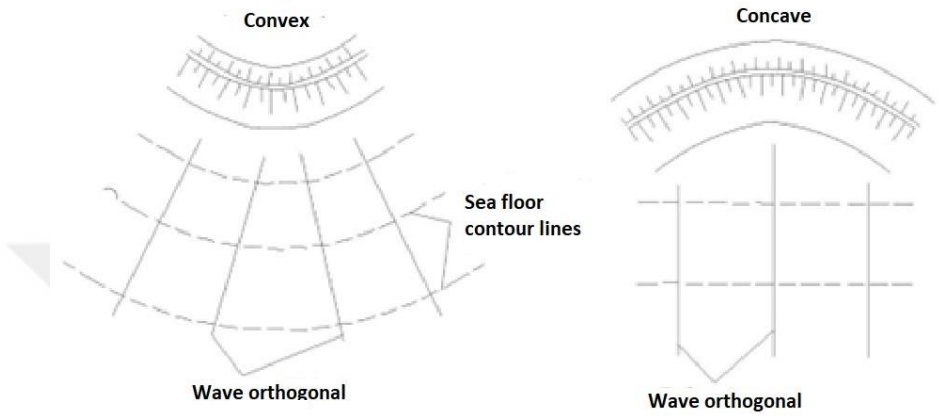

Figure 2.3 Convex and concave curves and corners (CERC, 2003), a) Wave energy concentration due to refraction b) Wave energy concentration due to refraction

Carver and Heimbaugh (1989) have suggested an expression to calculate the rock weight to be used in roundheads. This expression is valid for waves without overtopping, regular waves and both breaking and non-breaking waves.

$$\frac{H_s}{\Delta D_{n50}} = A\xi_p{}^2 + B\xi_p + C_c \tag{2.1}$$

$$\xi_p = \frac{\tan\alpha}{\sqrt{H_s/L_p}} \tag{2.2}$$

Where,

H_s : Significant wave height at structure's toe,

D_{n50} : Nominal stone diameter assuming that 50% of the stones by weight pass through the sieve,

$$\Delta = \frac{\rho_r}{\rho_w} - 1$$

ρ_r : Specific mass of stone (t/m^3),

ρ_w : Specific mass of water (t/m^3),

L_p : Peak wavelength that calculated by peak wave period at breakwater toe,

α : Slope angle of structure,

A, B, C_c : Experimental coefficients,

Detailed research on rubble mound breakwater roundheads has conducted by Vidal et al. (1991). Researchers showed that stone weights used on head section is 1.3 - 3.8 times bigger than the trunk section. As shown in Figure 2.4, damage starts at angle of 60^0 because of diffraction effects.

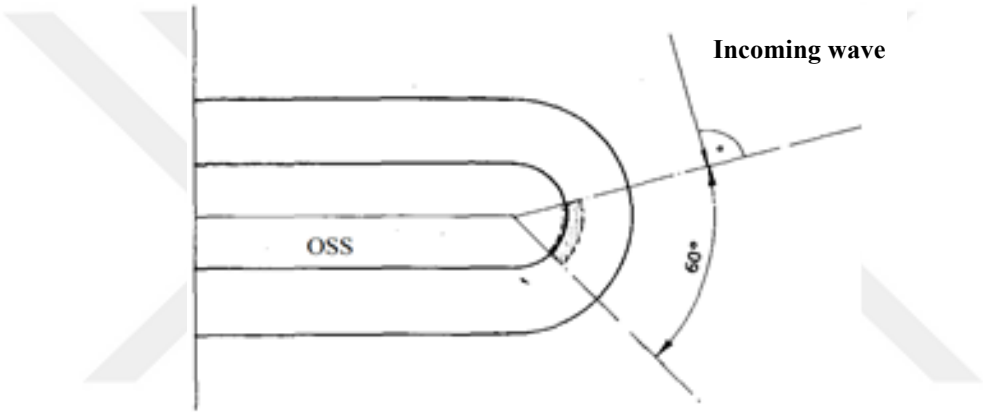

Figure 2.4 Starting of the damage at roundhead (Vidal et al. 1991)

Equation (2.3), developed by Maciñeira and Burcharth (2007), was derived from the analysis of breakwater heads with 1:1.5 and 1:2 slopes, armored with cube units, under the influence of both unidirectional and directional waves.

$$N_s = \frac{H_s}{\Delta D_n} = 0.57.\exp(0.07.R_n).\cot^{0.71}\alpha.D_{\%,crit}^{0.2}.S_{0p}^{0.4} + 2.08.S_{0p}^{0.14} - 0.17 \quad (2.3)$$

Here, N_s is the stability number, H_s is the significant wave height, Δ is the relative specific gravity ($\rho = \rho_r/\rho_w$ - 1), D_n is the nominal diameter of cubes, $D_{n50} = (M_{50}/\rho_r)^{1/3}$, ρ_r is the specific gravity of the armor layer, and ρ_w is the specific gravity of water. $D_{crit}E$ (0,1) is the damage level in the critical sector between 90° and 150° from the mean wave direction, according to Berenguer and Baonza (1999). $D_{crit}E$ (0,100) is the damage level in the critical sector between 90° and 150° from the mean wave direction according to Macineira and Burcharth (2007). R_n is the

dimensionless head radius at still water level ($R_n = R/D_{n50}$), and α is the slope angle. $S_{0p} = H_s/L_{0p} = 2\pi H_s/gT_p^2$ is the peak wave steepness (calculated by deep water peak wave period). $S_{0m} = H_s/L_{0m} = 2\pi H_s/gT_m^2$ is mean wave steepness (calculated by the deep water mean wave period).

Tests done by Berenguer and Baonza (1999) obtained the equation below as a stability formula:

$$N_s = \frac{H_s}{\Delta D_n} = 1.8 + 2.3\, D_{crit}^{0.4}\, S_{0m}^{0.5} \tag{2.4}$$

Comola et al., (2014) stated that the displacement of stones behind the breakwater did not occur due to wave overtopping. It was observed that the front sectors suffered significantly more damage at shorter wave periods, while the rear sectors experienced more damage at longer wave periods. Additionally, under shorter wave periods, the distribution of damage was more uniform compared to longer periods. As suggested by Burcharth and Hughes (2002), the damage assessment was conducted by considering the number of units displaced over a distance greater than D_{n50} in the active region. The reference region was defined as the area between the SWL ± nD_{n50} levels. Damage detection was performed by comparing photographs taken before and after the experiment. To characterize these observations, a damage model analysis was conducted using a probability density function p(β) that describes the likelihood of each stone being displaced to a position defined by an angle $\beta \in [\beta_0; \pi + \beta_0]$. The pdf function is defined as follows

$$p(\beta) = \frac{f(\beta; \mu, \sigma^2)}{f(\pi + \beta_0; \mu, \sigma^2) - f(\beta_0; \mu, \sigma^2)} \tag{2.5}$$

Here, f is the probability density function, and F is the cumulative distribution function of f and with β_0, μ and σ^2 being the parameters of this distribution.

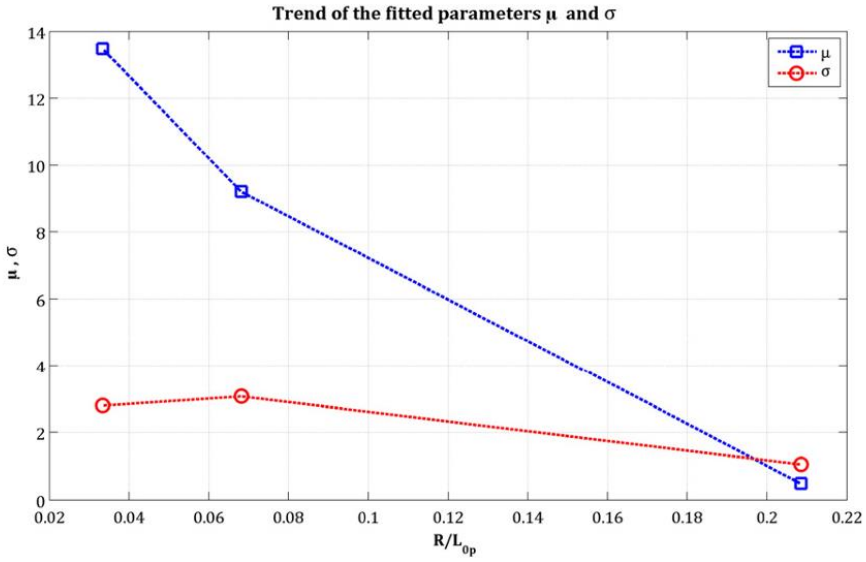

Figure 2.5 Values of μ and σ (Comola et al., 2014)

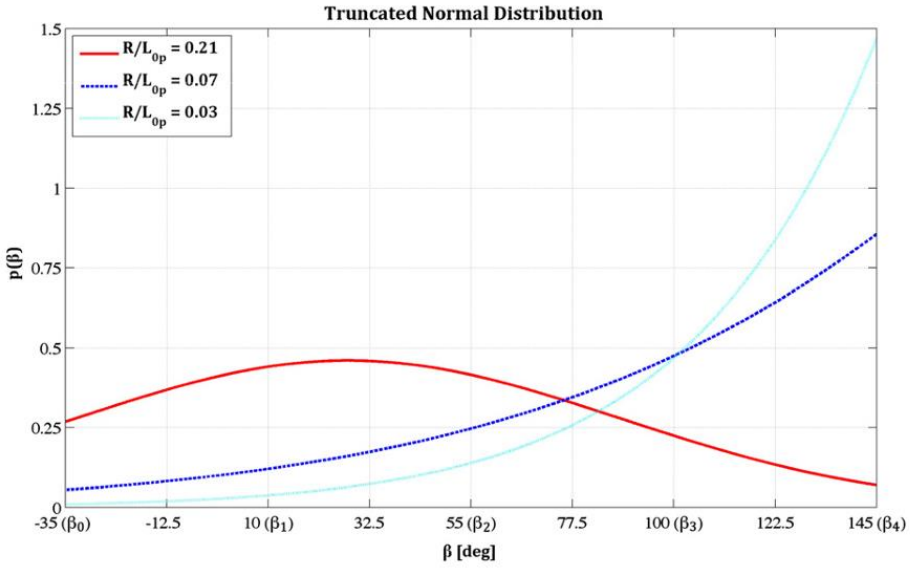

Figure 2.6 PDF graphs of damage distribution (Comola et al., 2014)

According to Comola et al. (2014), as a result, the front part of the structure is more prone to damage than the rear parts under the impact of short waves. As observed by Macineira and Burcharth (2008), the wave period is one of the most important parameters affecting the damage distribution. Moreover, under the influence of short wave periods, the damage at the breakwater roundhead is more uniform and small-scale damage was observed at the front of the breakwater. In long period waves, the damage is concentrated in the last 2 sectors. The directional dispersion parameter (s) and peak factor (γ) had no effect on the damage distribution.

$$D_{\%} = \frac{N_d}{N_t} 100 \tag{2.6}$$

where, N_d is the total number of stones displaced in the referencearea at the breakwater head, N_t is the total number of stones in the reference zone at the breakwater roundhead. The initial damage started to occur at the same stability number, independent of the peak wave period. This means that the initial damage is not affected by the wave steepness. However, damage progression is much faster at longer wave periods. The damage progression was not significantly affected by the peak factor (γ) and directional dispersion parameter (s). As a result of the tests and analysis, when Equation (2.4) is modified:

$$N_s = \frac{H_s}{\Delta D_{n50}} = 0.94 + 0.74 {D_{\%}}^{0.42} {S_{0p}}^{0.23} \tag{2.7}$$

At the breakwater head, failure occurs when the filter layer in the critical sector becomes visible. Therefore, it is stated that the $D_{\%}$ damage value in the critical sector can be a suitable parameter to characterize the full damage condition at the head. Overall damage is related to damage in the critical sector using Equation (2.8).

$$D_{\%} = \frac{D_{\%,crit}}{4P_{crit}} \tag{2.8}$$

Using $D_{\%, crit}$ as the design parameter, the appropriate size for the breakwater armor units could be obtained by modifying equation (2.7) in the stability formula.

The advantage of the new approach is that, as observed by Macineira and Burcharth (2007), it is assumed both when the critical sector is between [90°-135°] degrees from the main wave direction and when the critical sector is shifted to the forward sectors under short wave action. In this last case, as will be shown, the new approach can provide more reliable results.

According to the Comola et al. (2014), when equation (2.8) was written in equation (2.7), the following equation (2.9) was obtained, which expresses the relationship between N_s, S_{0p} and $D_{\%, crit}$.

$$N_s = 0.94 + 0.74\left(\frac{D_{\%,crit}}{P_{crit}}\right)^{0.42} {S_{0p}}^{0.23} \quad (2.9)$$

The spectra mentioned above are characterized by energy concentrations around two peak frequencies, the higher frequency corresponding to wind waves and the lower frequency corresponding to swell waves.

Expressions for double-peaked spectra is defined below as given by Comola et al. (2014):

$$H_{s,tot} = \sqrt{{H_{s,swell}}^2 + {H_{s,wind}}^2} \quad (2.10)$$

$$T_{p,eq} = \frac{T_{p,swell}{H_{s,swell}}^2 + T_{p,wind}{H_{s,wind}}^2}{{H_{s,swell}}^2 + {H_{s,wind}}^2} \quad (2.11)$$

Comola et al., (2014) indicated that the peak wave period is the primary factor in the formation of damage on the breakwater head. They observed that damage occurs at the front part of the breakwater head during short wave periods, while during long wave periods, the damage shifts to the rear parts (Comola et al., 2014). The two parameters of the truncated distribution were found to be primarily dependent on T_p and were related to the dimensionless ratio R/L_{0p}. Here, R is the roundhead radius at still water level (fixed in the experiments) and L_{0p} is the deep-water wavelength (dependent on T_p). It was confirmed that the wave period does not affect the onset of the initial damage.

However, once the initial stone displacements occur, the progression of damage is faster in long waves compared to short waves. It was observed that when the filter layer is exposed to wave action, the condition for considering the damage as complete occurs when the damage level is between 15% and 20%.

According to the derived stability formula, it has also been shown that this expression, combined with the damage structure analysis results, allows for a good prediction of damage progression in the critical sector.

Macineira and Burcharth (2016) investigated the stability of a breakwater head armored with cube units under the influence of long and short-crested waves. In this study, they highlighted the effects of R/L and R/H_s in addition to R/D_n. Based on these parameters:

- A large-radius head is considered for R/L > 0.15-0.2 or R/H_s > 3.5-4.0

- A small-radius head is considered for R/L < 0.15-0.2 or R/H_s < 3.5-4.0

In this study, expressions considering R/D_n and wave steepness as well as expressions considering the effects of R/L and R/H_s were discussed.

For short-crested waves (for wave conditions not limited by depth):

$$N_s = \frac{H_s}{\Delta D_n} = Z\left[0.56e^{0.07R/D_n}\cot\alpha^{0.71}D_{\%}^{0.19}s^{0.44} + 2.07s^{0.15}K_{size}^{scw}\right] \quad (2.12)$$

For long-crested waves (for wave conditions not limited by depth):

$$N_s = \frac{H_s}{\Delta D_n} = Z\left[0.44e^{0.07R/D_n}\cot\alpha^{0.71}D_{\%}^{0.25}s^{0.44} + 4.06s^{0.32}K_{size}^{lcw}\right] \quad (2.13)$$

Here, R is the radius of the breakwater head at still water level, D_n is the nominal diameter of the equivalent cube, α is the slope angle, $D_{\%}$ is the percentage of cubes displaced from the active region (SWL ± 1.25 H_s) in the sector between 90°-135° relative to the mean wave direction, and ‘’s’’ is the wave steepness (H_s/L, where L is the wavelength at the structure's toe corresponding to the spectral peak period).

Equation (2.14) was obtained based on the experimental results by Macineira and Burcharth, (2016):

$$K_{size} = K_{H_s}K_L\,;K_{H_s} = 1 + \frac{1}{e^{a1\times(R/H_s - b1)}}\;;\;K_L = 1 + \frac{1}{e^{a2\times(R/L - b2)}} \quad (2.14)$$

Parameter value for this expression is given in Table 2.1.

Table 2.1 Coefficients for Equation 2.14

	a_1	b_1	a_2	b_2
Short-Crested Waves	1.53	1.99	46	0.06
Long-Crested Waves	4.08	2.19	31	0.06

The formulas for the size coefficients to be used for short and long crest waves, respectively, are given below:

$$K_{size}^{scw} = \left(1 + \frac{1}{e^{1.53\times(R/H_s - 1.99)}}\right) . \left(1 + \frac{1}{e^{46\times(R/L - 0.06)}}\right) \quad (2.15)$$

$$K_{size}^{lcw} = \left(1 + \frac{1}{e^{4.08\times(R/H_s - 2.19)}}\right) . \left(1 + \frac{1}{e^{31\times(R/L - 0.06)}}\right) \quad (2.16)$$

The valid range of the parameters in Equations (2.15) and (2.16) is given in Table 2.2.

Table 2.2 Stability formula; the ranges, where the parameters in Equations. (2.15) and (2.16), are valid**.**

Parameters	Short Crested Waves	Long Crested Waves
Packing density (Ø)	1.472	1.32-1.472
Mass density of concrete	2.4-3.04 t/m^3	2.35-2.4 t/m^3
R/L	0.1-0.39	0.1 - 0.43
R/H_s	2.6-12.22	2.67-8.87
R/D_n	9.18-19.25	9.18 – 17.56
cotα	1.5-2.0	1.5 – 2.0
s	0.026-0.065	0.031- 0.066

Macineira and Burcharth (2016) found that although the initial damage occurs later in small-radius heads compared to large-radius heads, the progression of damage is much faster in small-radius heads. Additionally, small-radius heads are less stable. The most critical sector relative to the incoming wave direction is 90°-135°. In small-radius heads, damage spreads between 90°-180°. In large-radius heads, the 45°-90° sector is also affected by damage like the 90°-135° sector, but the 135°-180° sector is not affected. Short-crested waves cause more damage than long-crested waves, but this difference decreases as wave steepness increases. Damage increases as wave steepness decreases, and this effect is more pronounced in long-crested waves. Stability increases with increasing head radius. In the 1:1.5 and 1:2 slope angles considered in this study; the effect of the slope angle was found to be

very small. The researchers recommended the values in Table 1.3 for the KD stability coefficient.

Table 2.3 K_D stability coefficient for the critical 45° sector of the head (Macineira and Burcharth, 2016)

$D_{\%}$	Long Crested		Short Crested	
	s < 0.05	s> 0.05	s< 0.05	s> 0.05
2%	3.2	5.0	2.7	3.0
5%	4.0	7.0	3.7	4.5

Safari et al. (2016) emphasized that the most critical aspect of rubble mound breakwaters requiring special attention is the head section. They stated that the stability performance of armor layer elements on the conical head is affected not only by the increased wave intensity in some regions (shoaling, refraction, diffraction) but also by the reduced interlocking between neighboring units. Therefore, it is recommended to design the head with increased size and/or density of the armor layer elements compared to the trunk section. However, due to potential issues in placement technique or packing density, the researchers focused on a new armor unit, Vbloc®, which resembles a cube. This unit retains all the advantages of a cube (simple shape, ease of placement, easy construction) while mitigating some of the cube's disadvantages such as face-to-face fitting, heterogeneous porosity after damage, smooth exterior armor surface, and low hydraulic stability. Following 2D experiments showing high performance in terms of stability and overtopping, the researchers analyzed the hydraulic stability of the new Vbloc® in a wave basin (3D), comparing the head stability and behavior under oblique wave conditions to those under normal wave conditions.

They suggested that since the damage levels (initial damage and average damage) are very close, initial damage should be considered a criterion for design. Based on the results of 2D and 3D experiments, the following formulas were proposed for the new armor layer element.

For initial damage at trunk section:

$$\frac{H_s}{\Delta D_n} = 2.9 \tag{2.17}$$

For initial damage at head section:

$$\frac{H_s}{\Delta D_n} = 2.3 \tag{2.18}$$

Stability numbers for other armor units are given in Table 2.4

Table 2.4 Stability numbers of concrete elements (Safari et al., 2016)

Concrete Units	Stability Number ($H_s/\Delta D_n$)	
	Trunk	Head
Cube (1 layer)	2.2-2.3	-
Accropode	2.7	2.5
Core-loc	2.8	2.6
W-bloc	2.8	2.6
Cubipod (1 layer)	2.6	-

The damage was observed to start just below the still water level. It was reported that the damage to the head was mostly observed in two sectors, namely, the 0-degree sector, which is the direction of wave propagation, and the 105° - 135° degree sector, which is the wave direction.

Sande et al. (2016) analyzed the damage to the head of a breakwater with a single-layer Cubipod armor layer. The model scale was chosen to be 1/50. The breakwater model included a core with D_{n50} = 0.7 cm, a two-layer filter layer with D_{n50} = 1.7 cm, and a single-layer Cubipod armor layer (W = 128 g, D_n = 3.82 cm, and mass density = 2.28 g/cm³). The sector that experienced the most damage was found to be 45-90º.

2.2 Applications of Single Layer and High-Density Cube Units

Rubble mound breakwaters are constructed with three layers: the core, the filter, and the armor layer. The primary focus for the stability of these structures is the correct design of the armor layer. Armor layers are made either from quarry stone or various types of concrete blocks. Quarry stone armor layers are placed in two layers, and similarly, concrete blocks are placed in two layers over the filter. However, in recent years, patented blocks known as acropode, core-loc, and x-bloc have been placed in a single layer to achieve significant cost savings. The patenting of these blocks, however, incurs additional costs. Therefore, the limited number of recent studies have focused on single-layer cube blocks (Van Gent, 2003; Yuksel et al., 2022). The few studies on single-layer cube blocks have primarily considered the trunk section of the breakwater, but not on the roundhead section. Apart from this type of placement, the production of high-density concrete blocks has been gaining attention worldwide, and a few studies have begun to explore this (Ito, 1994; Van Gent et al., 2001; Yuksel et al., 2022). The aim of these researches on high-density concrete blocks is to achieve economic savings and to provide greater resistance to the increased wave heights caused by global climate change.

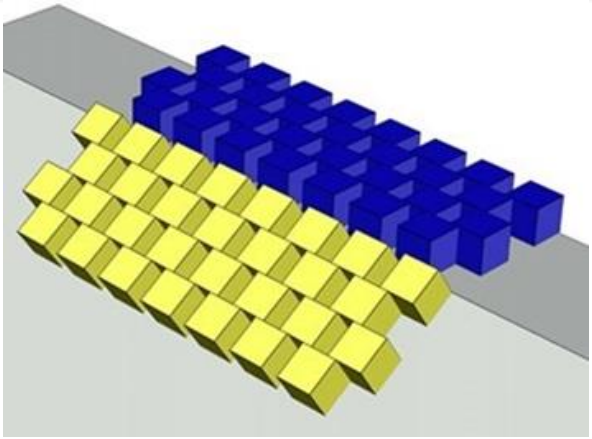

Figure 2.7 Regular single layer protection (Yüksel et al., 2022)

Regarding single-layer concrete blocks for trunk sections, there are studies by Van Gent et al. (1999), Yu et al. (2002), Van Gent (2014), Van Gent and Luis, L. (2013), Vieira et al. (2021), and Yuksel et al. (2022). However, these studies generally focus on the stability of the trunk section of the breakwater. Van Gent (2014), however, also considered the breakwater roundhead in his study. Figure 2.7 shows the placement of a single-layer cube block armor layer.

Van der Lem et al. (2016) stated that single-layer cubes could be a significant alternative to other single-layer armor units. Despite their larger size, single-layer cube elements are attractive both in shape and placement. Additionally, the application of concrete cube elements does not incur licensing fees, which is also considered an advantage.

The use of cube armor units in a single layer presents an innovative and cost-effective solution for the armor layers of rubble mound breakwaters. Research has demonstrated their effective usage and highlighted important considerations for their design (Van Gent and Luis, 2013).

Applying cubes in a single layer is an innovative solution. Single-layer cubes are viable and potentially economically competitive with other single-layer units (e.g., AccropodeTM, Core-locTM, and Xblocs®) as well as double-layer blocks (such as Antifer and Tetrapod). One of the advantages of using single-layer cubes, aside from stability benefits, is that they are easier to place in areas with limited underwater visibility compared to more complex armor units (Vergahen et al., 2002).

Furthermore, it is possible to achieve additional stability for the breakwater by arranging the cubes in a regular pattern (Frens et al., 2008). In single-layer cube armor, damage formation is observed to occur at a high stability number $H_s/\Delta D_n$. Another advantage of cube armor units over complex armor units is the ease of production and placement. Apart from the general performance assessment of cube blocks, factors such as packing density, placement method, filter layer material, wave steepness, water depth, and crest level have also been studied. Van Gent and Luis (2013) summarized these effects as follows:

Packing Density:

In single-layer cube arrangements, the void ratio should be approximately between 25% and 40%. An appropriate packing density is within the range of 25% to 30%, with a 25% void ratio being determined to reduce settlements in the armor layer.

Filter Layer:

The ratio of $M_{cube}/M_{50\text{-}filter}$ should be calculated as 10. Large filter stones cause irregularities and exert more force on the cubes, while small filter stones can wash through the gaps between the cubes.

Crest Level:

Due to settlements on the slope, cubes tend to move downward under wave action. Stones located at the crest, which are laid flat and without slope, do not show this tendency to move downward. This leads to a separation between the stones on the slope and those at the crest under wave action. This separation creates a weaker region that is more affected by incoming waves.

Toe Protection:

Toe protection is necessary to address erosion issues and supports the weight of all blocks laid along the slope. Therefore, the toe must be sufficiently secure and made from materials capable of supporting the cubes.

Stability Number and Damage Level:

Tests have shown that the initiation of damage for single-layer cubes occurs at approximately $H_s/\Delta D = 2$ to 3. For double-layer cubes of the same size and under similar wave conditions, the initial damage occurs at around $H_s/\Delta D$ =1.3-1.5. The results for single-layer cubes indicate failure at higher $H_s/\Delta D$ values. For double layers, $H_s/\Delta D$ = 2-3.5, and for single layers, $H_s/\Delta D$ = 3-3.5. Damage graphs also show that damage for double layers occurs more slowly compared to tests conducted for single-layer cubes.

Waves Approaching at an Angle:

For waves approaching at a certain angle, damage begins at larger waves compared to waves approaching perpendicularly. This increase in stability due to waves approaching at an angle varies for different armor layers (Figure 1.8). Tests by Van Gent, (2003) found that the positive effects of waves approaching at an angle are greater for single-layer cube placements compared to double-layer cubes.

In conclusion, research on single-layer cubes as the armor layer for rubble mound breakwaters has concluded that this type of armor layer performs well. The advantage of single-layer cube armor units includes the stability gained from their weight, support from neighboring cubes, and their flat surface, which makes them less affected by wave action. Additionally, single-layer armor is more economically advantageous compared to double-layer armor. The construction advantages include easier and more economical production, placement, and maintenance

compared to other complex armor units. The cube provides an effective solution against wave effects while being an economical option, making it an attractive choice for armor unit design. Between 1976 and 1978, a breakwater with a modified version of cube blocks, known as Antifer blocks, was constructed at a port in France. Many studies conducted for the design showed that the simple cube shape was not efficient for the stability of the armor layer. The studies demonstrated that having four sides of the block indented was advantageous. Antifer blocks have been used in various locations around the world. Different placement methods have been applied to breakwaters using Antifer blocks because no specific placement method has been defined.

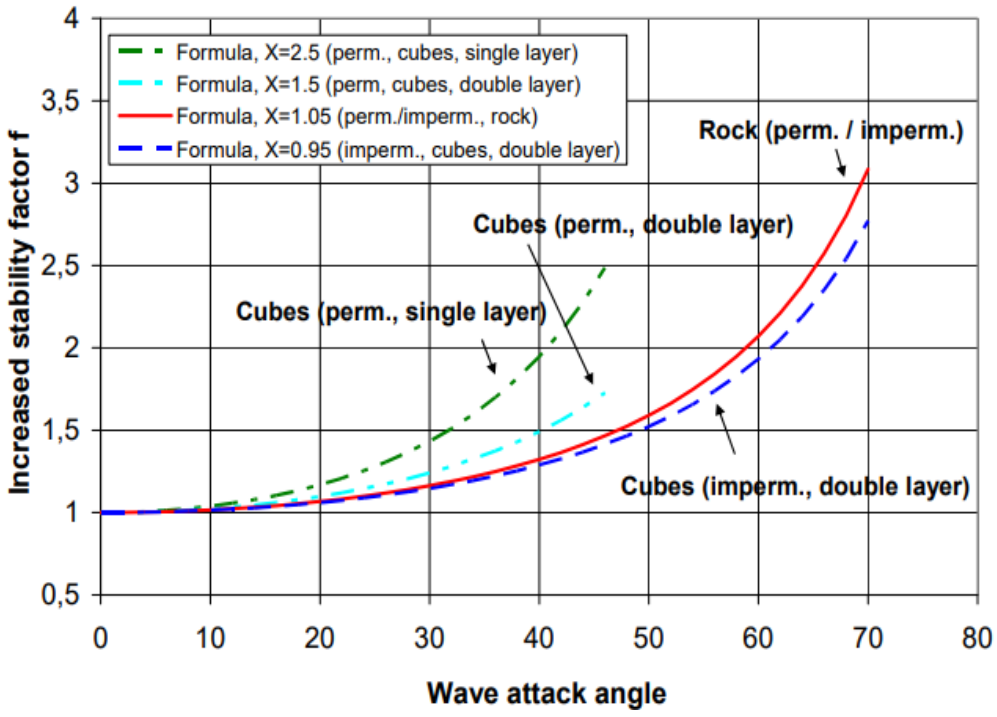

Figure 2.8 Effect of wave angle for various protection layers (Wolters and Van Gent, 2010)

Over the years, various placement methods have been applied, but no study has determined which method is most efficient.

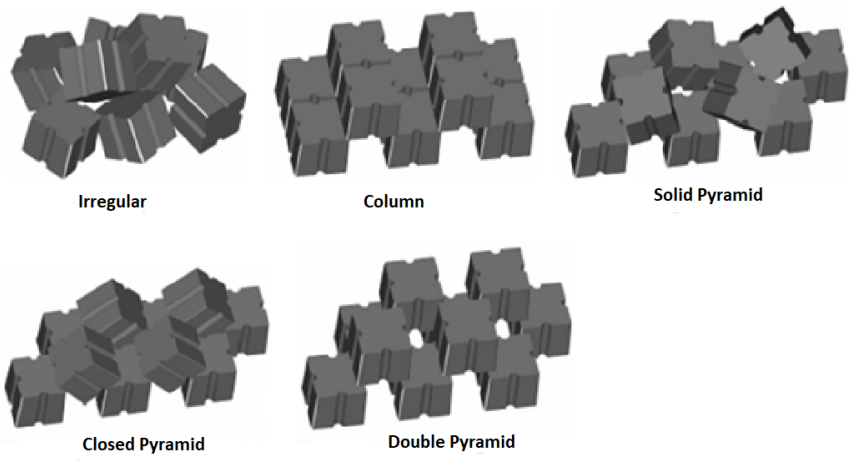

Figure 2.9 Types of placements (Frens et al., 2008)

The primary goal of the study by Frens et al. (2008) was to determine the most effective placement method. A total of 17 experiments were conducted using different densities and placement methods. The placement methods used are shown in Figure 2.2. These methods were categorized into two main groups: regular and irregular placement. According to the Rock Manual (CIRIA, 2007), various approaches have been developed for concrete armor units to achieve hydraulically stable armor layers:

The first approach is based on concrete units that primarily obtain their resistance through their **weight**.

The second approach involves armor layers that utilize concrete units with significant **interlocking** between adjoining units.

The third approach relies on armor layers with uniformly placed units, where a large portion of the resistance is derived from **friction** between the individual units.

For the irregular placement method, the smallest possible density has been determined to be 59%, as the cubes tend to settle after being placed. This settling continues throughout the experiment, resulting in a significantly higher rate of block movement compared to regular placement. The disadvantage of this method is that the settling occurring during the storm can cause damage near the crest level.

There are very few studies on high density concrete blocks in the literature, with these studies focusing only on the breakwater body and not the head section (Ito et al., 1994; Van Gent et al., 2001; Yuksel et al., 2022).

In the study by Yağcı et al. (2003), an alternative placement method for Antifer blocks was developed and compared with regular, irregular, and wall placement methods. Yağcı et al. (2003) observed that stability increases with the density in irregular placement, and that the regular placement method is less stable than the other methods, except for the low-density irregular placement method. The wall placement method's stability was found to be similar to that of the high-density irregular placement method and the alternative placement method. The alternative placement method's stability was observed to be like that of the high-density irregular placement method. Given that the alternative placement method would be easier to arrange in a prototype compared to the irregular placement method, Yağcı et al. (2003) recommended using this placement method.

Yuksel et al., (2022) investigated the stability of high-density (HD) and normal-density (ND) cubes used in the armor layers of breakwaters, focusing on the initiation of damage and overall stability under wave action. The tests demonstrated that the initiation of damage for single-layer cubes occurred at approximately $H_s/\Delta D = 2$ to 3, indicating that single-layer configurations can withstand relatively higher wave forces before showing signs of damage compared to double-layer configurations.

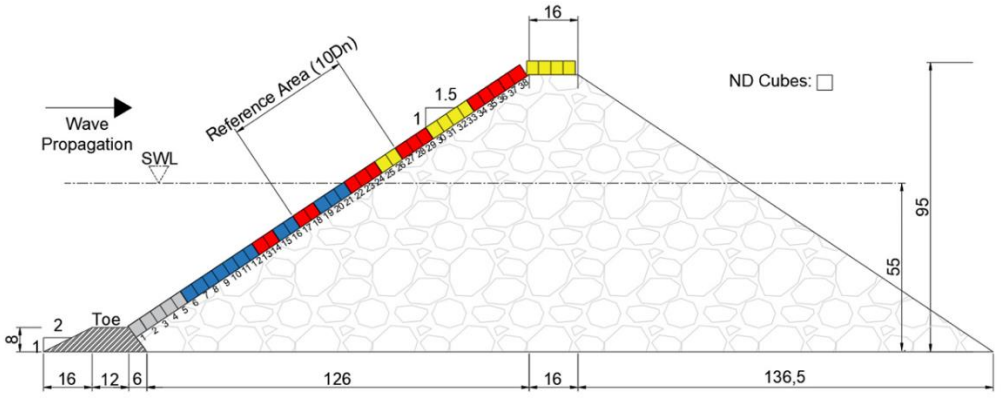

Figure 2.10 Positions of the ND cubes for the experiment Single Layer ND Cubes with Regular Placement (Yuksel et al., 2022)

The failure point for single-layer cubes was observed at $H_s/\Delta D = 3$ to 3.5, highlighting their resilience under wave action. For double-layer configurations, damage initiation was recorded at a lower range of $H_s/\Delta D = 1.3$ to 1.5. Despite the earlier onset of damage, double-layer configurations exhibited a slower

progression of damage, with final failure points observed at $H_s/\Delta D = 2$ to 3.5, showing that they maintain their integrity over a broader range of wave conditions.

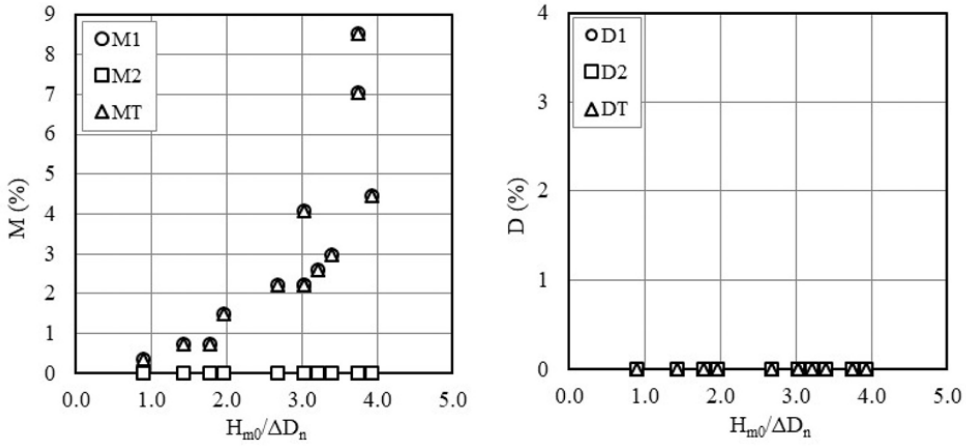

Figure 2.11 Movement (left: M) and displacement (right: D) in the Single Layer ND Cubes with Regular Placement (the stability number based on ND) (Yuksel et al., 2022)

As demonstrated in the study by Yuksel et al. (2022), the stability number N_s for HD cubes was approximately 1.5 times higher than for ND cubes. This suggests that HD cubes are more effective at resisting wave-induced forces, making them preferable in breakwater design, especially in scenarios anticipating higher wave conditions due to climate change. In berm-type breakwaters, HD cubes placed in the upper layer over ND cubes in the lower layer showed significantly better performance than ND cubes alone, reducing the likelihood of displacement and damage under wave action. The stability number for these configurations indicated strong resistance to sliding and displacement, even under challenging conditions.

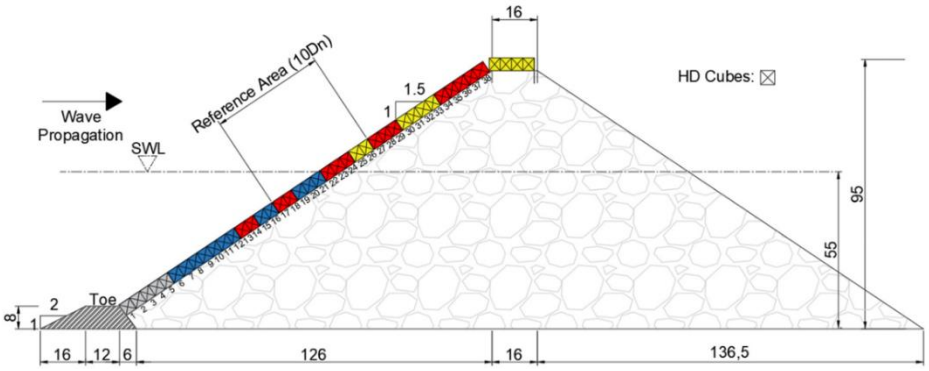

Figure 2.12 Positions of the HD cubes for the experiment Single Layer HD Cubes with Regular Placement (Yuksel et al., 2022)

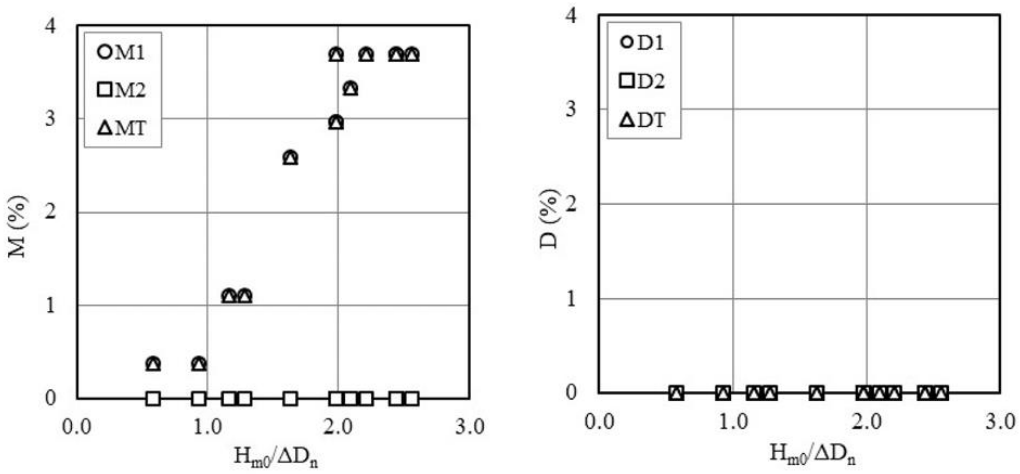

Figure 2.13 Movement (left: M) and displacement (right: D) in the Single Layer HD Cubes with Regular Placement (the stability number based on HD) (Yuksel et al., 2022)

Yuksel et al. (2022) also highlighted the economic advantages of using HD cubes, as their increased stability allows for a reduction in concrete volume, leading to cost savings without compromising structural integrity. This is particularly beneficial in large-scale coastal engineering projects where material costs can be significant. The findings underscore the importance of considering cube density and placement method in breakwater design. HD cubes, whether used in single or double layers, generally outperformed ND cubes, offering a higher level of protection against wave action. However, the study also pointed out that existing stability formulas derived for ND cubes might not be directly applicable to HD cubes, particularly in configurations prone to sliding. Overall, the results provide valuable insights for coastal engineers, suggesting that HD cubes should be the preferred choice in future breakwater designs, especially in areas exposed to high wave energy, and call for the development of new stability models tailored specifically to the unique properties of HD cubes.

3
EXPERIMENTAL STUDY

3.1 Experimental Setup and Conditions

The experimental study was conducted in the wave basin of the Hydrodynamic Research Laboratory at YTU. The wave basin dimensions are 28.84 m by 36.40 m (Figure 3.1). It is equipped with a multi-directional wave generator designed by HR Wallingford with 48 paddles of the piston type. The HR Wallingford-designed piston-type generator for regular/irregular directional waves consists of six modular units, each 4.8 m long, totaling 28.80 m in length. Each module contains eight 60 cm wide paddles (maximum stroke: 3.35 m). With a total of 48 paddles, the system offers flexible operation (snake type).

The wave generator can produce regular, irregular, long-crested, and short-crested (directional) waves. It has an active reflection absorption feature to absorb reflected wave energy. Additionally, the wave basin is equipped with a crane with a lifting capacity of 5 tons (Figure 3.2).

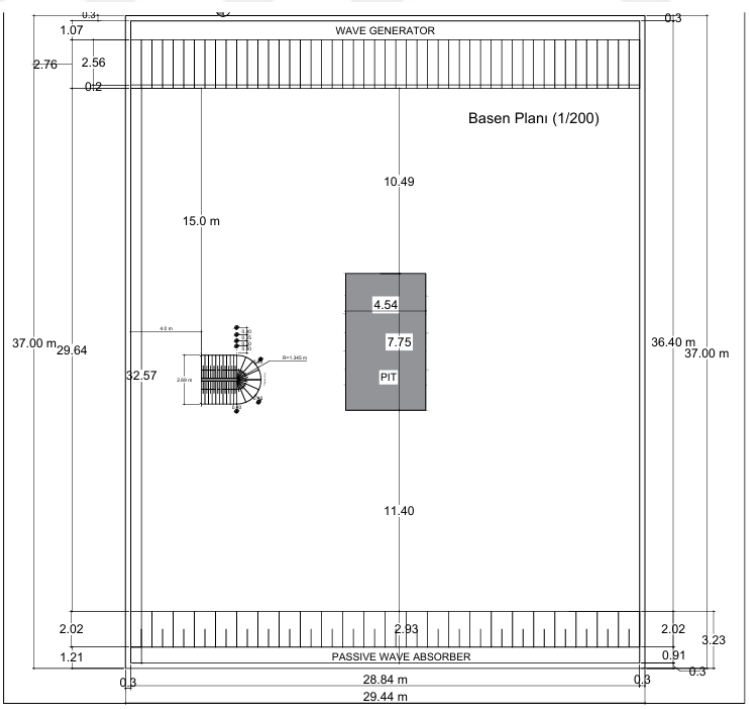

Figure 3.1 Wave basin plan and breakwater head model layout

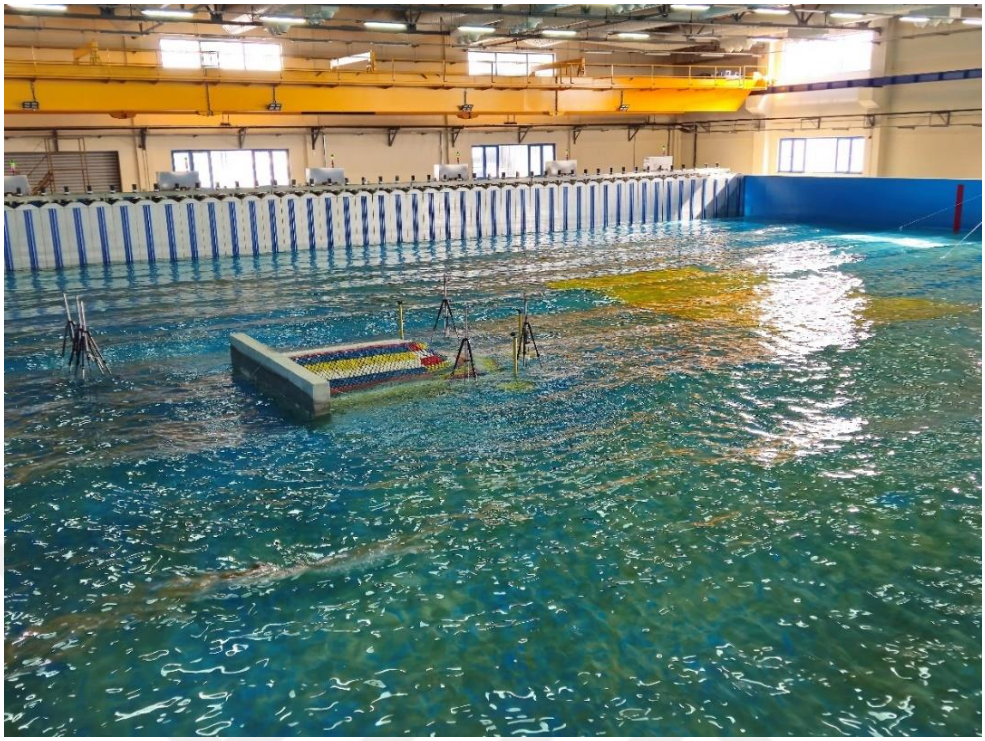

Figure 3.2 General view of wave basin and overhead crane

Besides the active reflection absorption function, there is also a passive absorber that can be adjusted according to the water depth near the shore. This depth-adjustable, parabolic-type passive wave absorption system is located on the shore opposite the wave generator. The three-dimensional breakwater head model was positioned $2L_p$ (15m) away from the wave generator. To avoid the effects of the side walls, the model was placed 4 meters away from the side wall. Geodesic measurements were conducted for this purpose.

3.2 Armor Unit Properties and Core Material

For the core material used in the breakwater model, quartz gravel with a nominal diameter D_{n50} of 1.90 cm, mass M_{50} of 18.25 grams, and specific gravity ρ_s of 2.65 tons/m³ was used. The relationship between the mass of the core material and the blocks was arranged according to Van Gent and Spaan (1998). This relationship is defined as:

$$\frac{M_{armor}}{M_{50,core}} \approx 10 - 20 \tag{3.1}$$

values between are a reliable range.

CEM (2003) recommends these values to be around 10. The material used in the core and the granulometry curve are given in Figures 3.3 and 3.4.

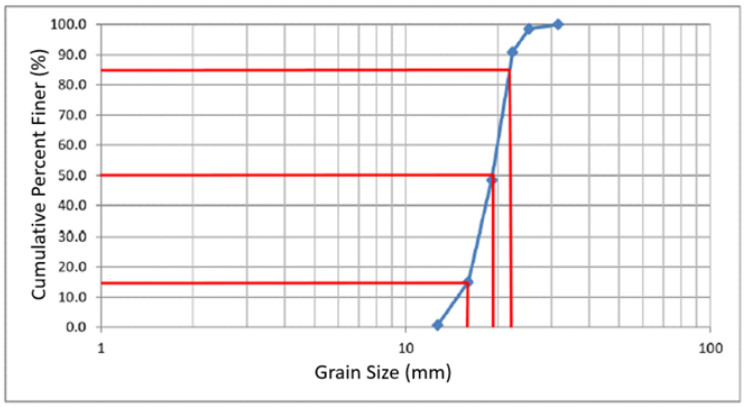

Figure 3.3 Particle-size distribution curve for core material

Figure 3.4 Core material of roundhead model

Figure 3.5 Cube blocks of the model

Mass ratio for armor layer and core material:

$$\frac{M_{armor}}{M_{50,core}} = \frac{202}{18.25} = 11.07$$

Nominal diameter ratio for armor layer and core material:

$$\frac{D_{n,armor}}{D_{n50,core}} = \frac{4.00}{1.90} = 2.11$$

In model study, cubes with 4 cm side length were used (Figure 3.6). In the experiments, two cubes of different densities were prepared to be placed in a single row. The properties of the cube blocks are given in Table 3.1

Table 3.1 Properties of high-density cube blocks

Nominal diameter, D_n (cm)	Weight, W (gr)	Volume, V (cm^3)	Density, ρ_{cube} (gr/cm^3)
4	202 (±4.53)	64	3.15

3.3 Packing Density and Porosity

In model studies, many different methods have been defined for calculating porosity and packing density. The packing density used in this research is based on the surface placement ratio. The superiority of this method is that it can evaluate the block volume together with the damage. It can be calculated simply by the total required concrete volume per unit area and the desired number of blocks. This defines the suitability of the placement method along with other criteria. The use of packing density allows for the comparison of two different placement methods. Due to the different layer thicknesses, the standard porosity calculation does not explain the layer packing density well.

Packing density Ψ_s is the ratio of the number of placed blocks (N_{BL}) to the maximum block volume per layer corresponding to one face (N_{PBL}) (Figure 3.6).

$$\Psi_s = \frac{N_{BL}}{N_{PBL}} = \frac{N_{BL}.D_n^2}{B.L} \quad (3.2)$$

N_{BL}: The number of blocks in the considered area of the B.L unit layer.

N_{PBL}: The maximum number of block volumes in the area of the unit layer = $B.L/D_n^2$.

D_n: Nominal block dimension = $\sqrt[3]{V_b}$

V_b: Block volume

B: Area width

L: Length of the area measured for each experiment on the slope.

In the conventional cube-block breakwater model, the blocks that move or are displaced are tracked considering the active or reference area, with the upper and lower limits taken as SWL ± $4D_n$ (± 16 cm). The reference area width being considered as 16 cm is approximately taken as the order of the maximum wave height.

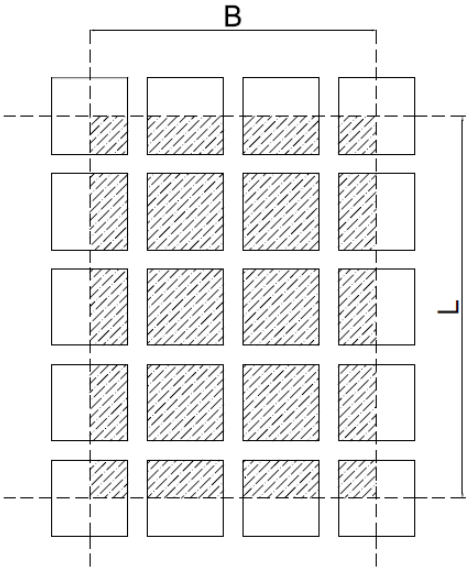

Figure 3.6 Reference area considered in existing models (schematic view)

In the regular placement method, it is also possible to apply different packing densities for each layer. The packing density is as follows:

$$\Psi_s = \frac{\Psi_{s1} + \Psi_{s2}}{2} \tag{3.3}$$

To find the N_{BL} in the irregular placement method, all blocks in the area are counted and the number of layers is divided by two (Frens, 2007).

This method gives the same results as the filled density (d) calculated from the thickness of the protection layer ($t = n.k_{\Delta}.\sqrt[3]{V_b}$, where the layer thickness coefficient, k_{Δ}=1). For the calculation of the filled density, the total volume of concrete per surface was divided by the volume of the protection layer in the reference area considered.

$$d = \frac{n.N_{BL}.V_b}{B.L.t} = \frac{N_{BL}.V_b^{2/3}}{B.L.k_{\Delta}} = \frac{\Psi_s}{k_{\Delta}}, V_b^{2/3} = D_n^2 \tag{3.4}$$

In the design of breakwaters, the total concrete volume required for each surface, V_t is calculated by multiplying the density, the number of layers, and the desired nominal block diameter. Thus, the following expression is obtained:

$$V_t = \Psi_s.n.\sqrt[3]{V_b} \ (m^3/m^2) \tag{3.5}$$

Here, according to the chosen placement method, ψ_s is a constant value. The relevant stability parameter determines the block volume. The number of cubic blocks per surface, N_t can be calculated by dividing the total concrete volume required for each surface by the required block volume.

$$N_t = \frac{V_t}{V_b} = \frac{\Psi_s.n}{V_b^{2/3}} \tag{3.6}$$

Figure 3.7 shows the schematic view of the model with 59% packing density that will be used in this study.

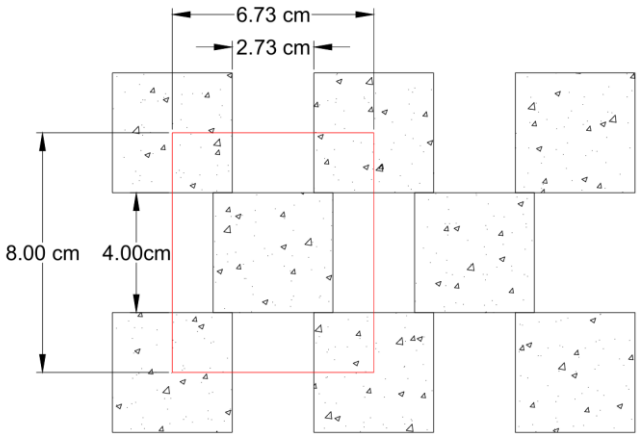

Figure 3.7 Schematical view of model with 59% packing density

$$\Psi_s = \frac{N_{BL}.D_n^2}{B.L} = \frac{2 \text{ x } 4^2}{6.73 \text{ x } 8} = 0.5943 \cong 59\ \%$$

It is known that due to different layer thicknesses, direct comparison of porosity in different placement methods is unnecessary (Frens, 2007). However, void ratio is an effective feature for the placement method. The actual porosities for the placement methods have been calculated. Therefore, the layer thickness has been determined for each experiment. P_r, the actual porosity, is expressed as follows:

$$P_r = 1 - d = 1 - \left(\frac{\Psi_s}{k_\Delta}\right) \tag{3.7}$$

For irregular placement, the layer thickness coefficient has been determined as 1.0 for cubes (blocks) by CEM (2003). The commonly used coefficient for a two-layer cube protection layer with irregular placement is 1.0. Accordingly, the layer thickness, t = 2a.

$$t = n.k_\Delta.\sqrt[3]{V_b}$$

$$t = 2.a = 2\left(\frac{V}{1.00}\right)^{1/3} = 2 \text{ x } 1.0 \text{ x } (V)^{1/3} \tag{3.8}$$

For regularly placed blocks, the layer thickness coefficient may vary due to the possible overlap of the second layer into the first layer. Porosity has been determined for each placement method by measuring and calculating the layer thickness.

Porosity calculation for the model with 59% packing density.

Total area: 6.73 x 8 = 53.84 cm²

Filled area: (4 x 4) x 2 = 32 cm²

Empty area: 53.84 - 32 = 21.84 cm²

Void ratio (porosity) = 21.84 / 53.84 ≅ 41%

In Section 3.4, the arrangement and placement of the cubes in the wave basin, along with the layout details, are provided.

In Section 3.7, the packing density ratios after the "As built" process are detailed. Here, each sector arc and the packing density ratios within the sectors are presented

in detail. Initially, the packing density was calculated as 59% using the theoretical formula, but it changed to 62% after the "As built" process.

3.4 Placement of the Cube Units on Roundhead Model

Considering that applying cubes on-site without a plan could be both difficult and incorrect, detailed calculations and trials were first made using AutoCAD. While placing the cubes on AutoCAD, the gaps between them and their positions relative to neighboring cubes were considered. Particularly, the placement was completed on AutoCAD with the condition that the cubes should not be stacked 3-4 rows high, and the gaps should not be too narrow or too wide.

The most important factor in the placement was ensuring that the packing density of each sector, the reference areas within each sector, the entire breakwater head, and the packing density in the entire reference area were as uniform as possible.

The number of cubes that could fit into a row was calculated using the required distance between cubes for a certain packing density and the nominal diameter (D_n=4cm) of the cubes.

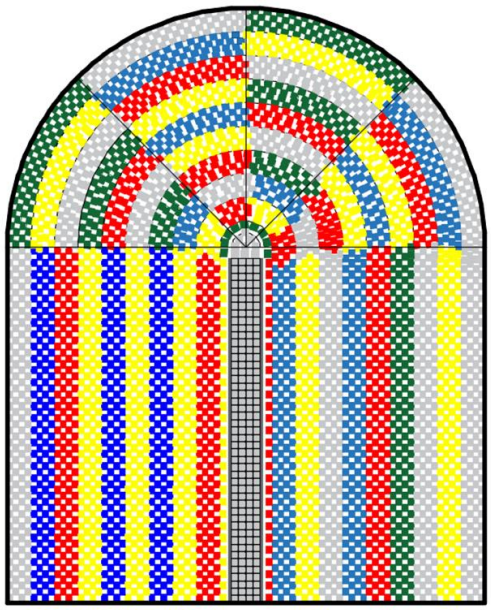

Figure 3.8 Finalized roundhead model with packing density of 62%

Once the number of cubes per row was determined and drawing plans are made, the placements for each sector were started from the bottom to upwards starting from 1st sector, towards the crown wall. After determining the density and cube numbers

on AutoCAD, the arrangement was applied on the prototype in the wave basin. Revisions were made to the arrangement, these revisions were incorporated back into the packing density calculations, and a final plan was prepared. All subsequent arrangements were made according to this final plan.

Figure 3.9 shows the breakwater roundhead with 62% packing density after finishing the implementation in basin.

Figure 3.9 Side view of roundhead model

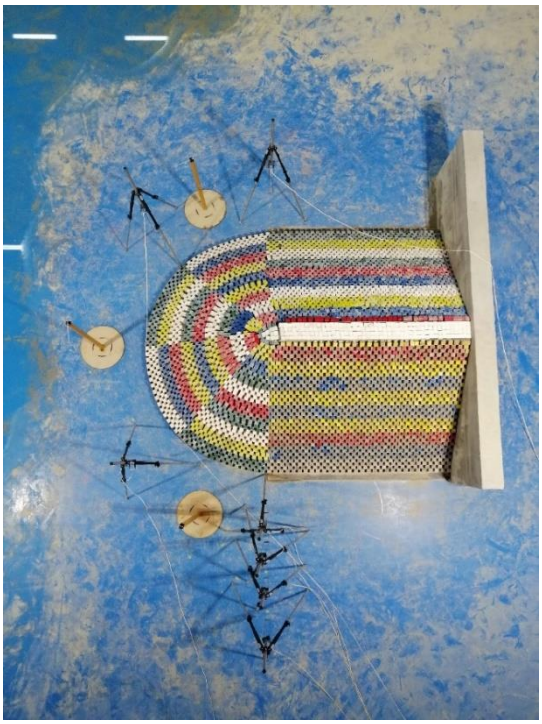

Figure 3.10 Top view of roundhead model

Construction of the roundhead model always started from trunk section to roundhead sectors. At first trunk section should be finished, after that placement started from first sector to second sector, second sector to third sector and to fourth sector. The methodology of the placement order is shown in the Figure 3.11.

Figure 3.11 Construction phase of the roundhead model

3.5 Definitions of Damage

In breakwaters with armor layers made of concrete blocks, block movements are a crucial parameter for defining damage. In this study, block movements were determined using image recordings from three separate cameras. Here, damage for moving blocks is defined as M_1 for 0-0.5 D_n, M_2 for 0.5-1 D_n, and M_T for <1 D_n, while for displaced blocks, damage is defined as D_1 for 1-2 D_n, D_2 for >2 D_n, and D_T for >1 D_n (Table 3.2 and Table 3.3).

Table 3.2 Damage criteria for moving blocks

M_1	0.0-0.5·D_n
M_2	0.5-1.0·D_n
M_T	0.0-1.0·D_n

Table 3.3 Damage criteria for displacing blocks

D_1	1.0-2.0·D_n
D_2	>2.0·D_n
D_T	>1.0·D_n

Damage ratio is calculated with percentage and determined by number of moving units over total number of units in reference area.

$$\text{Damage ratio (M or D)} = \frac{\text{Number of displaced block in reference area}}{\text{Number of total blocks in reference area}} \tag{3.9}$$

Damage due to displacement can also be defined in a different way than by percentages of movement or displacement. This is because it aims to define the movements of armor layer elements that are damaged and lose mass during movement. An armor layer element with reduced mass will move more easily during the next storm. Based on this, relative damage is defined as follows:

i. No damage

ii. Moving; movement of single units

$$N_{0<0.5} = \frac{n_r}{L/D_n} \tag{3.10}$$

$n_{r;}$ Number of moving units

iii. Sliding; movement of the units relatively to their initial position

$$N_{0<0.5} = \frac{n_{sl}}{L/D_n} \tag{3.11}$$

$n_{sl;}$ Number of sliding units

iv. Displacement (> 2.0 D_n)

$$N_{0<0.5} = \frac{n_0}{L/D_n} \tag{3.12}$$

$n_{0;}$ Number of displaced units

Relative damage for displaced units:

$$N_{0,mov} = N_{0d} + N_{0>0.5} \tag{3.13}$$

$$N_0 = \frac{\text{Number of displaced units more than 1.}D_n \text{ in reference area}}{\text{Total number of units in reference area}} \tag{3.14}$$

Before each experiment, three GoPro cameras were positioned at 45, 90, and 135 degrees to capture all four sectors of the breakwater head. Photos and video recordings were taken before and after each test to identify the movement of cube blocks and conduct damage analysis (Figure 3.12 and 3.13).

Figure 3.12 Wave-structure interaction at roundhead

Figure 3.13 Moving blocks after the tests

3.6 Scale Ratio and Scale Effects

In this study, scaling for the model was not done based on a specific prototype. The purpose of creating the studied model is to understand and solve the defined stability problem. In this section, the model scale and scale effects will be discussed.

3.6.1 Geometric Similarity

Since the ratios of geometric dimensions between the prototype and the model are equal, geometric similarity is shown as follows:

$$K = \frac{X_M}{X_P} = \frac{Y_M}{Y_P} = \frac{Z_M}{Z_P} \tag{3.15}$$

This relationship is independent of movement and only demonstrates similarity in terms of shape.

3.6.2 Kinematic Similarity

Kinematic similarity demonstrates the similarity in the motion of fluid particles between the model and the prototype. If the velocities at equivalent points in the model and the prototype are in the same direction and similar in scale, it can be said that "the model and the prototype are kinematically similar.

3.6.3 Dynamic Similarity

For two systems that are geometrically and kinematically similar to also be dynamically similar, the ratio of the vectorial forces in the model and the prototype must be the same. To achieve complete similarity, all dimensionless parameters between the model and the prototype must be similar. The systematic process used to form all dimensionless parameters given in variable sets is known as Buckingham Pi Theorem. In almost all coastal engineering problems, surface tension and elastic pressure are relatively insignificant and can be ignored. Therefore, the most important dimensionless parameters are the Froude and Reynolds numbers.

The Froude number represents the relative effect of inertial and gravitational forces in flow fields. For similarity to be achieved, the Froude number in the model and the prototype must be equal.

$$F_r = \left(\frac{U}{\sqrt{gL}}\right)_P = \left(\frac{U}{\sqrt{gL}}\right)_M \tag{3.16}$$

Here, U shows speed and L shows length.

$K_U = \frac{U_M}{U_P}, K_L = \frac{L_M}{L_P}$ and $K_g = 1.0$ (Gravity does not scaled)

Equation can be written below:

$$K_U = \sqrt{K_L} \tag{3.17}$$

The Froude scaling law typically simulates model flows involving inertial forces balanced by gravitational forces, which are effective in free-surface flows. The Reynolds number indicates the relative significance of inertial forces over viscous forces acting on fluid particles.

$$Re = \left(\frac{UL}{\nu}\right)_P = \left(\frac{UL}{\nu}\right)_M \tag{3.18}$$

ν show the kinematic viscosity

$K_U = \frac{U_M}{U_P}$, $K_L = \frac{L_M}{L_P}$ and $K_\nu = \frac{\nu_M}{\nu_P} = 1.0$ (Modelling done with water)

$$K_U = \frac{1}{K_L} \tag{3.19}$$

The Reynolds scaling law is observed in model flows where viscous forces are significant. In free-surface flows, gravitational forces are more influential than viscosity. Therefore, in this study, the Froude scaling law has been used. The required wave heights have been estimated for the stability analysis of cube blocks using the Hudson method.

3.6.4 Scale Effects

If a small-scale Froude model is tested with a liquid similar to that in the prototype, it does not simultaneously satisfy equations (3.16) and (3.18). This leads to viscous scale effects. Other scale effects include surface tension, friction, and aeration effects.

3.6.5 Viscous Scale Effects

According to the Froude scale law, linear scaling of prototype and model lengths at small Reynolds numbers leads to large viscous forces. This results in increased flow resistance, reducing internal and external flow in the filter and core layers. Hughes (1993) and Frens (2007) noted that at small Reynolds numbers, relatively more energy is reflected from the model structure, and less energy passes through the model. Additionally, wave run-up and rundown speeds are relatively higher. Higher wave run-up results in lower armor stability, leading to stability coefficients that are on the safer side. This issue can be addressed by calculating the geometric scale and increasing the size of the core layer material in the model.

In this study, the core layer and cube blocks were scaled, and the Reynolds number was calculated as follows:

$$U = \frac{P.H_s.L_m}{2.d.T} = \frac{0.49x0.16x6.60}{2x0.60x2.05} = 0.21\ m/s \tag{3.20}$$

$$R_e = \frac{U.D_n}{\upsilon} = \frac{0.21x0.019}{1.33x10^{-6}} = 2990 \tag{3.21}$$

The Reynolds number within the core layer was determined to be greater than $2x10^3$, indicating that the flow within the structure is turbulent. Therefore, the prototype and model were matched, and viscous scale effects were neglected.

3.6.6 Surface Tension Scale Effects

This scale effect becomes significant in cases where the water depth is very shallow or the waves are very short. Surface tension effects should be considered when water depths are less than 2 cm and wave periods are less than 0.35 seconds. In this study, the water depth and wave periods are significantly larger than the specified values. Therefore, the surface tension scale effect is neglected.

3.6.7 Friction Scale Effects

In cases where the wave travel distance is long, the effects of bottom friction scale emerge in the model. This situation is not considered in relatively large rubble mound models. Another friction effect is due to the interaction between the armor layer elements in contact with each other. In rubble mound structure models, contact friction forces are important for structural behavior, but in the presence of wave

effects, friction forces can be neglected compared to wave effects. However, in small-scale physical models, the friction force between armor layer elements does not correspond to that in the prototype. This is because the surfaces of the armor layer elements are rougher in small-scale models.

In this study, the armor layer elements were sanded and painted to achieve smooth surfaces. It has been noted that if the model elements are smoother than the prototype, the results for stability will be more consistent.

3.6.8 Aeration Scale Effects

As a result of wave breaking on the structure, the movement and interactions of air bubbles entering the armor layer elements have been investigated. It has been noted that there will not be a similarity between the prototype and the model due to the lack of similarity in the Weber number. Air bubbles will cause more energy loss in the model than in the prototype. Therefore, the energy loss occurring in the rubble mound slope will be greater than estimated, and wave run-up will be affected by this situation. In this study, the physical model experiment is conducted with the head stability armor layer composed of single-row, normally and highly dense cube blocks.

3.7 Methods and Model Setup

Irregular waves were generated using the JONSWAP spectrum in the experiments. The cumulative relative damage was determined by image processing technique as the wave heights were increased while keeping the wave steepness constant. For this purpose, three cameras were used.

All experiments were conducted at a constant water depth of 60 cm. Based on damage measurements on the head section, the most critical damage areas were identified. In the model, single-layer regular placement of 4×4×4 cm cube concrete blocks were used for the armor layer. The high-density cube blocks has a density of 31.5 kN/m^3.

The regular and staggered placement method with a packing density of 0.62 was applied as the placement method for the single-layer cube blocks.

The placement of the cube blocks in the head section of the established model is shown in Figure 3.14. The head section consists of four 45-degree sectors.

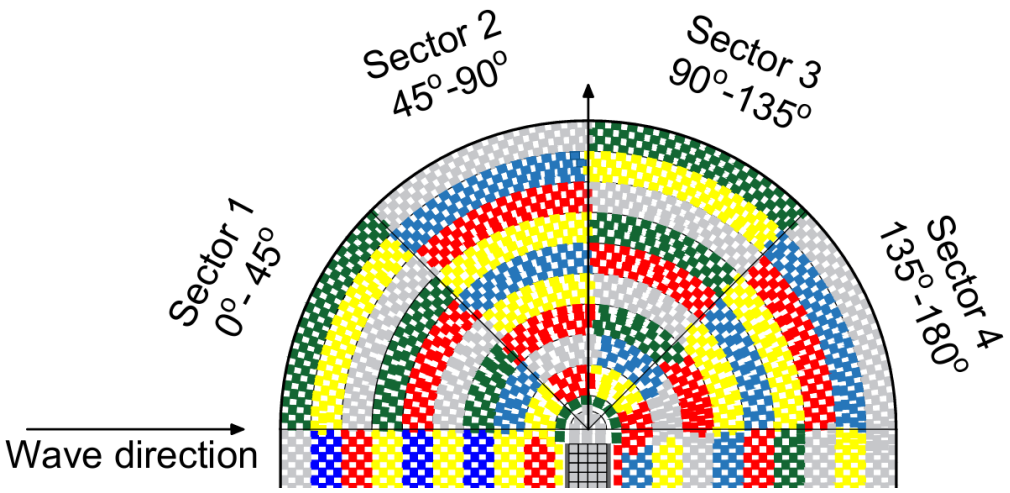

Figure 3.14 Cube placement and sectors at roundhead section

Before placing the cube blocks on the armor layer in the model, the block placement was designed using AutoCAD software to achieve a 62% packing density. Due to the circular conical shape of the head section, some deviations in packing density occurred in certain rows when placing the fixed-size cubes. The number of cube blocks and packing densities for each row and sector are provided in Table 3.4. As shown in Table 3.4, 37 rows of cubes were placed from the first row of the rigid toe up to the crest, which was kept stable.

Table 3.4 Number of cubes and packing densities (S1, S2, S3 and S4 represents sector 1, sector 2, sector 3 and sector 4 respectively)

		Number of Cubes					**Packing density for each sector arc (%)**			
Row	**Arc Length**	**S1**	**S2**	**S3**	**S4**	**Arc length for sectors**	**S1**	**S2**	**S3**	**S4**
1	417.44	15	15	15	15	104.4	57.49	57.49	57.49	57.49
2	406.98	15	15	15	15	101.7	58.97	58.97	58.97	58.97
3	396.52	15	15	15	14	99.1	60.53	60.53	60.53	56.49
4	386.05	15	15	15	15	96.5	62.17	62.17	62.17	62.17
5	375.59	14	14	14	14	93.9	59.64	59.64	59.64	59.64
6	365.13	14	14	14	14	91.3	61.35	61.35	61.35	61.35

Table 3.4 Number of cubes and packing densities (S1, S2, S3 and S4 represents sector 1, sector 2, sector 3 and sector 4 respectively) (cont.)

7	354.67	14	14	13	14	88.7	63.16	63.16	58.65	63.16
8	344.21	13	13	13	13	86.1	60.43	60.43	60.43	60.43
9	333.75	12	12	12	12	83.4	57.53	57.53	57.53	57.53
10	323.29	12	13	12	12	80.8	59.39	64.34	59.39	59.39
11	312.82	12	12	12	12	78.2	61.38	61.38	61.38	61.38
12	302.36	11	12	11	11	75.6	58.21	63.50	58.21	58.21
13	291.90	11	11	10	11	73.0	60.29	60.29	54.81	60.29
14	281.44	11	11	11	11	70.4	62.54	62.54	62.54	62.54
15	270.98	10	10	9	10	67.7	59.05	59.05	53.14	59.05
16	260.52	10	10	10	10	65.1	61.42	61.42	61.42	61.42
17	250.06	9	9	9	9	62.5	57.59	57.59	57.59	57.59
18	239.59	9	10	9	9	59.9	60.10	66.78	60.10	60.10
19	229.13	8	8	8	8	57.3	55.86	55.86	55.86	55.86
20	218.67	8	9	8	8	54.7	58.54	65.85	58.54	58.54
21	208.21	8	8	8	8	52.1	61.48	61.48	61.48	61.48
22	197.75	8	7	7	8	49.4	64.73	56.64	56.64	64.73
23	187.29	7	7	7	7	46.8	59.80	59.80	59.80	59.80
24	176.82	8	7	7	7	44.2	72.39	63.34	63.34	63.34
25	166.36	6	7	6	6	41.6	57.71	67.32	57.71	57.71
26	155.90	6	7	6	6	39.0	61.58	71.84	61.58	61.58
27	145.44	6	6	6	6	36.4	66.01	66.01	66.01	66.01
28	134.98	5	5	5	6	33.7	59.27	59.27	59.27	71.12
29	124.52	5	5	5	5	31.1	64.25	64.25	64.25	64.25
30	114.06	5	5	5	4	28.5	70.14	70.14	70.14	56.11
31	103.59	4	4	4	4	25.9	61.78	61.78	61.78	61.78
32	93.13	4	4	4	4	23.3	68.72	68.72	68.72	68.72
33	82.67	4	3	4	3	20.7	77.42	58.06	77.42	58.06
34	72.21	3	3	3	3	18.1	66.47	66.47	66.47	66.47
35	61.75	3	3	3	3	15.4	77.74	77.74	77.74	77.74
36	51.29	3	2	2	3	12.8	93.59	62.39	62.39	93.59
37	40.82	3	2	2	2	10.2	117.58	78.38	78.38	78.38
Total		**326**	**327**	**319**	**322**	Mean	**64.76**	**63.07**	**61.97**	**62.77**
Ref Cube Number		54	54	52	54					

The placement plan was prepared in Figure 3.15, and the blocks were manually placed according to this plan after each experiment.

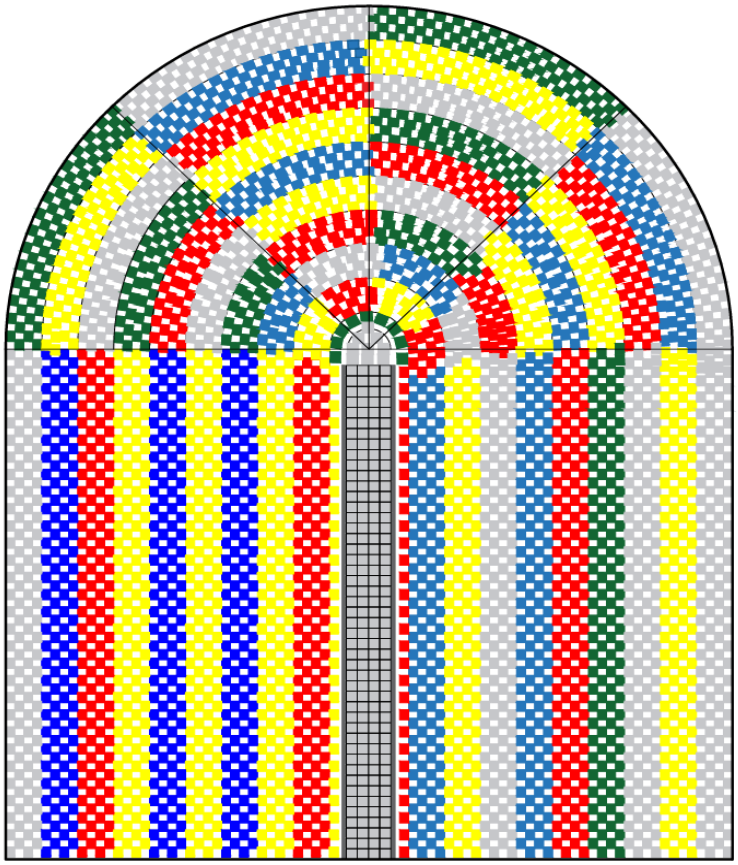

Figure 3.15 Layout of whole section with 62% packing density

The width of the reference area in each sector was considered to be $8D_n$, given a design wave height of H_{m0}=0.16m, considering SWL± H_{m0} or SWL± nD_n. The number of cubes and packing densities in the reference area after application are provided in Table 3.5 and Table 3.6. After the application, the average packing density in the reference area was found to be 62.5%. A total of 1294 cubes were placed throughout the entire head section.

Table 3.5 Packing density and number of cubes in reference area

After application					
	Reference Area				**Reference Area**
	1.Sector	**2. Sector**	**3. Sector**	**4. Sector**	5481.15
Number of cubes	54	54	52	54	214
Packing density (%)	62.87	63.21	60.73	63.22	62.51

Table 3.6 Packing densities of each sector and reference areas in each sector

After application	1. Sector	2. Sector	3. Sector	4. Sector	Mean
Packing density of each sector (%)	64.76	63.07	61.97	62.77	63.14
Packing density of each reference area (%)	62.87	63.21	60.73	63.22	62.51

3.7.1 Model Setup

The physical model was prepared according to the Froude scaling conditions with a 1/30 geometric scale, avoiding the effects of side walls. A local right-angle coordinate system, as defined below, was established around the wave basin. Measurements were taken using the Leica TCRA 1201 Total Station device, available in the inventory of the Department of Geomatics Engineering. Reference points N.101, N.102, N.103, and N.104, shown in Figure 3.16, were established on the pool and structure walls. Leica panel reflectors were used in the establishment of these points (Figures 3.16 and 3.17). The coordinate values of these points were calculated based on the measurements of distances and directions, and the results are provided in Table 3.7.

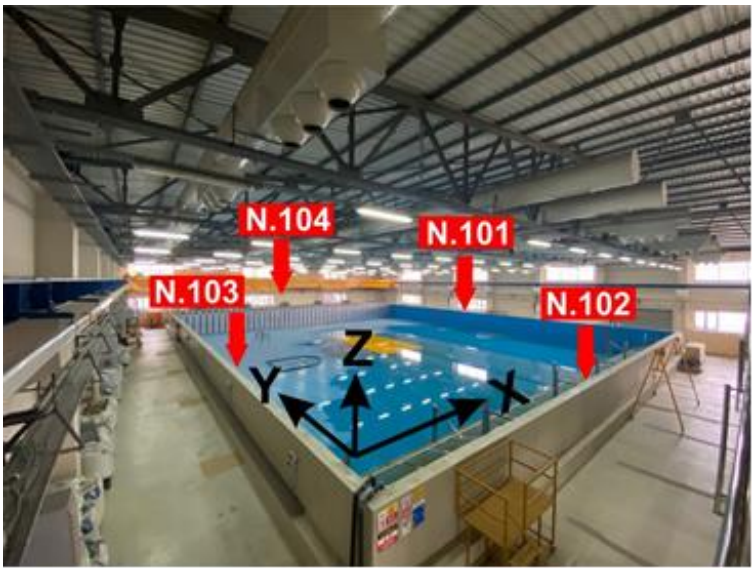

Figure 3.16 Hydrodynamics laboratory basin coordinate systems and reference points

Table 3.7 Local values of reference points

Point No	Y (m)	X (m)	Z (m)
N.101	1006.5645	514.4275	102.105
N.102	987.5865	497.526	102.1275
N.103	1006.3215	485.589	102.101
N.104	1029.546	499.548	103.454

Figure 3.17 Reference points and measurements

In all works to be carried out within the basin, the coordinate values of these points, established through geodetic measurements, will be taken as reference, and the work continued in a single coordinate system.

The breakwater model, defined by coordinates, was placed as shown in Figure 3.18. For this model placement, plywood templates were made, and the body and head sections were constructed with the help of these templates. After the model section was placed, the templates were removed using a crane. The other end of the model was fixed with a wall constructed 4.00 meters away from the basin wall. To ensure the stability of the model's toe, a steel toe was constructed. The completed core of the breakwater model is shown in Figure 3.19. The height of the model core is 91 cm, and the slope is 1/1.5.

Figure 3.18 Creation of model cross-section

Figure 3.19 Core material of the breakwater model

3.8 Reflection Analysis and Wave Conditions

Before building the breakwater model, reflection tests were done in the wave basin (Figure 3.20). Although the generator system includes an active absorption system and a passive wave absorption slope structure was installed on the opposite shore, the waves generated at the area where the breakwater would be placed were tested using a four-probe system. Potential reflections were analyzed using the Mansard and Funke (1980) method. At first case four of these probes were positioned just in front of the breakwater head section for reflection analysis, while the others were placed around the head. While three of other probes are positioned same (Probe 5-6-7), location of these four probes (Probe 1-2-3-4) changed and moved between breakwater and wave basin walls. All these placements of the wave probes are aimed to analyze the wave reflection properly. In Figure 3.20 first probe location is shown.

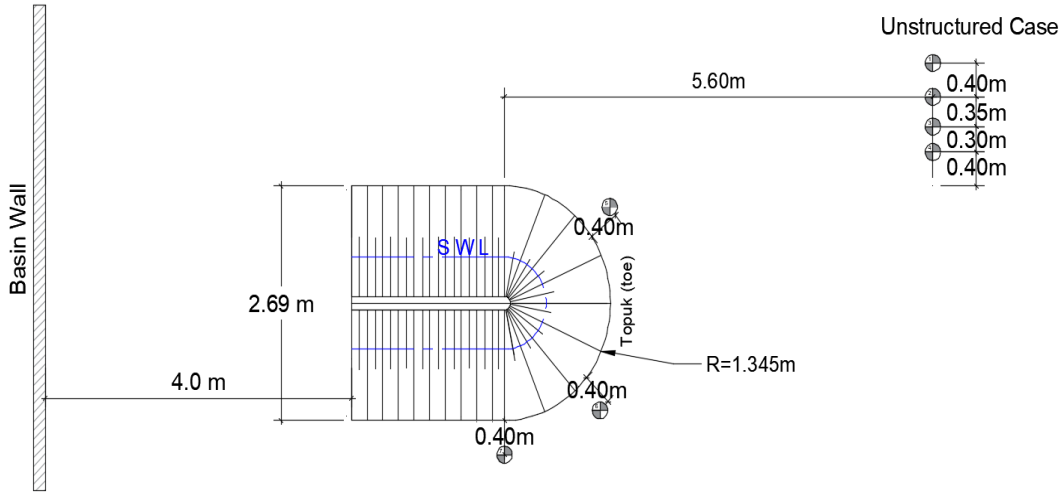

Figure 3.20 Reflection analysis without structure

First four probe is located at starting of the roundhead where the sector is 0° degree. Figure 3.21 shows 2nd locations of the four probes are located at middle of the trunk section of the breakwater. Figure 3.22 shows the 3rd location of the four probes. To avoid reflection from trunk section at 2nd location, four probes have moved middle of basin wall and breakwater's end (Figure 3.23).

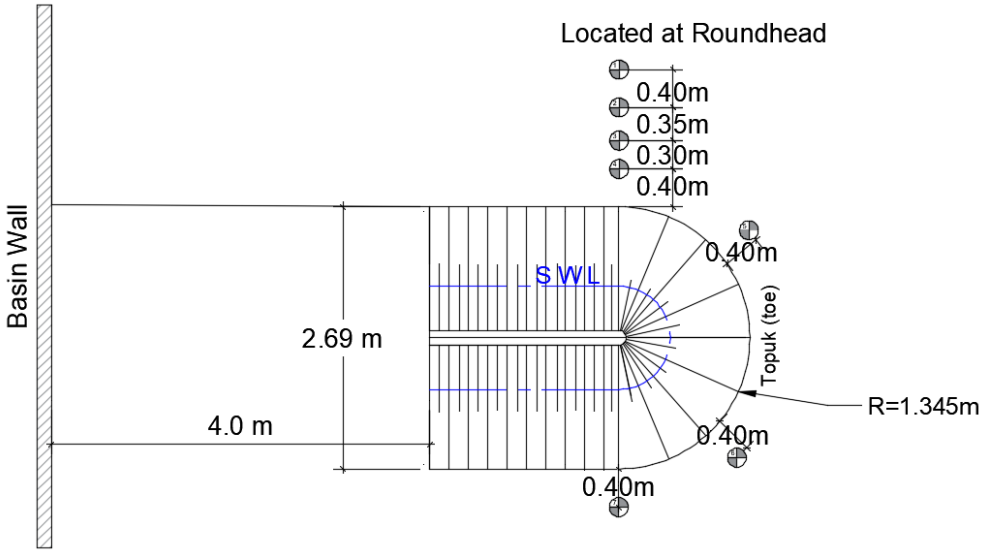

Figure 3.21 Probes located at roundhead case for reflection analysis

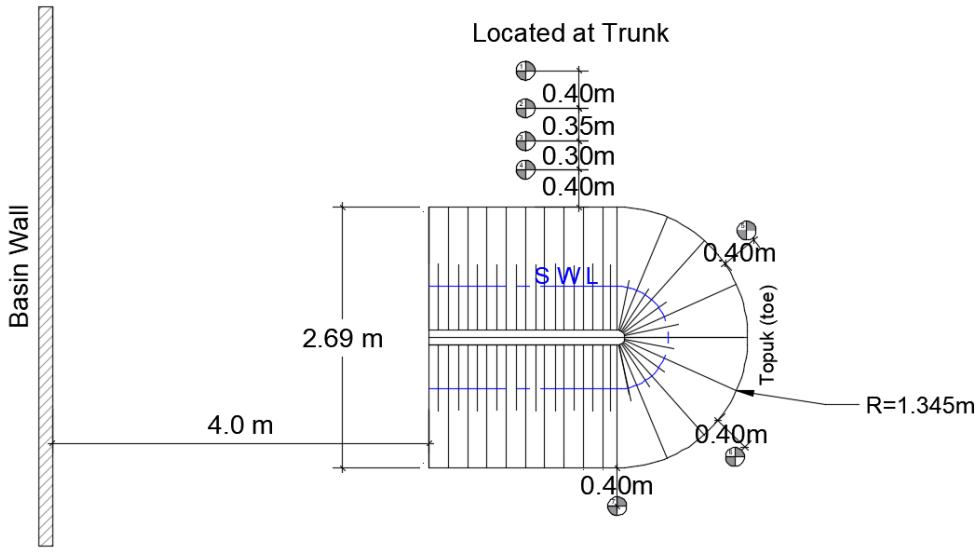

Figure 3.22 Probes located at trunk case for reflection analysis

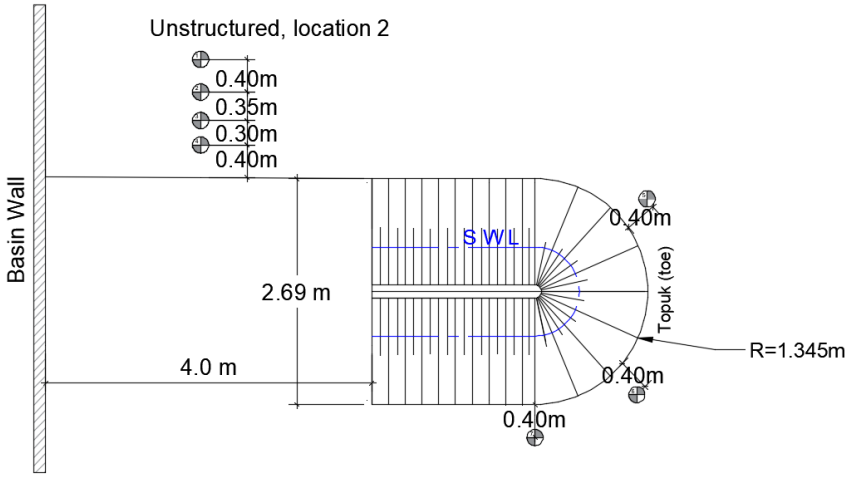

Figure 3.23 2nd case for reflection analysis without structure

Reflection analysis were done for each probe location case to obtain the best wave conditions around the breakwater roundhead and results of these analyses are given tables below for each wind and swell wave conditions. WS is used as an abbreviation for "without structure" condition.

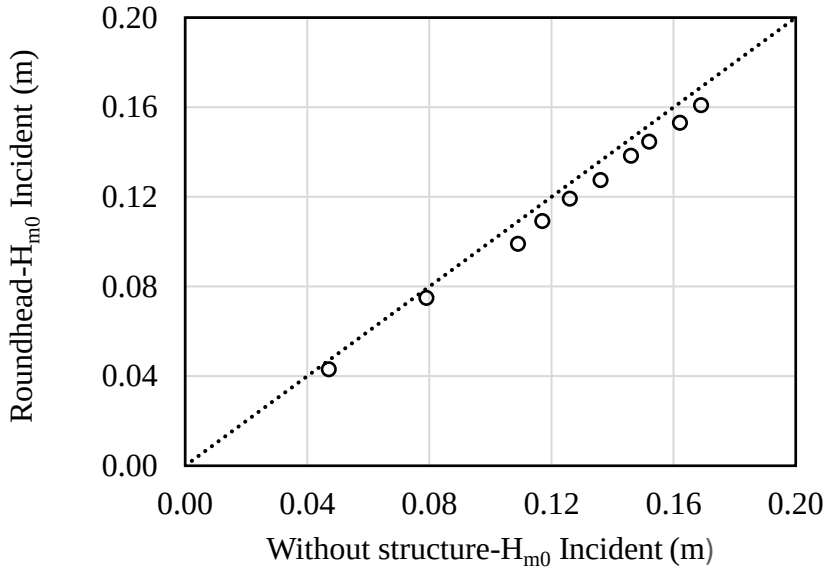

Figure 3.24 Without structure-Roundhead Comparison for wind waves

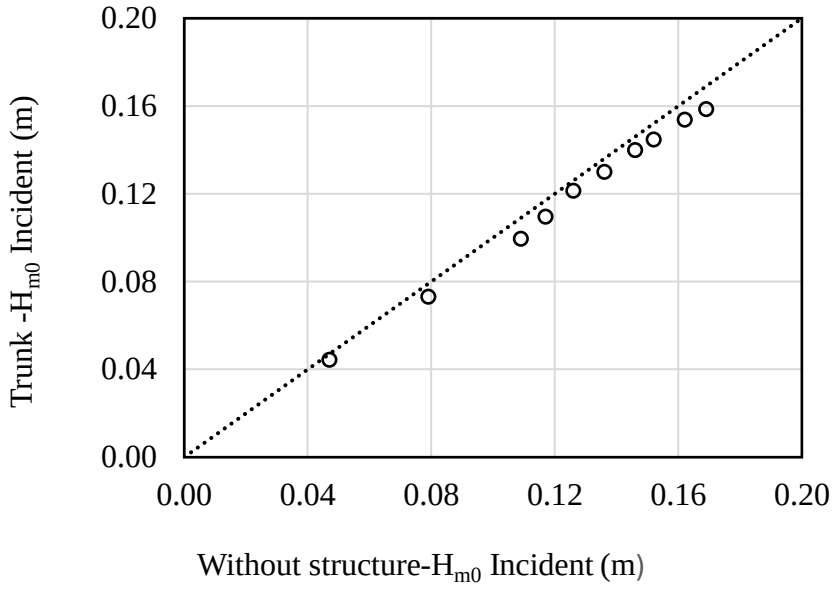

Figure 3.25 Without structure-Trunk Comparison for wind waves

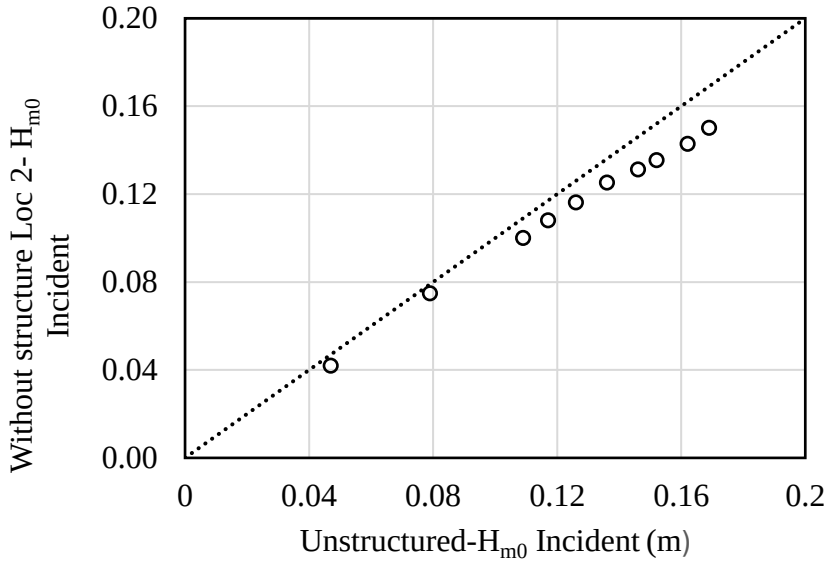

Figure 3.26 WS-WS Location-2 Comparison for wind waves

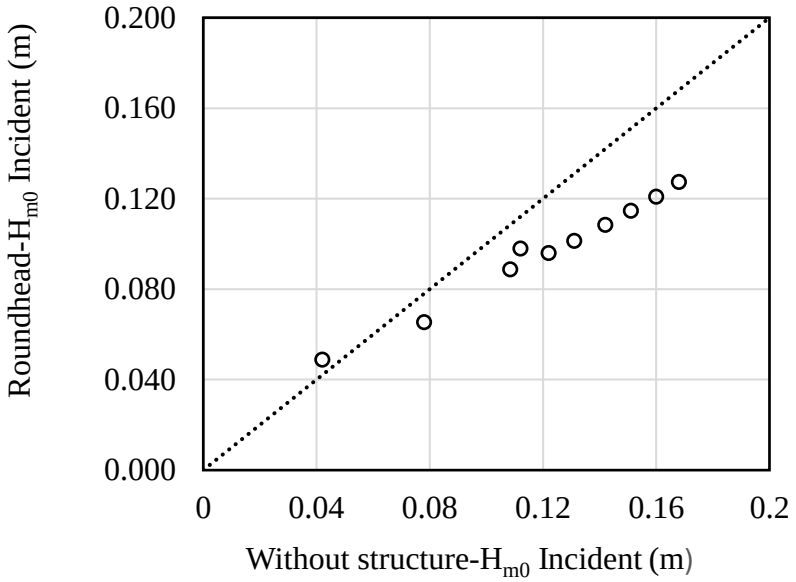

Figure 3.27 Without structure-Roundhead Comparison for swell waves

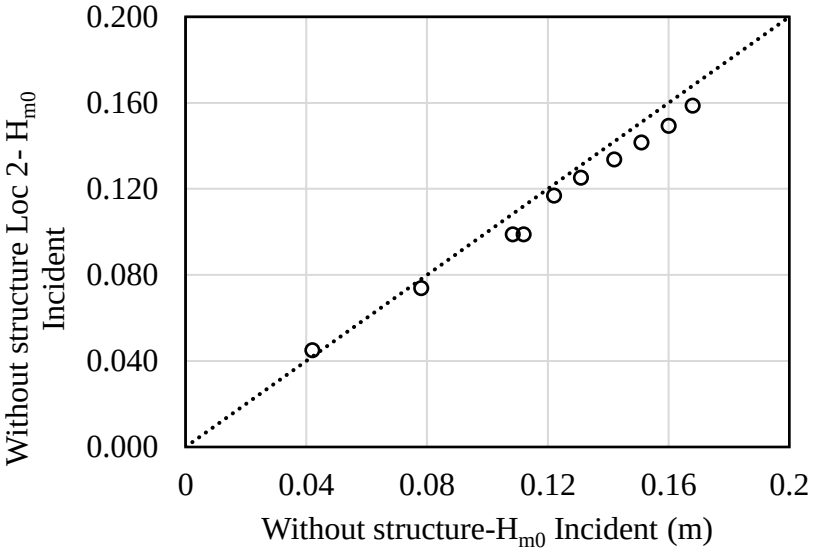

Figure 3.28 WS-WS Location-2 Comparison for swell waves

For wind waves, when probes are placed on the breakwater roundhead and trunk, the reflection effects are quite small. In swell waves, when probes are placed on the breakwater roundhead, the height of incident waves has decreased due to reflections caused by the presence of the structure.

When the probes are positioned between the breakwater and the wave basin walls, the incident wave heights have shown better results compared to the previous

situation. In this situation, target wave conditions are obtained even with presence of the reflections in the basin and shown in tables below.

Table 3.8 Wave parameters for without structure condition for wind waves

Without structure					
Case	**H_{m0} Incident (m)**	**H_{m0} Reflected (m)**	**K_r**	**T_p (s)**	**$T_{m-1,0}$ (s)**
WW1	0.047	0.008	0.170	1.000	0.950
WW2	0.079	0.012	0.160	1.250	0.940
WW3	0.109	0.018	0.163	1.470	1.320
WW4	0.117	0.018	0.156	1.471	1.390
WW5	0.126	0.021	0.162	1.560	1.430
WW6	0.136	0.023	0.163	1.563	1.490
WW7	0.146	0.024	0.160	1.667	1.550
WW8	0.152	0.026	0.170	1.667	1.600
WW9	0.162	0.027	0.161	1.667	1.600
WW10	0.169	0.027	0.157	1.667	1.600

Table 3.9 Wave parameters for roundhead condition for wind waves

Roundhead					
Case	**H_{m0} Incident (m)**	**H_{m0} Reflected (m)**	**K_r**	**T_p (s)**	**$T_{m-1,0}$ (s)**
WW1	0.043	0.010	0.235	0.962	0.973
WW2	0.075	0.017	0.229	1.250	1.175
WW3	0.099	0.023	0.234	1.429	1.400
WW4	0.109	0.027	0.247	1.471	1.450
WW5	0.119	0.031	0.260	1.563	1.506
WW6	0.128	0.033	0.262	1.667	1.556
WW7	0.138	0.037	0.266	1.667	1.608
WW8	0.145	0.040	0.276	1.724	1.642
WW9	0.153	0.042	0.274	1.724	1.640
WW10	0.161	0.044	0.274	1.724	1.646

Table 3.10 Wave parameters for trunk condition for wind waves

Trunk					
Case	**H_{m0} Incident (m)**	**H_{m0} Reflected (m)**	**K_r**	**T_p (s)**	**$T_{m-1,0}$ (s)**
WW1	0.045	0.015	0.330	0.962	0.972
WW2	0.073	0.025	0.339	1.191	1.159
WW3	0.100	0.035	0.351	1.471	1.388
WW4	0.110	0.038	0.349	1.515	1.453
WW5	0.122	0.042	0.345	1.563	1.485
WW6	0.130	0.045	0.345	1.613	1.532
WW7	0.140	0.048	0.343	1.667	1.587
WW8	0.145	0.052	0.355	1.786	1.629
WW9	0.154	0.055	0.353	1.724	1.624
WW10	0.159	0.056	0.354	1.724	1.644

Table 3.11 Wave parameters for without structure location 2 condition for wind waves

Without structure - location 2					
Case	**H_{m0} Incident (m)**	**H_{m0} Reflected (m)**	**K_r**	**T_p (s)**	**$T_{m-1,0}$ (s)**
WW1	0.042	0.009	0.222	0.962	0.973
WW2	0.075	0.015	0.200	1.250	1.181
WW3	0.100	0.021	0.205	1.471	1.378
WW4	0.108	0.023	0.211	1.515	1.444
WW5	0.116	0.024	0.206	1.563	1.488
WW6	0.125	0.028	0.221	1.613	1.536
WW7	0.131	0.030	0.231	1.667	1.604
WW8	0.135	0.032	0.236	1.724	1.651
WW9	0.143	0.033	0.233	1.724	1.652
WW10	0.150	0.035	0.231	1.724	1.653

Table 3.12 Wave parameters for without structure condition for swell waves

Without structure					
Case	**H_{m0} Incident (m)**	**H_{m0} Reflected (m)**	**K_r**	**T_p (s)**	**$T_{m-1,0}$ (s)**
SW1	0.042	0.009	0.209	1.667	1.620
SW2	0.078	0.002	0.256	2.273	2.040
SW3	0.1084	0.032	0.287	2.500	2.390
SW4	0.112	0.035	0.301	2.778	2.490
SW5	0.122	0.035	0.286	2.500	2.240
SW6	0.131	0.038	0.287	2.500	2.220
SW7	0.142	0.042	0.285	2.500	2.210
SW8	0.151	0.044	0.282	2.500	2.210
SW9	0.16	0.048	0.285	2.500	2.200
SW10	0.168	0.050	0.286	2.500	2.210

Table 3.13 Wave parameters for roundhead condition for swell waves

Roundhead					
Case	**H_{m0} Incident (m)**	**H_{m0} Reflected (m)**	**K_r**	**T_p (s)**	**$T_{m-1,0}$ (s)**
SW1	0.049	0.014	0.289	1.724	1.651
SW2	0.065	0.027	0.393	2.273	2.184
SW3	0.089	0.044	0.473	2.778	2.492
SW4	0.098	0.049	0.478	2.778	2.528
SW5	0.096	0.048	0.503	2.381	2.429
SW6	0.101	0.051	0.506	2.381	2.430
SW7	0.108	0.055	0.508	2.381	2.432
SW8	0.115	0.058	0.512	2.500	2.435
SW9	0.121	0.061	0.511	2.500	2.438
SW10	0.127	0.065	0.509	2.500	2.439

Table 3.14 Wave parameters for without structure location 2 condition for swell waves

Without structure - Location 2					
Case	**H_{m0} Incident (m)**	**H_{m0} Reflected (m)**	**K_r**	**T_p (s)**	**$T_{m-1,0}$ (s)**
SW1	0.045	0.013	0.282	1.724	1.664
SW2	0.074	0.022	0.295	2.273	2.171
SW3	0.099	0.027	0.270	2.632	2.495
SW4	0.100	0.026	0.261	2.632	2.636
SW5	0.117	0.032	0.278	2.381	2.400
SW6	0.125	0.034	0.270	2.381	2.401
SW7	0.134	0.035	0.264	2.381	2.402
SW8	0.142	0.036	0.256	2.381	2.405
SW9	0.149	0.038	0.254	2.381	2.407
SW10	0.159	0.039	0.246	2.500	2.398

Before the breakwater section was placed, preliminary experiments were conducted, and the wave parameters obtained from these experiments were referred to as "without structure." Subsequently, after the breakwater section was constructed, experiments were conducted, and wave probes were positioned at different locations to collect wave data. The probes were first positioned in the absence of the structure (Without structure), then at the location of the breakwater head (Roundhead), at the trunk section (Trunk), and finally between the breakwater and the basin wall (Without structure location 2) to measure the waves.

When the probes were placed on the roundhead, less wave reflection was observed compared to the trunk, and this reflection was negligible. Therefore, for stability numbers, the calculations were performed considering the conditions without structure.

The wave parameters obtained from these experiments are presented in Tables 3.8, 3.9, 3.10, and 3.11 for wind wave conditions, and in Tables 3.12, 3.13, and 3.14 for swell wave conditions. Based on the values obtained from these tables, Figures 3.24, 3.25, 3.26, 3.27, and 3.28 were generated to conduct and compare the wave reflection analysis.

G is the gain factor of the wave generator and chosen as 1.15 to obtain the target wave conditions.

Table 3.15 Target wave conditions for wind waves

$S_{p,\,mean}$ = 0.034 Wind wave									
H_{m0} (m)	**T_m**	**S_m**	**T_p**	**S_p**	**T_{m-1}**	**S_{m-1}**	**Ts**	**Ss**	**G**
0.05	0.789	0.052	0.986	0.033	0.891	0.040	0.917	0.038	1.15
0.08	0.998	0.052	1.247	0.033	1.126	0.040	1.160	0.038	1.15
0.11	1.170	0.052	1.462	0.033	1.321	0.040	1.360	0.038	1.15
0.12	1.222	0.052	1.527	0.033	1.379	0.040	1.420	0.038	1.15
0.13	1.271	0.052	1.589	0.033	1.435	0.040	1.478	0.038	1.15
0.14	1.319	0.052	1.649	0.033	1.490	0.040	1.534	0.038	1.15
0.15	1.366	0.052	1.707	0.033	1.542	0.040	1.588	0.038	1.15
0.16	1.410	0.052	1.763	0.033	1.593	0.040	1.640	0.038	1.15
0.17	1.408	0.054	1.760	0.035	1.590	0.043	1.645	0.040	1.15
0.18	1.408	0.058	1.760	0.037	1.590	0.046	1.645	0.043	1.15

Table 3.16 Target wave conditions for swell waves

Sp = 0.0133 Swell wave									
H_{m0} (m)	**T_m**	**S_m**	**T_p**	**S_p**	**T_{m-1}**	**S_{m-1}**	**Ts**	**Ss**	**G**
0.05	1.432	0.016	1.790	0.010	1.617	0.012	1.665	0.012	1.15
0.08	1.816	0.016	2.270	0.010	2.051	0.012	2.111	0.012	1.15
0.11	2.128	0.016	2.660	0.010	2.403	0.012	2.474	0.012	1.15
0.12	2.224	0.016	2.780	0.010	2.511	0.012	2.585	0.012	1.15
0.13	2.000	0.021	2.500	0.013	2.258	0.016	2.325	0.015	1.15
0.14	2.000	0.022	2.500	0.014	2.258	0.018	2.325	0.017	1.15
0.15	2.000	0.024	2.500	0.015	2.258	0.019	2.325	0.018	1.15
0.16	2.000	0.026	2.500	0.016	2.258	0.020	2.325	0.019	1.15
0.17	2.000	0.027	2.500	0.017	2.258	0.021	2.325	0.020	1.15
0.18	2.000	0.029	2.500	0.018	2.258	0.023	2.325	0.021	1.15

Table 3.17 Actual wave conditions for wind waves

$S_{p,\,mean}$= 0.034 Wind Wave										
Case	**H_{m0} Total (m)**	**H_{m0} Incident (m)**	**H_{m0} Reflected (m)**	**T_p (s)**	**S_p**	**$T_{m-1,0}$ (s)**	**S_{m-1}**	**K_r**	**Duration (s)**	**Number of Overtopping**
ww1	0.048	0.042	0.009	0.962	0.033	0.973	0.033	0.222	800	-
ww2	0.080	0.075	0.015	1.250	0.033	1.181	0.035	0.200	1000	-
ww3	0.111	0.100	0.021	1.471	0.033	1.378	0.035	0.205	1200	3
ww4	0.120	0.108	0.023	1.515	0.034	1.444	0.035	0.211	1250	6
ww5	0.130	0.116	0.024	1.563	0.034	1.488	0.036	0.206	1300	10
ww6	0.139	0.125	0.028	1.613	0.034	1.536	0.036	0.221	1350	16
ww7	0.149	0.131	0.030	1.667	0.034	1.604	0.036	0.231	1400	22
ww8	0.156	0.135	0.032	1.724	0.034	1.651	0.035	0.236	1440	25
ww9	0.165	0.143	0.033	1.724	0.035	1.652	0.037	0.233	1440	36
ww10	0.173	0.150	0.035	1.724	0.037	1.653	0.039	0.231	1440	44

Table 3.18 Actual wave conditions for swell waves

$S_{p,mean}$=0.013 Swell Wave										
Case	**H_{m0} Total (m)**	**H_{m0} Incident (m)**	**H_{m0} Reflected (m)**	**T_p (s)**	**S_p**	**$T_{m-1,0}$ (s)**	**S_{m-1}**	**K_r**	**Duration (s)**	**Number of Overtopping**
sw1	0.051	0.045	0.013	1.724	0.011	1.664	0.011	0.282	1450	-
sw2	0.085	0.074	0.022	2.273	0.011	2.171	0.011	0.295	1850	-
sw3	0.120	0.099	0.027	2.632	0.011	2.495	0.012	0.270	2150	3
sw4	0.128	0.100	0.026	2.632	0.012	2.636	0.012	0.261	2230	8
sw5	0.141	0.117	0.032	2.381	0.016	2.400	0.016	0.278	2010	10
sw6	0.152	0.125	0.034	2.381	0.017	2.401	0.017	0.270	2000	14
sw7	0.162	0.134	0.035	2.381	0.018	2.402	0.018	0.264	2000	18
sw8	0.173	0.142	0.036	2.381	0.020	2.405	0.019	0.256	2000	28
sw9	0.183	0.149	0.038	2.381	0.021	2.407	0.020	0.254	2000	35
sw10	0.193	0.159	0.039	2.500	0.020	2.398	0.021	0.246	2000	56

3.9 Wave Diffraction at the Breakwater Roundhead

When waves propagate from deep water to shallow water and encounter an obstacle such as a breakwater, island, or headland, wave heights change. This phenomenon is referred to as wave diffraction. Diffraction is the most important parameter affecting wave height within a harbor. The ratio of the diffracted wave height H_d to the incoming wave height H_i is termed the diffraction coefficient K_d and is defined as:

$$K_d = \frac{H_d}{H_i}$$

Due to diffraction effect of waves that approaching the breakwater roundhead, there have been changes in the wave height. These changes were determined by measuring the waves and represented with a 10 cm grid and show in Figure 3.29.

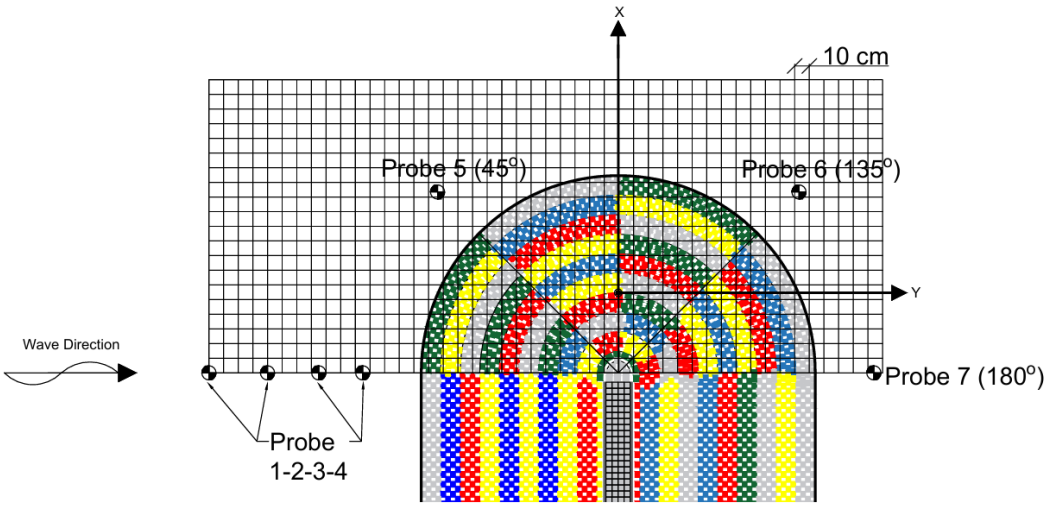

Figure 3.29 Grid spacing and probe locations

Diffraction occurs at roundhead and changes the velocities at roundhead. The wave ray concept may make it easier to explain this phenomenon. Water wave rays, in the context of wave theory, refer to the conceptual lines or paths that are perpendicular to wave crests and show the direction of wave energy propagation. These rays are useful in analyzing how water waves travel through different environments, especially when dealing with irregular coastlines, varying water depths, or other complex conditions. When wave rays become close to each other at the roundhead, velocity increases around the roundhead, generally between 70°

to 135° degrees. When waves pass the 3rd sector, distance between the rays increases and velocities decreases when compared to the 2nd and 3rd sector of the roundhead.

Required parameters for diffraction analysis are given below in Table 3.12 and Table 3.13 for both wind and swell wave conditions. The X distance refers to the distance along the direction of the breakwater, while the Y distance refers to the distance perpendicular to the direction of the breakwater. T_p and T_{m-1} are wave periods, and L_p and L_{m-1} are the wavelengths obtained from these periods. The X/L ratios are values derived from the ratios of these parameters.

Table 3.19 X/L ratios for wind wave conditions

Wind Wave							
	Probe 1	**Probe 2**	**Probe 3**	**Probe 4**	**Probe 5**	**Probe 6**	**Probe 7**
X (cm)	-54.62	-54.62	-54.62	-54.62	68.8	68.8	-54.62
Y (cm)	-279.5	-239.5	-204.5	-174.5	-123.4	123.42	174.54
T_{m-1} (s)	1.654	1.654	1.654	1.654	1.654	1.654	1.654
T_p (s)	1.724	1.724	1.724	1.724	1.724	1.724	1.724
L_{m-1} (m)	4.268	4.268	4.268	4.268	4.268	4.268	4.268
L_p (m)	4.637	4.637	4.637	4.637	4.637	4.637	4.637
X/L_{m-1}	-12.798	-12.798	-12.798	-12.798	16.121	16.121	-12.798
Y/L_{m-1}	-65.501	-56.128	-47.927	-40.898	-28.919	28.919	40.898
X/L_p	-11.780	-11.780	-11.780	-11.780	14.838	14.838	-11.780
Y/L_p	-60.290	-51.663	-44.114	-37.644	-26.619	26.619	37.644

Table 3.20 X/L ratios for swell wave conditions

Swell Wave							
	Probe 1	**Probe 2**	**Probe 3**	**Probe 4**	**Probe 5**	**Probe 6**	**Probe 7**
X (cm)	-54.62	-54.62	-54.62	-54.62	68.8	68.8	-54.62
Y (cm)	-279.54	-239.54	-204.54	-174.54	-123.42	123.42	174.54
T_{m-1} (s)	2.406	2.406	2.406	2.406	2.406	2.406	2.406
T_p (s)	2.381	2.381	2.381	2.381	2.381	2.381	2.381
L_{m-1} (m)	9.031	9.031	9.031	9.031	9.031	9.031	9.031
L_p (m)	8.844	8.844	8.844	8.844	8.844	8.844	8.844
X/L_{m-1}	-6.048	-6.048	-6.048	-6.048	7.619	7.619	-6.048
Y/L_{m-1}	-30.955	-26.525	-22.650	-19.328	-13.667	13.667	19.328
X/L_p	-6.176	-6.176	-6.176	-6.176	7.779	7.779	-6.176
Y/L_p	-31.608	-27.085	-23.128	-19.736	-13.955	13.955	19.736

Table 3.21 Diffraction coefficient for wind wave conditions

$K_D = H_D/H_i$, H_D = Diffracted wave height, H_i = incoming wave height		
K_D-45º	**K_D-135º**	**K_D-180º**
0.911	0.673	0.337
1.018	0.736	0.417
1.079	0.735	0.444
1.073	0.748	0.449
1.060	0.766	0.456
1.054	0.787	0.469
1.037	0.803	0.475
1.040	0.828	0.494
1.041	0.834	0.493
1.032	0.835	0.487

Table 3.22 Diffraction coefficient for swell wave conditions

$K_D = H_D/H_i$, H_D = Diffracted wave height, H_i = incoming wave height		
K_D-45º	**K_D-135º**	**K_D-180º**
1.015	0.741	0.488
0.870	0.823	0.499
0.787	0.869	0.467
0.817	0.902	0.462
0.806	0.855	0.469
0.790	0.841	0.462
0.783	0.837	0.466
0.780	0.836	0.460
0.776	0.834	0.459
0.782	0.842	0.466

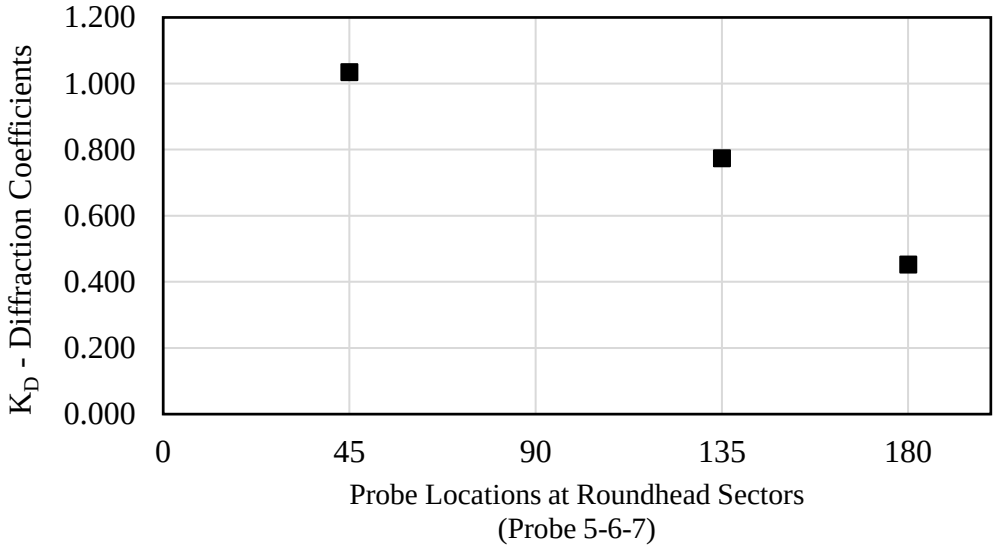

Figure 3.30 Diffraction values at roundhead - wind wave condition

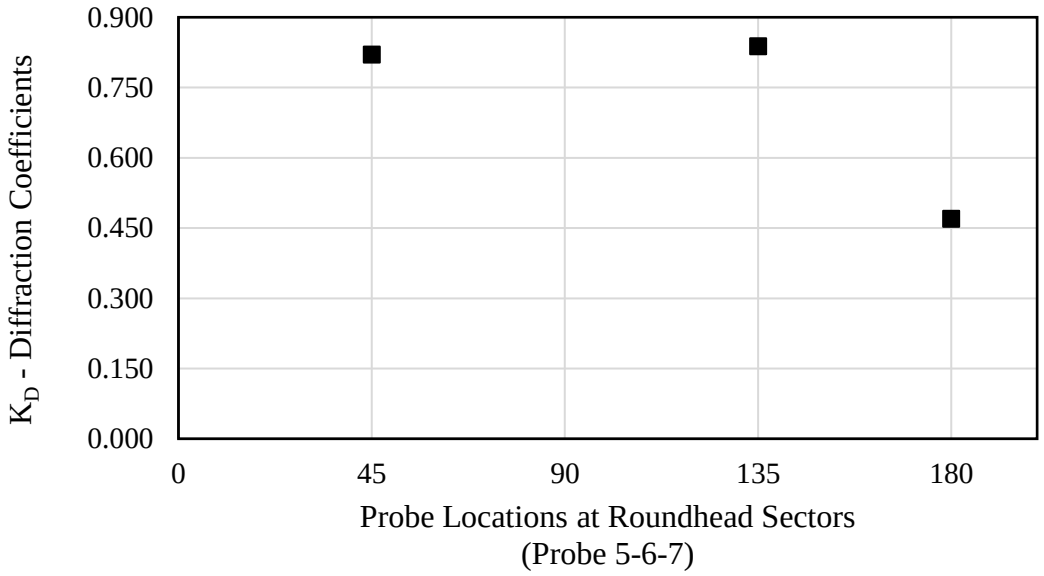

Figure 3.31 Diffraction values at roundhead - swell wave condition

4
EXPERIMENTAL RESULTS AND DISCUSSION

4.1 Experimental Results and Discussion

In this study, cube blocks made of heavy concrete with a density of 31.5 kN/m³ were placed in a single layer with 62% packing density. Their stability was tested under both wind waves with $s_{p,mean}$ = 0.034 and swell waves with $s_{p,mean}$ = 0.013. In the tests, movement ratios and stability were separately evaluated for each of the four 45-degree sectors of the roundhead using image recordings. Each test lasted 800-1440 seconds and 1450-2000 seconds for wind waves and swell waves, respectively.

4.2 Stability of Breakwater Roundheads with a Single Layer of High-Density Cube Armor Units

4.2.1 Wind Wave Conditions

After conducting a reflection analysis under wind wave conditions, the incoming wave conditions in front of the structure were determined and presented in Table 4.9. Irregular waves were generated in wind wave conditions, and 10 different wave series were generated in successively increasing wave conditions. Thus, the cumulative damage was determined.

It was determined that the moving cube blocks (M) started to mobilize in the second sector (WW3, H_{m0}=0.100) from the third wave onwards. The number of moving blocks, their damage ratios are given in Table 4.1 and Table 4.2, and their stability numbers and variations are also shown in Figure 4.1, Figure 4.2, Figure 4.3 and Figure 4.4. For the high-density blocks, only M1 type movement occured except in the fourth sector. The damage ratio of the blocks that moved in the second sector reached up to 16.7%. This ratio is 5.56% in the first sector, 1.92% in the third sector, and no movement was observed in the fourth sector. The initial movement occurred in the 2nd sector under WW3 wave condition, in the 1st sector under WW4 wave condition, and in the 3rd sector under WW8 wave condition. The stability numbers

at the start of movement in these sectors (2nd, 1st and 3rd) are 1.79, 1.93, and 2.42, respectively.

The damage ratios of the displaced cube blocks and their variations with the stability number are presented in Table 4.3 and Figure 4.6, Figure 4.7, Figure 4.8 and Figure 4.9 respectively. No displacement was observed in the entire cross-section of the breakwater roundhead single-layer high-density. This indicates that the high-density blocks placed in a single layer with 0.62 packing density remained stable, and no damage was observed.

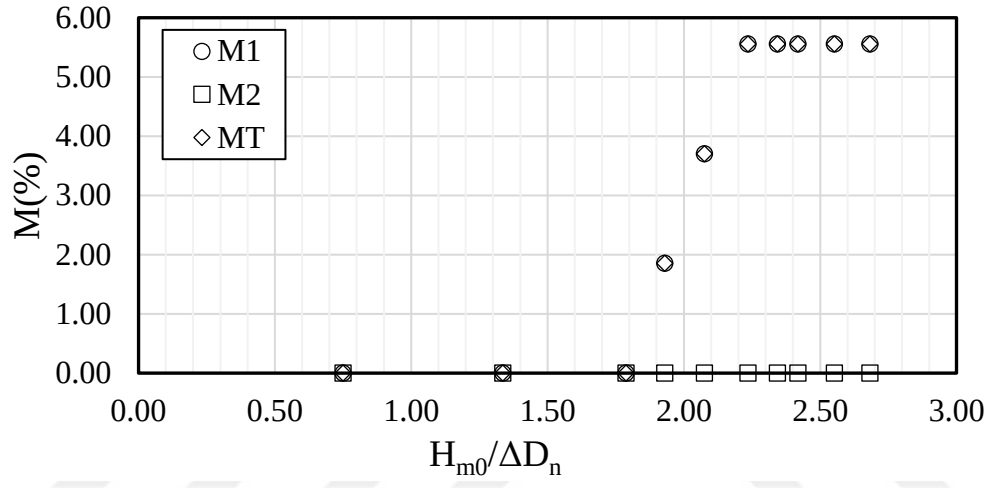

Figure 4.1 Movement ratios for 1st sector in reference area

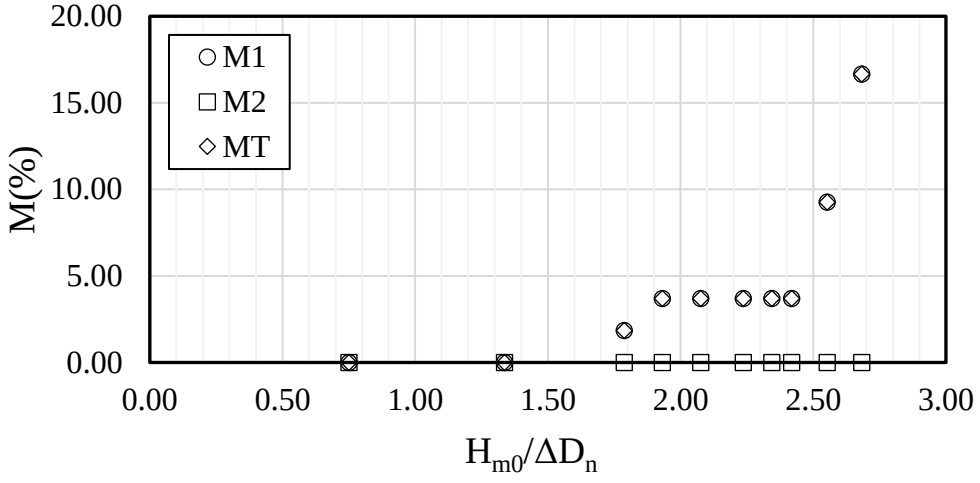

Figure 4.2 Movement ratios for 2nd sector in reference area

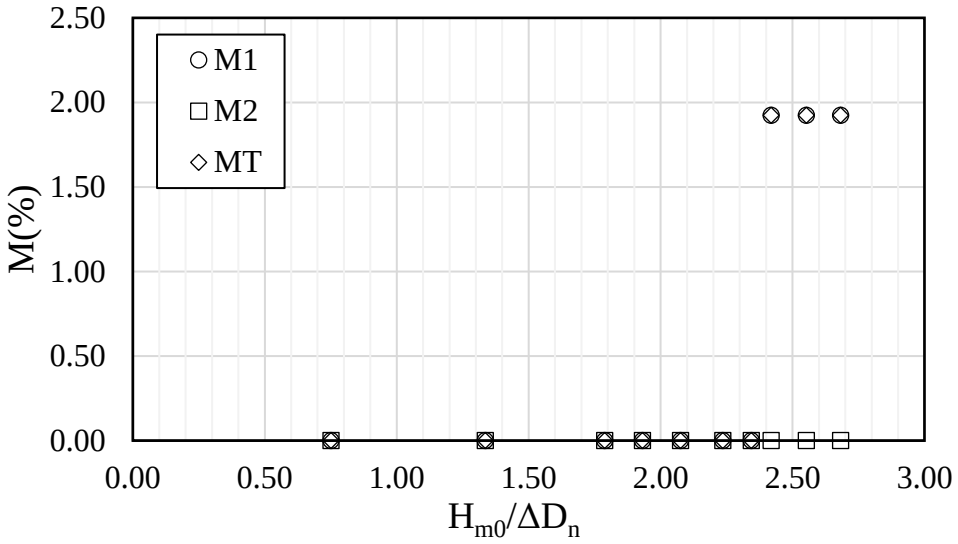

Figure 4.3 Movement ratios for 3rd sector in reference area

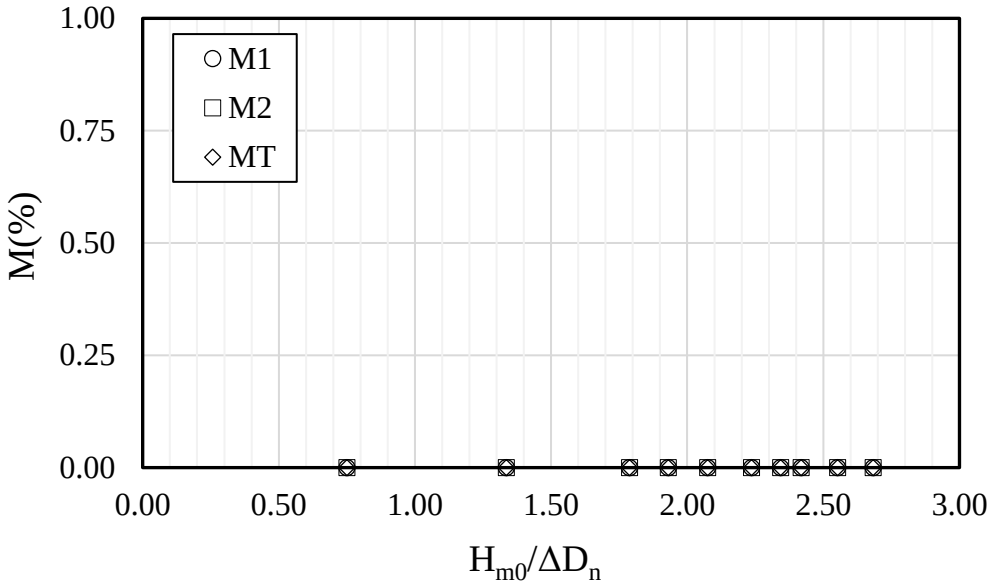

Figure 4.4 Movement ratios for 4th sector in reference area

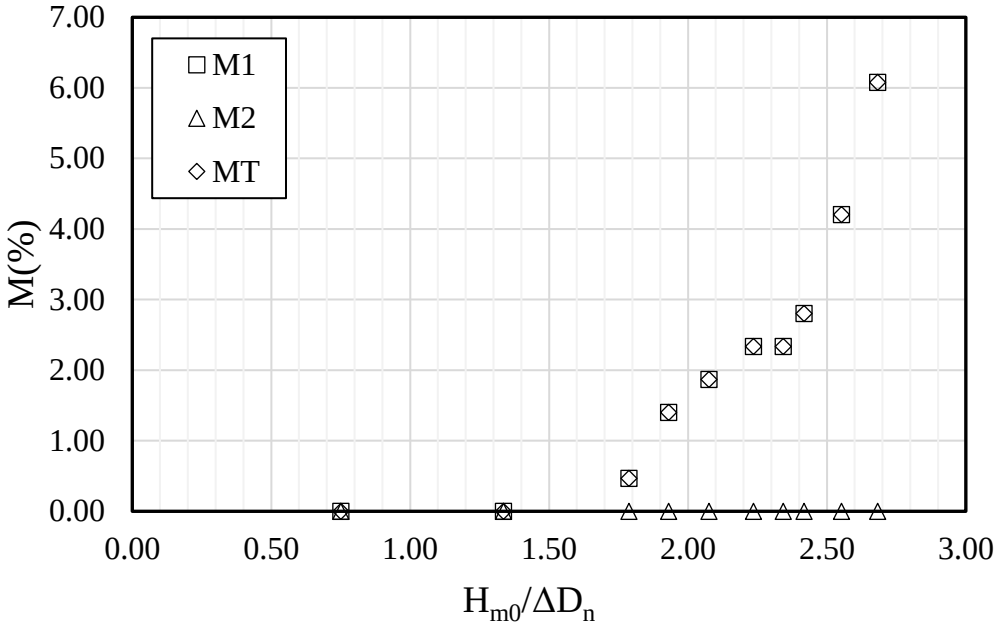

Figure 4.5 Movement ratios for all roundhead section in reference area

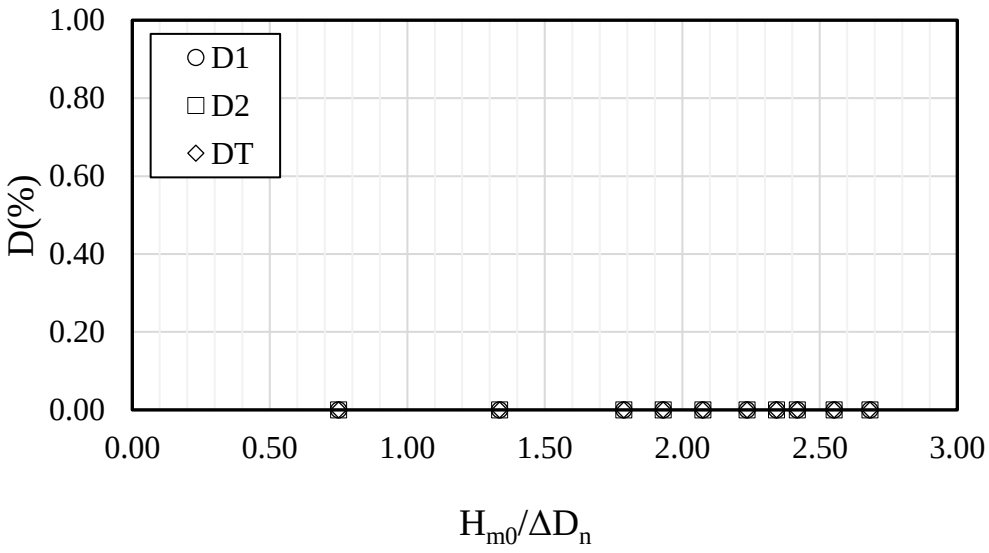

Figure 4.6 Displacement ratios for 1st sector in reference area

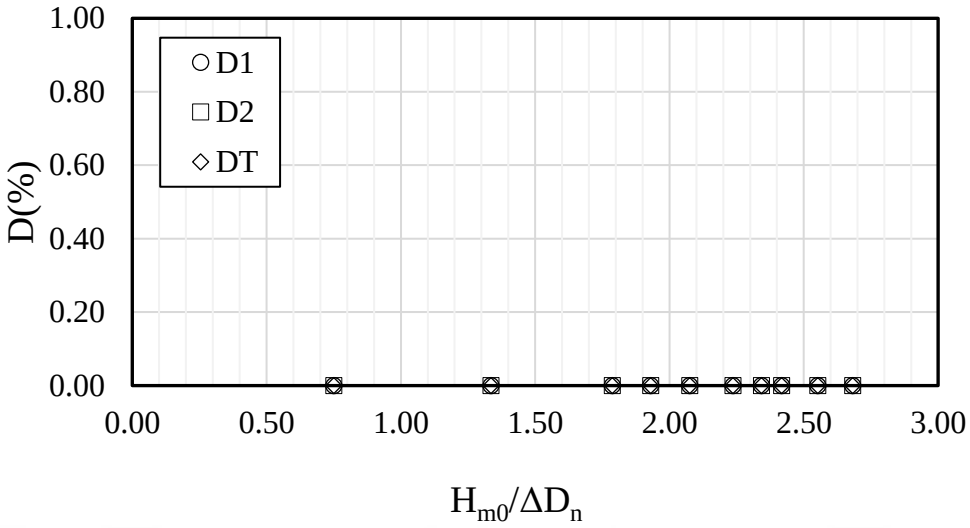

Figure 4.7 Displacement ratios for 2nd sector in reference area

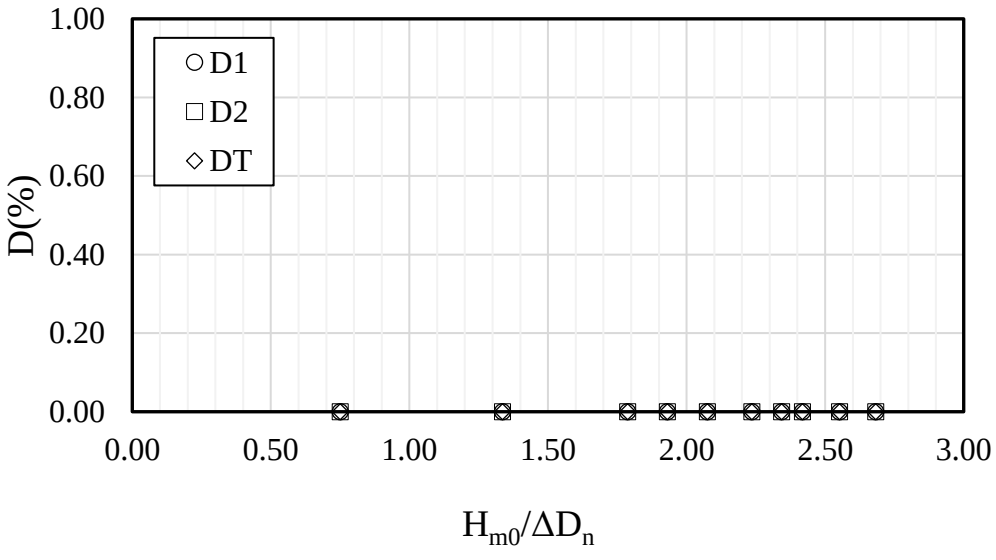

Figure 4.8 Displacement ratios for 3rd sector in reference area

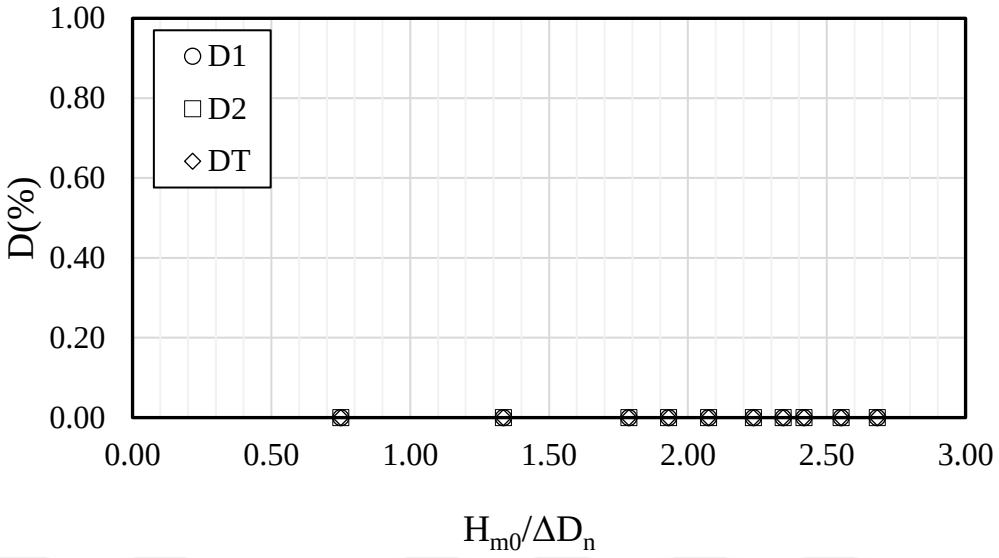

Figure 4.9 Displacement ratios for 4th sector in reference area

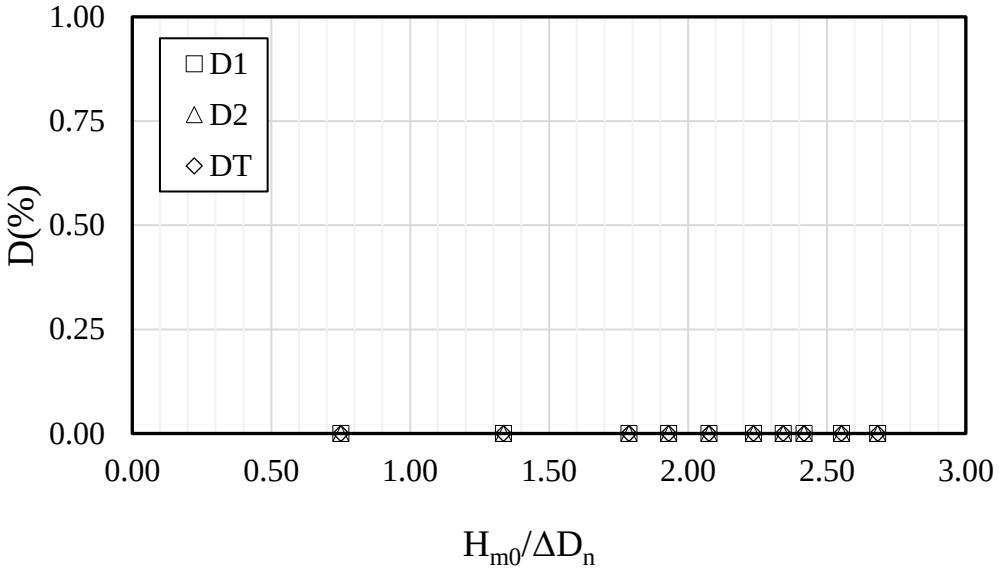

Figure 4.10 Displacement ratios for all roundhead section in reference area

Table 4.1 Quantity and movement ratios of blocks moving in the reference area

Wind wave, Water depth d=60 cm												
Movement Ratio for Blocks Moving in the Reference Area												
	1st Sector (0°- 45°)						**2nd Sector (45°-90°)**					
	M_1 (Quantity)	**M_1 (%)**	**M_2 (Quantity)**	**M_2 (%)**	**M_T (Quantity)**	**Mov. Ratio (%)**	**M_1 (Quantity)**	**M_1 (%)**	**M_2 (Quantity)**	**M_2 (%)**	**M_T (Quantity)**	**Mov. Ratio (%)**
WW1	0	0.00	0	0.00	0	0.00	0	0.00	0	0.00	0	0.00
WW2	0	0.00	0	0.00	0	0.00	0	0.00	0	0.00	0	0.00
WW3	0	0.00	0	0.00	0	0.00	1	1.85	0	0.00	1	1.85
WW4	1	1.85	0	0.00	1	1.85	2	3.70	0	0.00	2	3.70
WW5	2	3.70	0	0.00	2	3.70	2	3.70	0	0.00	2	3.70
WW6	3	5.56	0	0.00	3	5.56	2	3.70	0	0.00	2	3.70
WW7	3	5.56	0	0.00	3	5.56	2	3.70	0	0.00	2	3.70
WW8	3	5.56	0	0.00	3	5.56	2	3.70	0	0.00	2	3.70
WW9	3	5.56	0	0.00	3	5.56	5	9.26	0	0.00	5	9.26
WW10	3	5.56	0	0.00	3	5.56	9	16.67	0	0.00	9	16.67

Table 4.1 Quantity and movement ratios of blocks moving in the reference area (cont.)

Wind Wave, Water Depth d=60 cm												
Movement Ratio for Blocks Moving in the Reference Area												
	3rd Sector (90°-135°)						**4th Sector (135°-180°)**					
	M_1 (Quantity)	**M_1 (%)**	**M_2 (Quantity)**	**M_2 (%)**	**M_T (Quantity)**	**Mov. Ratio (%)**	**M_1 (Quantity)**	**M_1 (%)**	**M_2 (Quantity)**	**M_2 (%)**	**M_T (Quantity)**	**Mov. Ratio (%)**
WW1	0	0.00	0	0.00	0	0.00	0	0.00	0	0.00	0	0.00
WW2	0	0.00	0	0.00	0	0.00	0	0.00	0	0.00	0	0.00
WW3	0	0.00	0	0.00	0	0.00	0	0.00	0	0.00	0	0.00
WW4	0	0.00	0	0.00	0	0.00	0	0.00	0	0.00	0	0.00
WW5	0	0.00	0	0.00	0	0.00	0	0.00	0	0.00	0	0.00
WW6	0	0.00	0	0.00	0	0.00	0	0.00	0	0.00	0	0.00
WW7	0	0.00	0	0.00	0	0.00	0	0.00	0	0.00	0	0.00
WW8	1	1.92	0	0.00	1	1.92	0	0.00	0	0.00	0	0.00
WW9	1	1.92	0	0.00	1	1.92	0	0.00	0	0.00	0	0.00
WW10	1	1.92	0	0.00	1	1.92	0	0.00	0	0.00	0	0.00

Table 4.2 Movement ratio and stability numbers for blocks moving in the reference area

1st Sector (0°-45°)				2nd Sector (45°-90°)			
Ns	**M_T (%)**	**M_1 (%)**	**M_2 (%)**	**Ns**	**M_T (%)**	**M_1 (%)**	**M_2 (%)**
0.750	0.000	0.000	0.000	0.750	0.000	0.000	0.000
1.336	0.000	0.000	0.000	1.336	0.000	0.000	0.000
1.788	0.000	0.000	0.000	1.788	1.852	1.852	0.000
1.930	1.852	1.852	0.000	1.930	3.704	3.704	0.000
2.075	3.704	3.704	0.000	2.075	3.704	3.704	0.000
2.236	5.556	5.556	0.000	2.236	3.704	3.704	0.000
2.343	5.556	5.556	0.000	2.343	3.704	3.704	0.000
2.418	5.556	5.556	0.000	2.418	3.704	3.704	0.000
2.552	5.556	5.556	0.000	2.552	9.259	9.259	0.000
2.682	5.556	5.556	0.000	2.682	16.667	16.667	0.000

Table 4.2 Movement ratio and stability numbers for blocks moving in the reference area (cont.)

3rd Sector (90°-135°)				4th Sector (135°-180°)			
Ns	**M_T (%)**	**M_1 (%)**	**M_2 (%)**	**Ns**	**M_T (%)**	**M_1 (%)**	**M_2 (%)**
0.750	0.000	0.000	0.000	0.750	0.000	0.000	0.000
1.336	0.000	0.000	0.000	1.336	0.000	0.000	0.000
1.788	0.000	0.000	0.000	1.788	0.000	0.000	0.000
1.930	0.000	0.000	0.000	1.930	0.000	0.000	0.000
2.075	0.000	0.000	0.000	2.075	0.000	0.000	0.000
2.236	0.000	0.000	0.000	2.236	0.000	0.000	0.000
2.343	0.000	0.000	0.000	2.343	0.000	0.000	0.000
2.418	1.923	1.923	0.000	2.418	0.000	0.000	0.000
2.552	1.923	1.923	0.000	2.552	0.000	0.000	0.000
2.682	1.923	1.923	0.000	2.682	0.000	0.000	0.000

Table 4.3 Quantity and damage ratio of blocks displacing in the reference area

Wind Wave, Water Depth d=60 cm												
Damage Ratio for Displaced Blocks in the Reference Area												
	1st Sector (0°-45°)						**2nd Sector (45°-90°)**					
	D_1 (Quantity)	**D_1 (%)**	**D_2 (Quantity)**	**D_2 (%)**	**D_T (Quantity)**	**Damage Ratio (%)**	**D_1 (Quantity)**	**D_1 (%)**	**D_2 (Quantity)**	**D_2 (%)**	**D_T (Quantity)**	**Damage Ratio (%)**
WW1	0	0.00	0	0.00	0	0.00	0	0.00	0	0.00	0	0.00
WW2	0	0.00	0	0.00	0	0.00	0	0.00	0	0.00	0	0.00
WW3	0	0.00	0	0.00	0	0.00	0	0.00	0	0.00	0	0.00
WW4	0	0.00	0	0.00	0	0.00	0	0.00	0	0.00	0	0.00
WW5	0	0.00	0	0.00	0	0.00	0	0.00	0	0.00	0	0.00
WW6	0	0.00	0	0.00	0	0.00	0	0.00	0	0.00	0	0.00
WW7	0	0.00	0	0.00	0	0.00	0	0.00	0	0.00	0	0.00
WW8	0	0.00	0	0.00	0	0.00	0	0.00	0	0.00	0	0.00
WW9	0	0.00	0	0.00	0	0.00	0	0.00	0	0.00	0	0.00
WW10	0	0.00	0	0.00	0	0.00	0	0.00	0	0.00	0	0.00

Table 4.3 Quantity and damage ratio of blocks displacing in the reference area (cont.)

Wind Wave, Water Depth d=60 cm												
Damage Ratio for Displaced Blocks in the Reference Area												
	3rd Sector (90°-135°)						**4th Sector (135°-180°)**					
	D_1 (Quantity)	**D_1 (%)**	**D_2 (Quantity)**	**D_2 (%)**	**D_T (Quantity)**	**Damage Ratio (%)**	**D_1 (Quantity)**	**D_1 (%)**	**D_2 (Quantity)**	**D_2 (%)**	**D_T (Quantity)**	**Damage Ratio (%)**
WW1	0	0.00	0	0.00	0	0.00	0	0.00	0	0.00	0	0.00
WW2	0	0.00	0	0.00	0	0.00	0	0.00	0	0.00	0	0.00
WW3	0	0.00	0	0.00	0	0.00	0	0.00	0	0.00	0	0.00
WW4	0	0.00	0	0.00	0	0.00	0	0.00	0	0.00	0	0.00
WW5	0	0.00	0	0.00	0	0.00	0	0.00	0	0.00	0	0.00
WW6	0	0.00	0	0.00	0	0.00	0	0.00	0	0.00	0	0.00
WW7	0	0.00	0	0.00	0	0.00	0	0.00	0	0.00	0	0.00
WW8	0	0.00	0	0.00	0	0.00	0	0.00	0	0.00	0	0.00
WW9	0	0.00	0	0.00	0	0.00	0	0.00	0	0.00	0	0.00
WW10	0	0.00	0	0.00	0	0.00	0	0.00	0	0.00	0	0.00

Table 4.4 Damage ratio and stability numbers for blocks displaced in the reference area

1st Sector (0°-45°)				2nd Sector (45°-90°)			
N_s	D_T (%)	D_1 (%)	D_2 (%)	N_s	D_T (%)	D_1 (%)	D_2 (%)
0.750	0.000	0.000	0.000	0.750	0.000	0.000	0.000
1.336	0.000	0.000	0.000	1.336	0.000	0.000	0.000
1.788	0.000	0.000	0.000	1.788	0.000	0.000	0.000
1.930	0.000	0.000	0.000	1.930	0.000	0.000	0.000
2.075	0.000	0.000	0.000	2.075	0.000	0.000	0.000
2.236	0.000	0.000	0.000	2.236	0.000	0.000	0.000
2.343	0.000	0.000	0.000	2.343	0.000	0.000	0.000
2.418	0.000	0.000	0.000	2.418	0.000	0.000	0.000
2.552	0.000	0.000	0.000	2.552	0.000	0.000	0.000
2.682	0.000	0.000	0.000	2.682	0.000	0.000	0.000

Table 4.4 Damage ratio and stability numbers for blocks displaced in the reference area (cont.)

3rd Sector (90°-135°)				4th Sector (135°-180°)			
N_s	D_T (%)	D_1 (%)	D_2 (%)	N_s	D_T (%)	D_1 (%)	D_2 (%)
0.750	0.000	0.000	0.000	0.750	0.000	0.000	0.000
1.336	0.000	0.000	0.000	1.336	0.000	0.000	0.000
1.788	0.000	0.000	0.000	1.788	0.000	0.000	0.000
1.930	0.000	0.000	0.000	1.930	0.000	0.000	0.000
2.075	0.000	0.000	0.000	2.075	0.000	0.000	0.000
2.236	0.000	0.000	0.000	2.236	0.000	0.000	0.000
2.343	0.000	0.000	0.000	2.343	0.000	0.000	0.000
2.418	0.000	0.000	0.000	2.418	0.000	0.000	0.000
2.552	0.000	0.000	0.000	2.552	0.000	0.000	0.000
2.682	0.000	0.000	0.000	2.682	0.000	0.000	0.000

4.2.2 Swell Wave Conditions

With the reflection analysis of swell waves, the incident wave conditions in front of the structure were determined and are presented in Table 4.10. Irregular waves were generated in swell conditions, and 10 different wave series were generated in successively increasing wave conditions. Thus, the cumulative damage was determined.

In swell wave conditions, movement started in the first and second sectors (SW2) and was later seen in the third and fourth sectors. The most movement occurred in the third sector. The number of moving blocks, their movement ratios, are provided in Tables 4.5 and 4.6, and their variations with respect to the stability number are shown in Figures 4.11, 4.12, 4.13 and 4.14 for each sector. Movement occurred in the fourth sector under swell conditions, as opposed to wind wave conditions for high-density blocks. The most significant movement occurred in the third sector and started with the SW4 wave. In the third sector, both M1 and M2 type movements were observed. After the first and second sectors, movement occurred in the third and fourth sectors as the wave energy increased. Damage ratios were determined to be 7.41% in the second sector and 21% in the third sector. Movement started earlier compared to wind waves. It was observed that only in the third sector, the damage ratio was higher compared to wind waves.

The damage ratios of the displaced cube blocks and their variations with respect to the stability number are presented in Table 4.7 and Table 4.8, respectively. No displacement occurred throughout the entire head section where high-density blocks were placed in a single layer. This indicates that the high-density blocks, placed in a single layer with a packing density of 0.62, remained stable, without any damage.

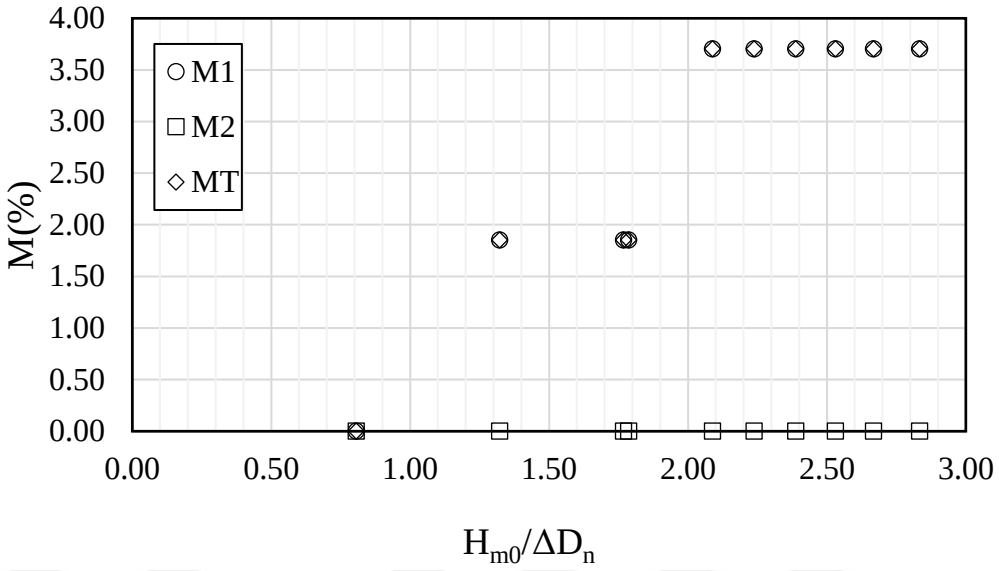

Figure 4.11 Movement ratios for 1st sector in reference area

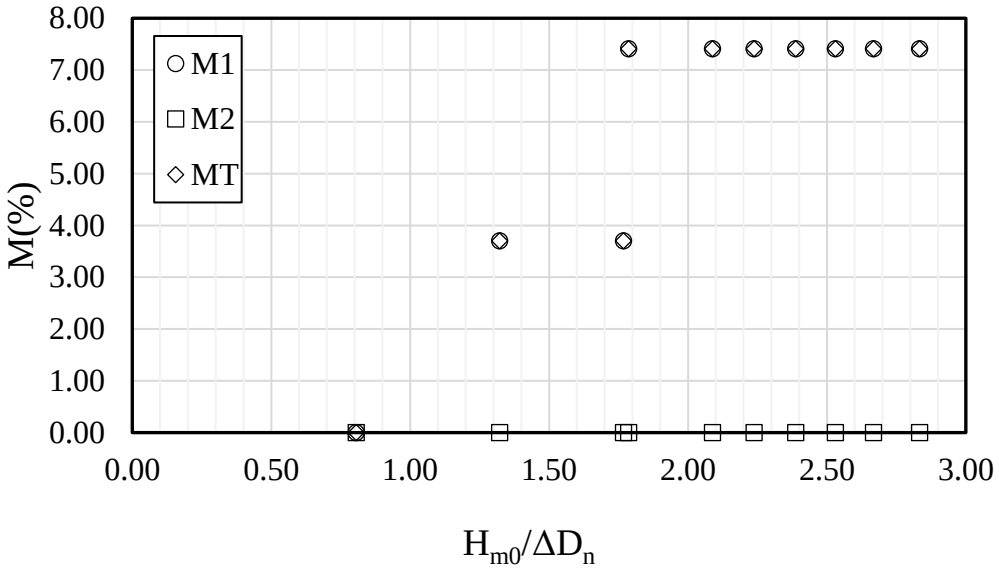

Figure 4.12 Movement ratios for 2nd sector in reference area

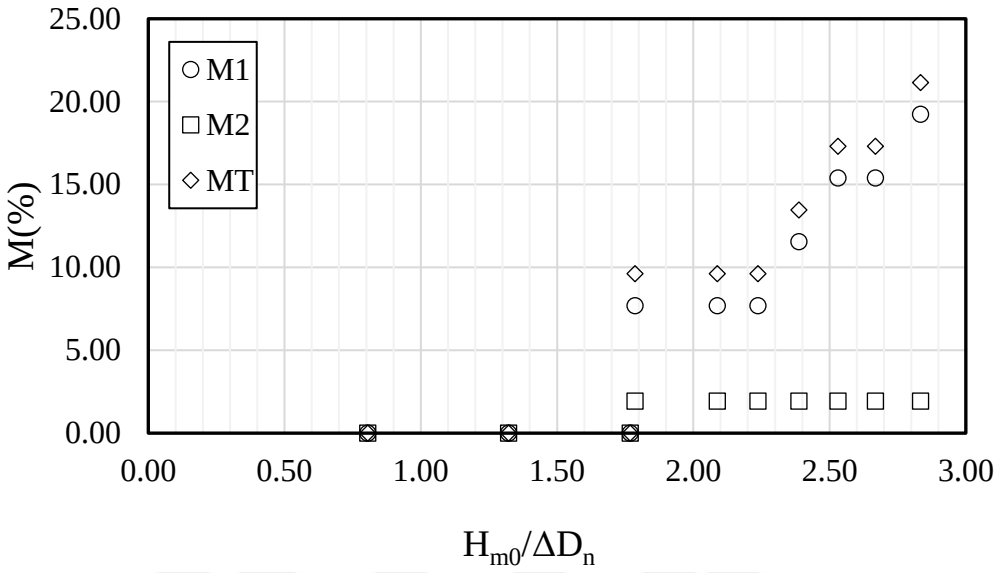

Figure 4.13 Movement ratios for 3rd sector in reference area

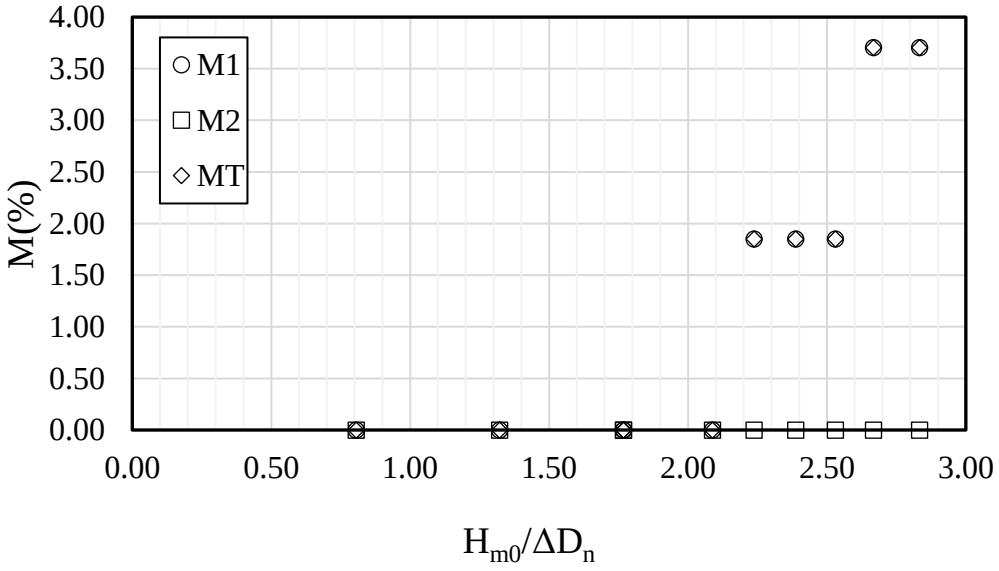

Figure 4.14 Movement ratios for 4th sector in reference area

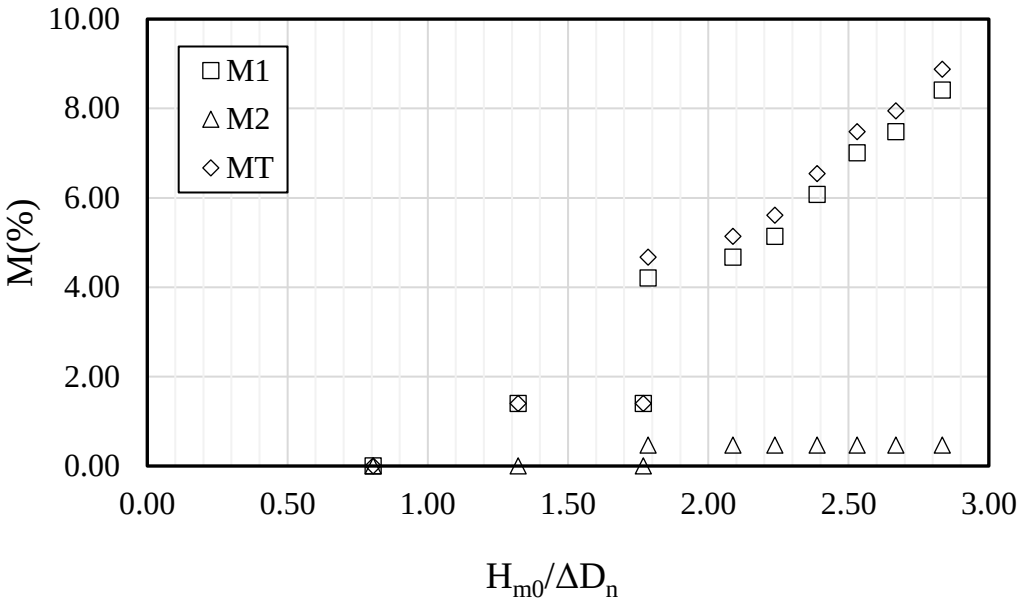

Figure 4.15 Movement ratios for all roundhead section in reference area

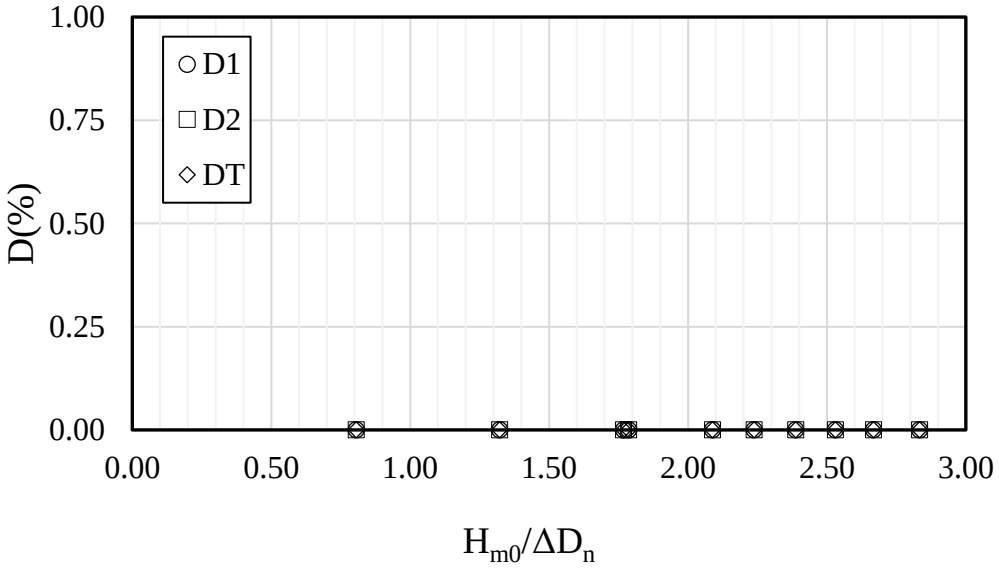

Figure 4.16 Displacement ratios for 1st sector in reference area

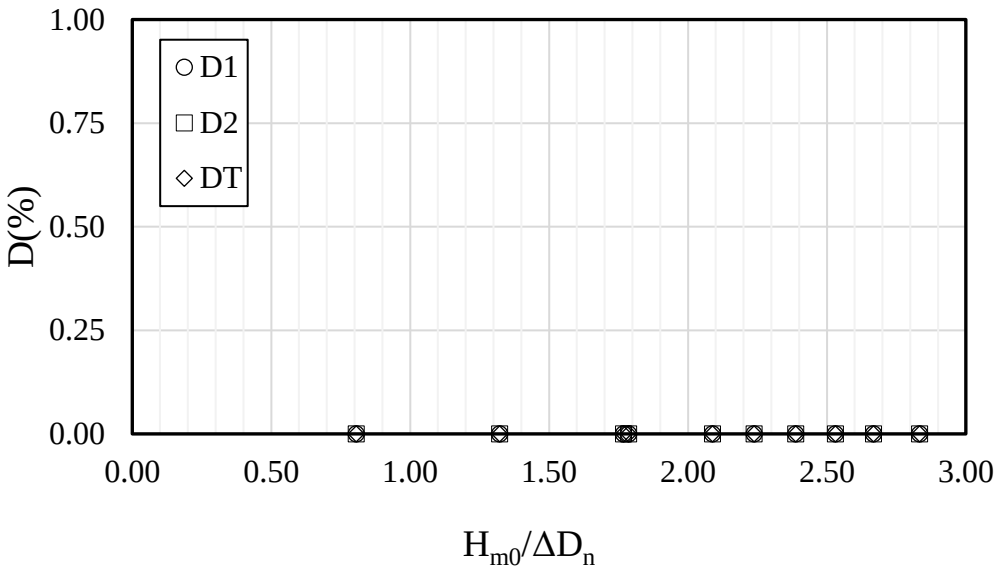

Figure 4.17 Displacement ratios for 2nd sector in reference area

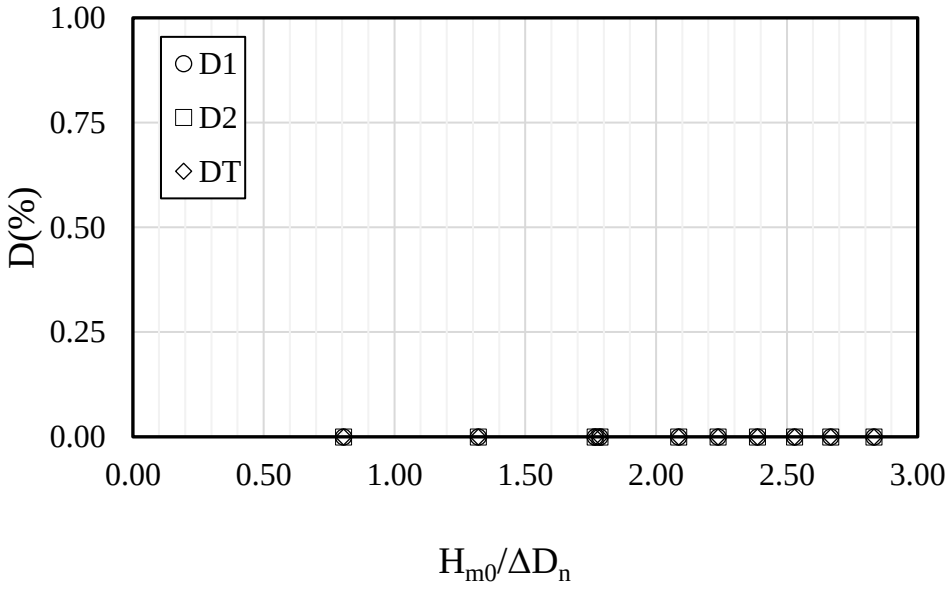

Figure 4.18 Displacement ratios for 3rd sector in reference area

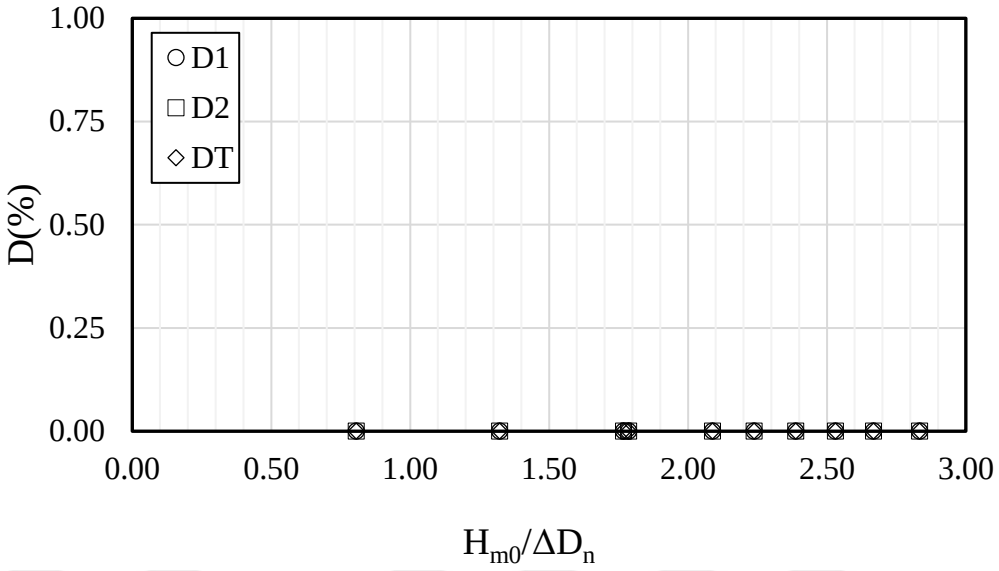

Figure 4.19 Displacement ratios for 4th sector in reference area

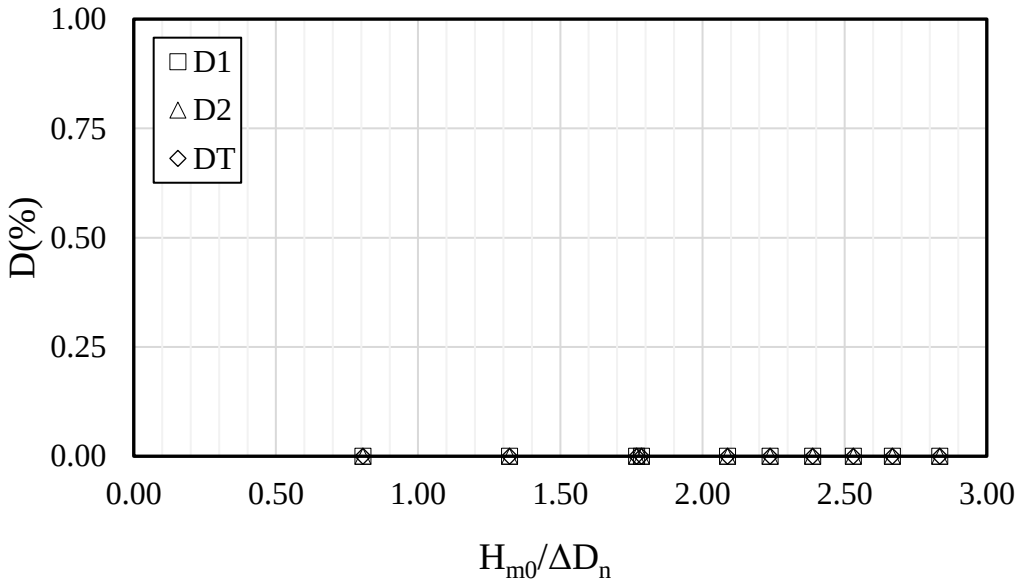

Figure 4.20 Displacement ratio for all roundhead section in reference area

Table 4.5 Quantity and movement ratio of blocks moving in the reference area

Swell Wave, Water Depth d=60 cm												
Movement Ratio for Blocks Moving in the Reference Area												
	1st Sector (0°-45°)						**2nd Sector (45°-90°)**					
	M_1 (Quantity)	**M_1 (%)**	**M_2 (Quantity)**	**M_2 (%)**	**M_T (Quantity)**	**Mov. Ratio (%)**	**M_1 (Quantity)**	**M_1 (%)**	**M_2 (Quantity)**	**M_2 (%)**	**M_T (Quantity)**	**Mov. Ratio (%)**
SW1	0	0.00	0	0.00	0	0.00	0	0.00	0	0.00	0	0.00
SW2	1	1.85	0	0.00	1	1.85	2	3.70	0	0.00	2	3.70
SW3	1	1.85	0	0.00	1	1.85	2	3.70	0	0.00	2	3.70
SW4	1	1.85	0	0.00	1	1.85	4	7.41	0	0.00	4	7.41
SW5	2	3.70	0	0.00	2	3.70	4	7.41	0	0.00	4	7.41
SW6	2	3.70	0	0.00	2	3.70	4	7.41	0	0.00	4	7.41
SW7	2	3.70	0	0.00	2	3.70	4	7.41	0	0.00	4	7.41
SW8	2	3.70	0	0.00	2	3.70	4	7.41	0	0.00	4	7.41
SW9	2	3.70	0	0.00	2	3.70	4	7.41	0	0.00	4	7.41
SW10	2	3.70	0	0.00	2	3.70	4	7.41	0	0.00	4	7.41

Table 4.5 Quantity and movement ratio of blocks moving in the reference area (cont.)

Swell Wave, Water Depth d=60 cm												
Movement Ratio for Blocks Moving in the Reference Area												
	3rd Sector (90°-135°)						**4th Sector (135°-180°)**					
	M_1 (Quantity)	**M_1 (%)**	**M_2 (Quantity)**	**M_2 (%)**	**M_T (Quantity)**	**Mov. Ratio (%)**	**M_1 (Quantity)**	**M_1 (%)**	**M_2 (Quantity)**	**M_2 (%)**	**M_T (Quantity)**	**Mov. Ratio (%)**
SW1	0	0.00	0	0.00	0	0.00	0	0.00	0	0.00	0	0.00
SW2	0	0.00	0	0.00	0	0.00	0	0.00	0	0.00	0	0.00
SW3	0	0.00	0	0.00	0	0.00	0	0.00	0	0.00	0	0.00
SW4	4	7.69	1	1.92	5	9.62	0	0.00	0	0.00	0	0.00
SW5	4	7.69	1	1.92	5	9.62	0	0.00	0	0.00	0	0.00
SW6	4	7.69	1	1.92	5	9.62	1	1.85	0	0.00	1	1.85
SW7	6	11.54	1	1.92	7	13.46	1	1.85	0	0.00	1	1.85
SW8	8	15.38	1	1.92	9	17.31	1	1.85	0	0.00	1	1.85
SW9	8	15.38	1	1.92	9	17.31	2	3.70	0	0.00	2	3.70
SW10	10	19.23	1	1.92	11	21.15	2	3.70	0	0.00	2	3.70

Table 4.6 Movement ratio and stability numbers for blocks moving in the reference area

1st Sector (0°-45°)				2nd Sector (45°-90°)			
N_s	M_T (%)	M_1 (%)	M_2 (%)	N_s	M_T (%)	M_1 (%)	M_2 (%)
0.805	0.000	0.000	0.000	0.805	0.000	0.000	0.000
1.321	1.852	1.852	0.000	1.321	3.704	3.704	0.000
1.768	1.852	1.852	0.000	1.768	3.704	3.704	0.000
1.786	1.852	1.852	0.000	1.786	7.407	7.407	0.000
2.088	3.704	3.704	0.000	2.088	7.407	7.407	0.000
2.238	3.704	3.704	0.000	2.238	7.407	7.407	0.000
2.388	3.704	3.704	0.000	2.388	7.407	7.407	0.000
2.530	3.704	3.704	0.000	2.530	7.407	7.407	0.000
2.668	3.704	3.704	0.000	2.668	7.407	7.407	0.000
2.834	3.704	3.704	0.000	2.834	7.407	7.407	0.000

Table 4.6 Movement ratio and stability numbers for blocks moving in the reference area (cont.)

3rd Sector (90°-135°)				4th Sector (135°-180°)			
N_s	M_T (%)	M_1 (%)	M_2 (%)	N_s	M_T (%)	M_1 (%)	M_2 (%)
0.805	0.000	0.000	0.000	0.805	0.000	0.000	0.000
1.321	0.000	0.000	0.000	1.321	0.000	0.000	0.000
1.768	0.000	0.000	0.000	1.768	0.000	0.000	0.000
1.786	9.615	7.692	1.923	1.786	0.000	0.000	0.000
2.088	9.615	7.692	1.923	2.088	0.000	0.000	0.000
2.238	9.615	7.692	1.923	2.238	1.852	1.852	0.000
2.388	13.462	11.538	1.923	2.388	1.852	1.852	0.000
2.530	17.308	15.385	1.923	2.530	1.852	1.852	0.000
2.668	17.308	15.385	1.923	2.668	3.704	3.704	0.000
2.834	21.154	19.231	1.923	2.834	3.704	3.704	0.000

Table 4.7 Quantity and damage ratio of blocks displacing in the reference area

Swell Wave, Water Depth d=60 cm												
Damage Ratio for Displaced Blocks in the Reference Area												
	1st Sector (0°-45°)						**2nd Sector (45°-90°)**					
	D_1 (Quantity)	**D_1 (%)**	**D_2 (Quantity)**	**D_2 (%)**	**D_T (Quantity)**	**Damage Ratio (%)**	**D_1 (Quantity)**	**D_1 (%)**	**D_2 (Quantity)**	**D_2 (%)**	**D_T (Quantity)**	**Damage Ratio (%)**
SW1	0	0.00	0	0.00	0	0.00	0	0.00	0	0.00	0	0.00
SW2	0	0.00	0	0.00	0	0.00	0	0.00	0	0.00	0	0.00
SW3	0	0.00	0	0.00	0	0.00	0	0.00	0	0.00	0	0.00
SW4	0	0.00	0	0.00	0	0.00	0	0.00	0	0.00	0	0.00
SW5	0	0.00	0	0.00	0	0.00	0	0.00	0	0.00	0	0.00
SW6	0	0.00	0	0.00	0	0.00	0	0.00	0	0.00	0	0.00
SW7	0	0.00	0	0.00	0	0.00	0	0.00	0	0.00	0	0.00
SW8	0	0.00	0	0.00	0	0.00	0	0.00	0	0.00	0	0.00
SW9	0	0.00	0	0.00	0	0.00	0	0.00	0	0.00	0	0.00
SW10	0	0.00	0	0.00	0	0.00	0	0.00	0	0.00	0	0.00

Table 4.7 Quantity and damage ratio of blocks displacing in the reference area (cont.)

Swell Wave, Water Depth d=60 cm												
Damage Ratio for Displaced Blocks in the Reference Area												
	3rd Sector (90°-135°)						**4th Sector (135°-180°)**					
	D_1 (Quantity)	**D_1 (%)**	**D_2 (Quantity)**	**D_2 (%)**	**D_T (Quantity)**	**Damage Ratio (%)**	**D_1 (Quantity)**	**D_1 (%)**	**D_2 (Quantity)**	**D_2 (%)**	**D_T (Quantity)**	**Damage Ratio (%)**
SW1	0	0.00	0	0.00	0	0.00	0	0.00	0	0.00	0	0.00
SW2	0	0.00	0	0.00	0	0.00	0	0.00	0	0.00	0	0.00
SW3	0	0.00	0	0.00	0	0.00	0	0.00	0	0.00	0	0.00
SW4	0	0.00	0	0.00	0	0.00	0	0.00	0	0.00	0	0.00
SW5	0	0.00	0	0.00	0	0.00	0	0.00	0	0.00	0	0.00
SW6	0	0.00	0	0.00	0	0.00	0	0.00	0	0.00	0	0.00
SW7	0	0.00	0	0.00	0	0.00	0	0.00	0	0.00	0	0.00
SW8	0	0.00	0	0.00	0	0.00	0	0.00	0	0.00	0	0.00
SW9	0	0.00	0	0.00	0	0.00	0	0.00	0	0.00	0	0.00
SW10	0	0.00	0	0.00	0	0.00	0	0.00	0	0.00	0	0.00

Table 4.8 Damage ratio and stability numbers for blocks displacing in the reference area

1st Sector (0°-45°)				2nd Sector (45°-90°)			
N_s	D_T (%)	D_1 (%)	D_2 (%)	N_s	D_T (%)	D_1 (%)	D_2 (%)
0.805	0.000	0.000	0.000	0.805	0.000	0.000	0.000
1.321	0.000	0.000	0.000	1.321	0.000	0.000	0.000
1.768	0.000	0.000	0.000	1.768	0.000	0.000	0.000
1.786	0.000	0.000	0.000	1.786	0.000	0.000	0.000
2.088	0.000	0.000	0.000	2.088	0.000	0.000	0.000
2.238	0.000	0.000	0.000	2.238	0.000	0.000	0.000
2.388	0.000	0.000	0.000	2.388	0.000	0.000	0.000
2.530	0.000	0.000	0.000	2.530	0.000	0.000	0.000
2.668	0.000	0.000	0.000	2.668	0.000	0.000	0.000
2.834	0.000	0.000	0.000	2.834	0.000	0.000	0.000

Table 4.8 Damage ratio and stability numbers for blocks displacing in the reference area (cont.)

3rd Sector (90°-135°)				4th Sector (135°-180°)			
N_s	D_T (%)	D_1 (%)	D_2 (%)	N_s	D_T (%)	D_1 (%)	D_2 (%)
0.805	0.000	0.000	0.000	0.805	0.000	0.000	0.000
1.321	0.000	0.000	0.000	1.321	0.000	0.000	0.000
1.768	0.000	0.000	0.000	1.768	0.000	0.000	0.000
1.786	0.000	0.000	0.000	1.786	0.000	0.000	0.000
2.088	0.000	0.000	0.000	2.088	0.000	0.000	0.000
2.238	0.000	0.000	0.000	2.238	0.000	0.000	0.000
2.388	0.000	0.000	0.000	2.388	0.000	0.000	0.000
2.530	0.000	0.000	0.000	2.530	0.000	0.000	0.000
2.668	0.000	0.000	0.000	2.668	0.000	0.000	0.000
2.834	0.000	0.000	0.000	2.834	0.000	0.000	0.000

Table 4.9 Wind wave conditions

	H_{m0} (m)	T_p (s)	N_s
WW1	0.042	0.962	0.750
WW2	0.075	1.191	1.336
WW3	0.100	1.429	1.788
WW4	0.108	1.471	1.930
WW5	0.116	1.563	2.075
WW6	0.125	1.613	2.236
WW7	0.131	1.667	2.343
WW8	0.135	1.724	2.418
WW9	0.143	1.724	2.552
WW10	0.150	1.724	2.682

Table 4.10 Swell wave conditions

	H_{m0} (m)	T_p (s)	N_s
SW1	0.045	1.724	0.805
SW2	0.074	2.273	1.321
SW3	0.099	2.632	1.768
SW4	0.100	2.632	1.786
SW5	0.117	2.381	2.088
SW6	0.125	2.381	2.238
SW7	0.134	2.381	2.388
SW8	0.142	2.381	2.530
SW9	0.149	2.381	2.668
SW10	0.159	2.381	2.834

4.3 Discussion

Overtopping were also evaluated in all experiments. Wave overtopping varied between 0.3% and 5.36% for wind waves and between 0.28% and 5.80% for swell waves.

No displacement occurred in high-density blocks. Only movement was observed, the variation of movement ratios with the stability number is presented in Figure 4.21 for both wind and swell waves together. As seen in Figure 4.21, movement in HD cube blocks begins earlier under swell wave conditions compared to wind wave conditions.

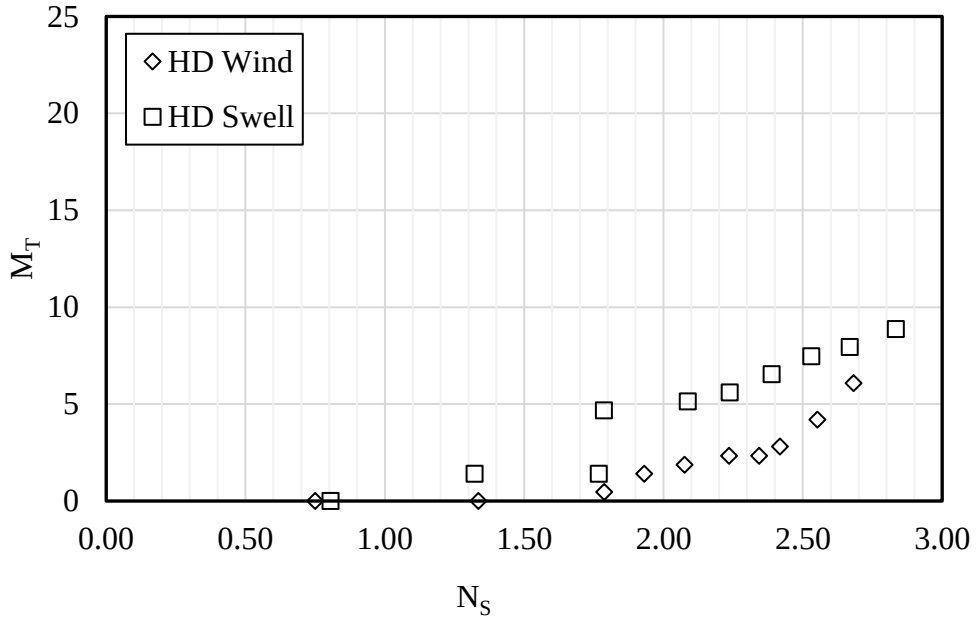

Figure 4.21 Movement ratios of all roundhead section of high-density blocks under wind and swell waves in reference area

In Figures 4.22 and 4.23, the movement rates of normal and high-density blocks in reference area are compared. The movement rates of HD cubes are significantly lower than those of ND cubes. Under the influence of wind waves, ND blocks reached a movement rate of 45% across the entire slope, while for HD blocks, this rate was only 6%. A similar trend is observed under the influence of swell waves, where the movement rate for ND blocks reached 36%, while for HD blocks, it only reached 9% across the entire slope.

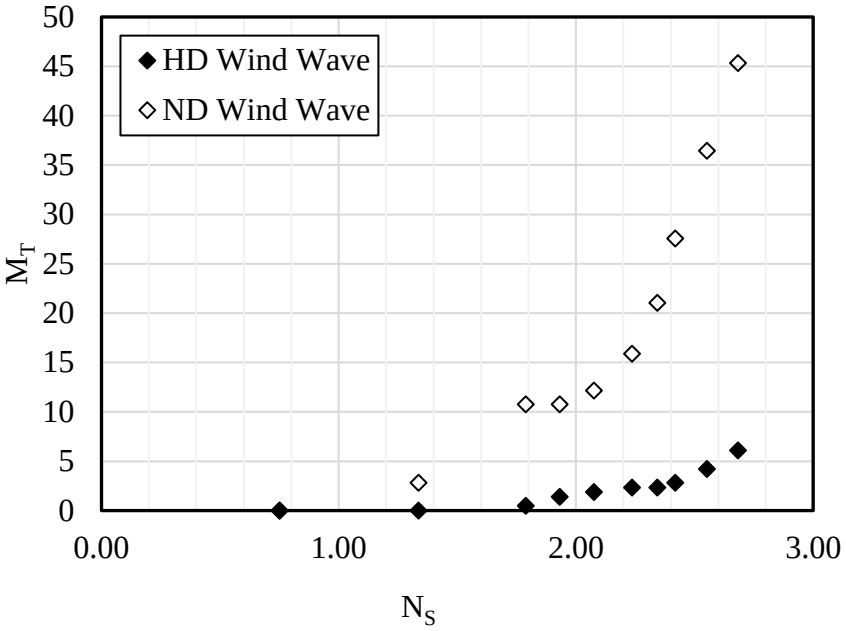

Figure 4.22 Movement ratios of ND and HD blocks under wind waves in reference area (Yuksel et al., 2024)

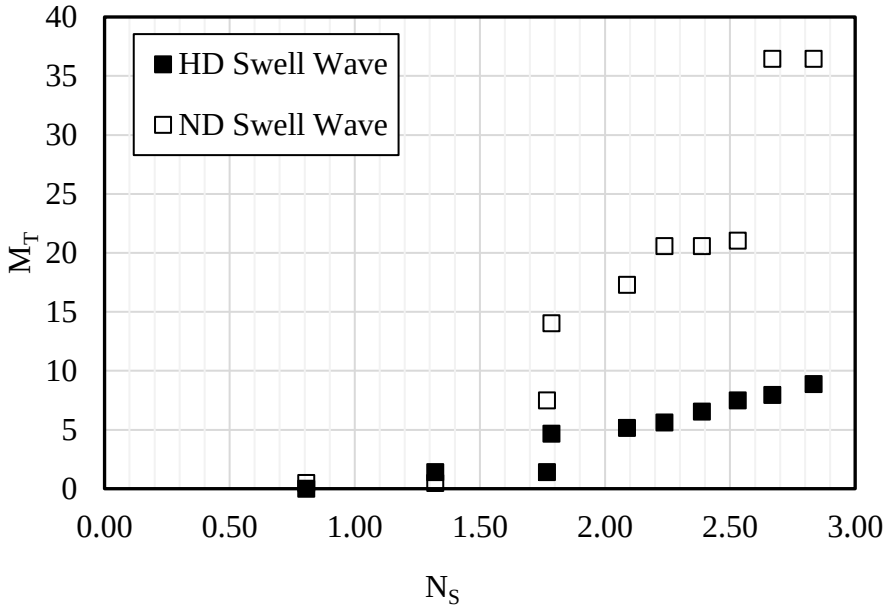

Figure 4.23 Movement ratios of ND and HD blocks under swell waves in reference area (Yuksel et al., 2024)

Yuksel et al. (2022) conducted stability tests under wind wave conditions by placing both normal and high-density cube blocks in a single layer on the trunk section with the same packing density. For HD cubes, no damage due to displacement was observed in the trunk section for wind and swell wave condition. However, damage occurred in the head section due to displacement in the normal-density cube blocks. Figure 4.24 shows the comparison of the moveing blocks in both the trunk and head sections. The movement rates of both normal and high-density blocks were larger in the head section, and the initiation of movement occurred earlier, which can be attributed to the three-dimensional flow structure around the head. The movement rate of normal and high-density blocks in the head section was four times greater than that in the trunk section.

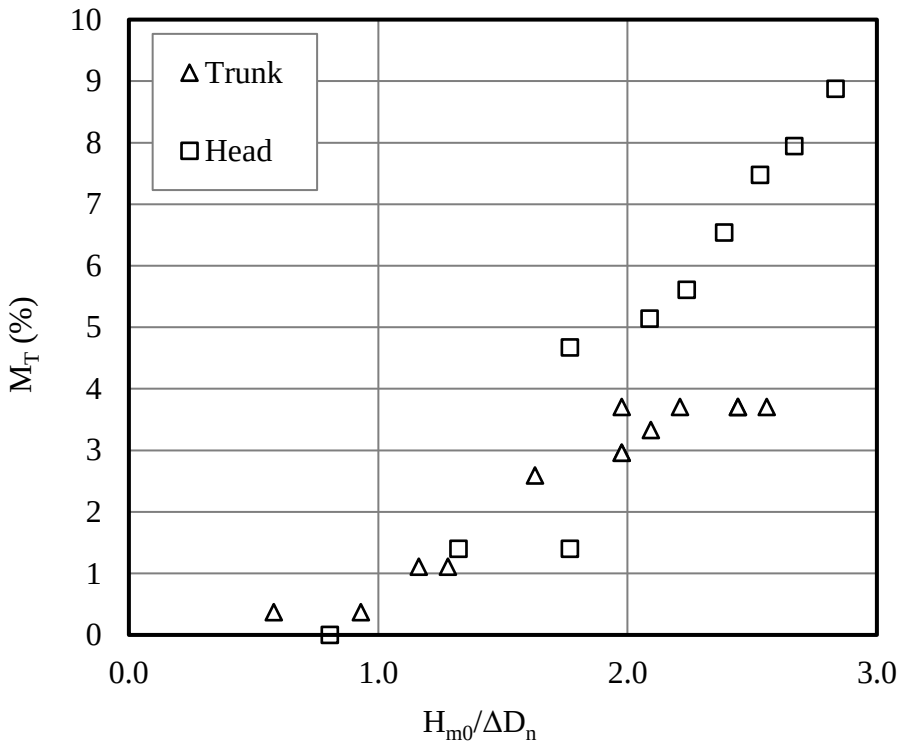

Figure 4.24 Movement ratios of trunk and roundhead with single-layer armor units of high density

In the figures below, comparison of the wind and swell waves in each sector; also, sectoral comparison of the four sectors for two different wave conditions (wind and swell) are shown in Figures 4.25, 4.26, 4.27 and 4.28

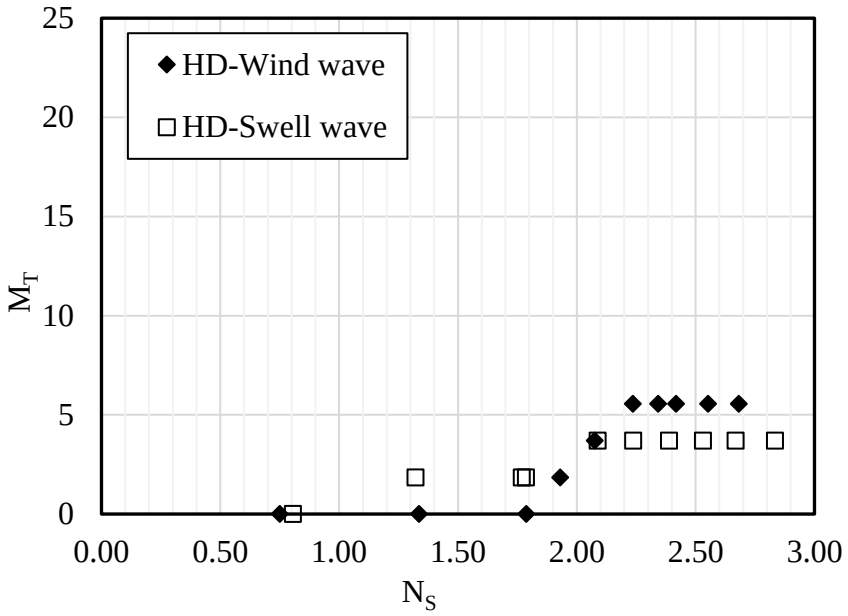

Figure 4.25 M_T versus N_s for wind and swell waves in 0°-45° degree in reference area

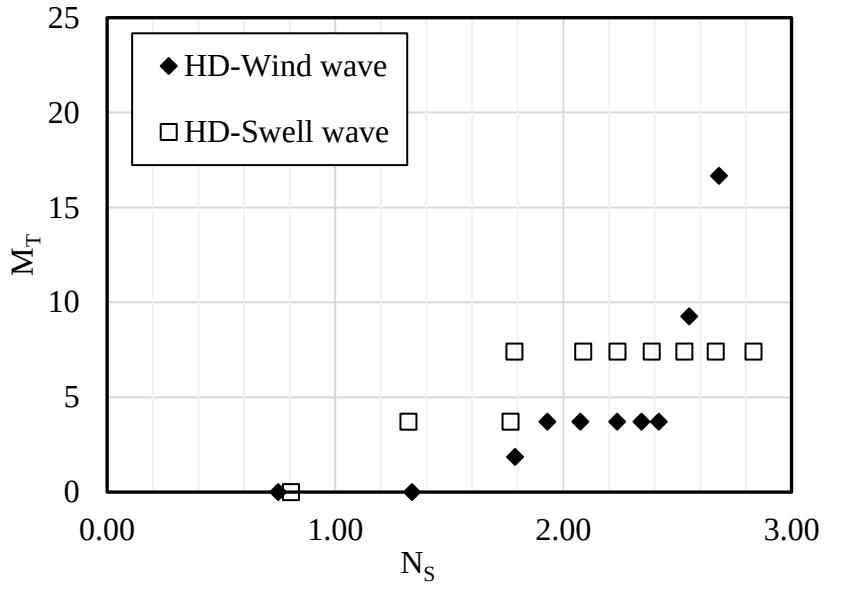

Figure 4.26 M_T versus N_s for wind and swell waves in 45°-90° degree in reference area

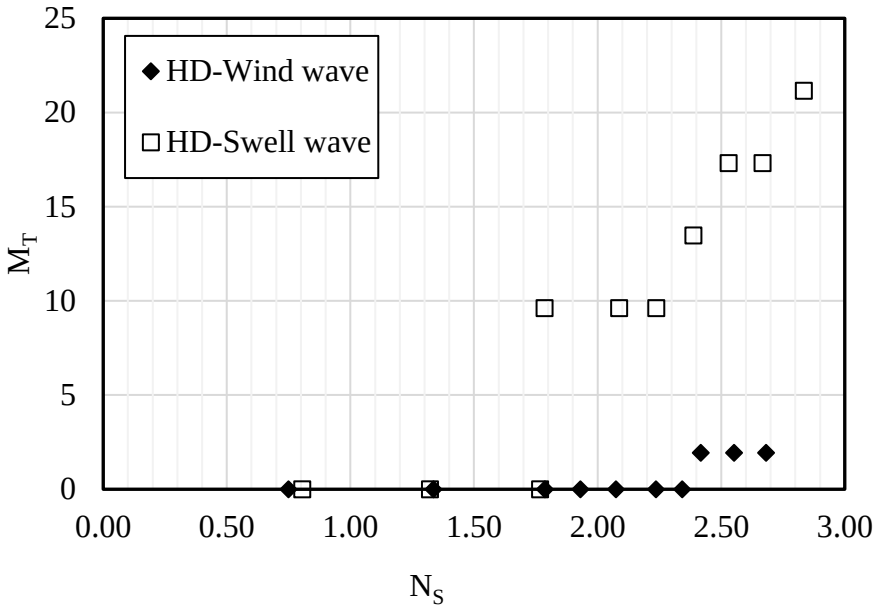

Figure 4.27 M_T versus N_s for wind and swell waves in 90°-135° degree in reference area

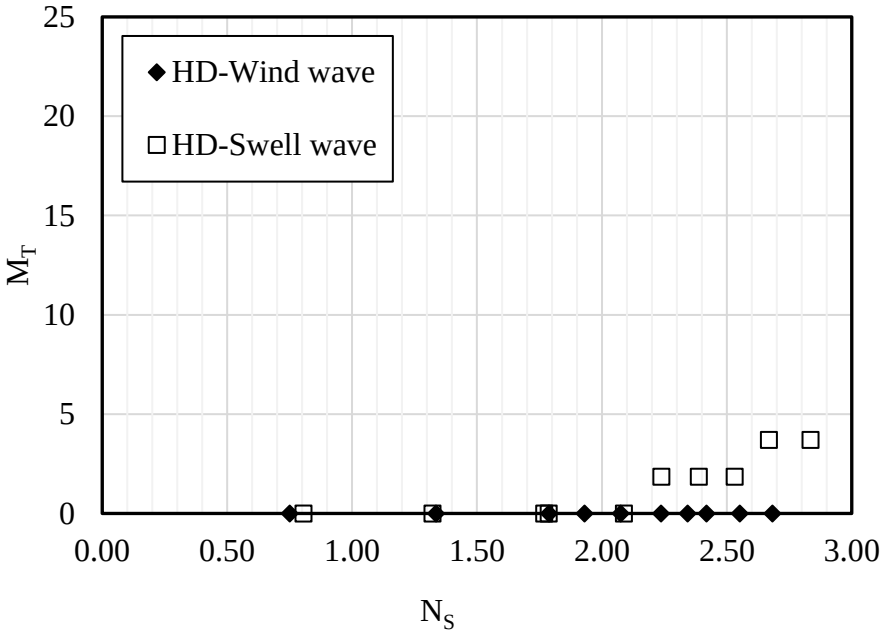

Figure 4.28 M_T versus N_s for wind and swell waves in 135°-180° degree in reference area

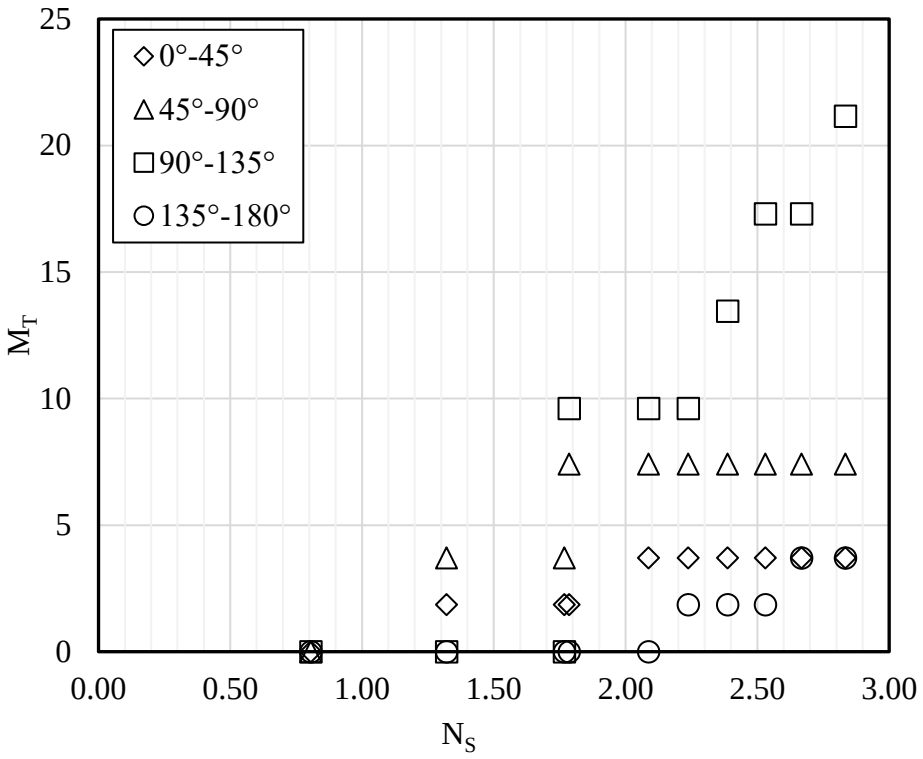

Figure 4.29 Sectoral comparison of M_T for swell waves in reference area

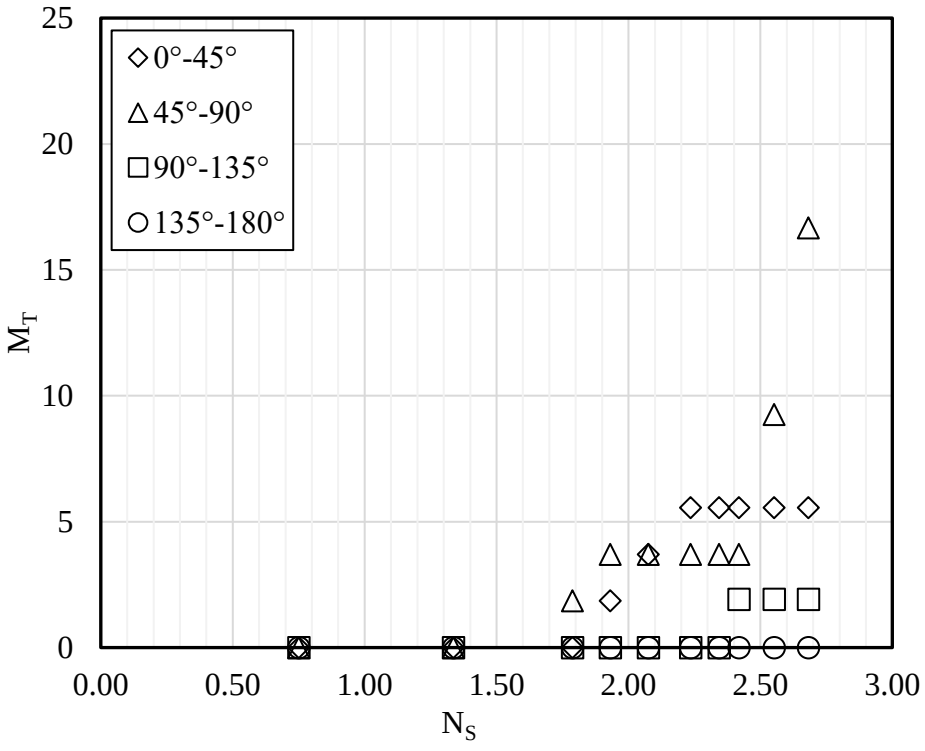

Figure 4.30 Sectoral comparison of M_T for wind waves in reference area

In Figure 4.31, the three-dimensional flow structure at the roundhead section is schematically illustrated under wind wave conditions.

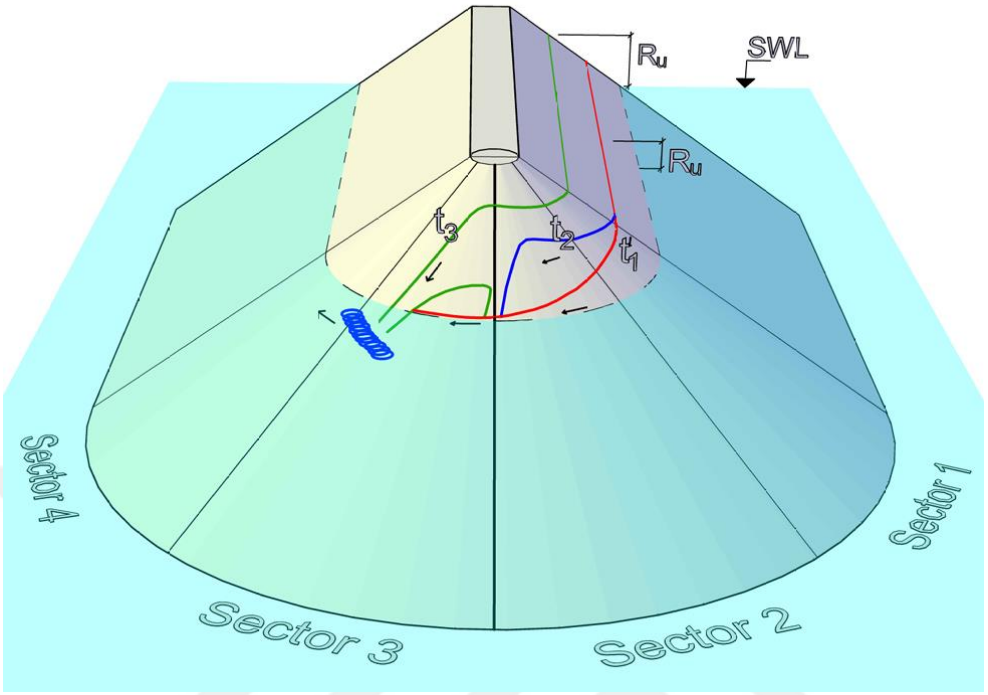

Figure 4.31 Three-dimensional flow structure under wind wave conditions

High-energetic waves initially run up (at time t1) and then diffract around the roundhead. Subsequently, the wave progressing around the roundhead (at time t2) begins to break in the second sector, and as it continues around the roundhead (at time t3), the plunging jet strikes the last segment at the end of the third sector. Therefore, high-energy waves particularly cause larger movement and displacement of blocks in the third sector. Breaking type can be calculated according to Formula 4.1.

$$\xi_0 = \frac{m}{\sqrt{\frac{H_{m0}}{L_{m-1,0}}}} \tag{4.1}$$

$$\xi_0 = \frac{m}{\sqrt{\frac{H_{m0}}{L_{m-1,0}}}} = \frac{0.667}{\sqrt{\frac{0.16}{4.14}}} = 3.39$$

It has been observed that plunging-type breaking occurs at the roundhead under wind wave conditions.

In Figure 4.32, the progression of swell waves along the roundhead section is schematically illustrated.

$$\xi_0 = \frac{m}{\sqrt{\frac{H_{m0}}{L_{m-1,0}}}} = \frac{0.667}{\sqrt{\frac{0.16}{9.022}}} = 5.00$$

Under these conditions, it has been observed that the waves break in a surging type. Swell waves with a larger period break further around the roundhead. High-energy waves, particularly under these conditions, break in the fourth sector in larger waves, leading to an increase in the rate of blocks that move and shift in this sector.

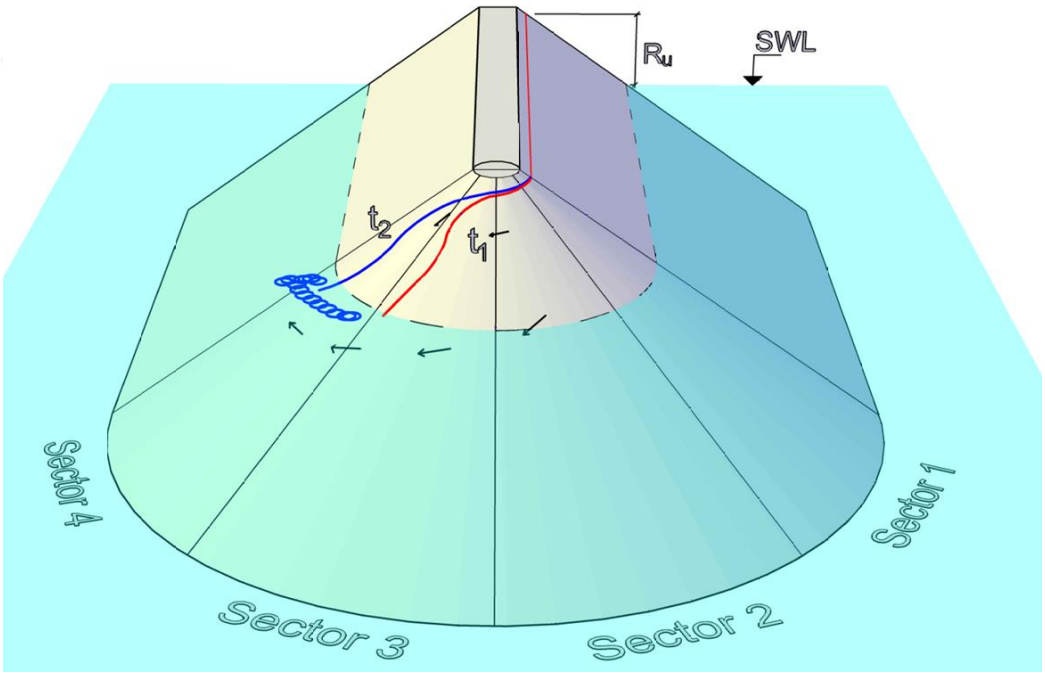

Figure 4.32 Three-dimensional flow structure under swell wave conditions

There is no displacement occurred in HD cubes, therefore, the stability coefficient was determined only for the normal-density cubes. Figures 4.33 and 4.34 are giving summary of all results. From these figures, initial movement, amount of movements of each sector and shifting of the movement percentages can be analyzed.

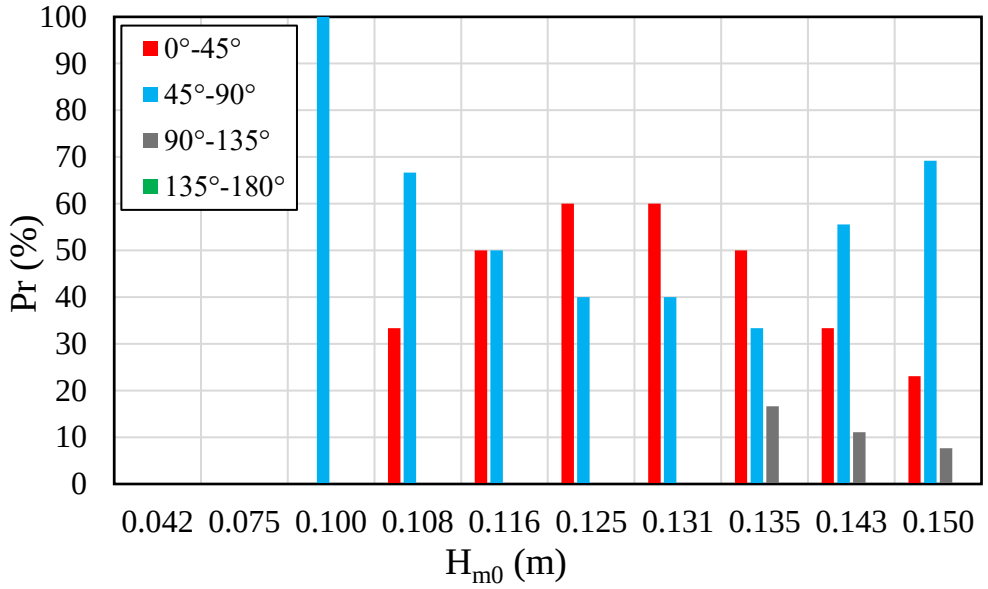

Figure 4.33 Movement percentages of HD cubes in wind waves

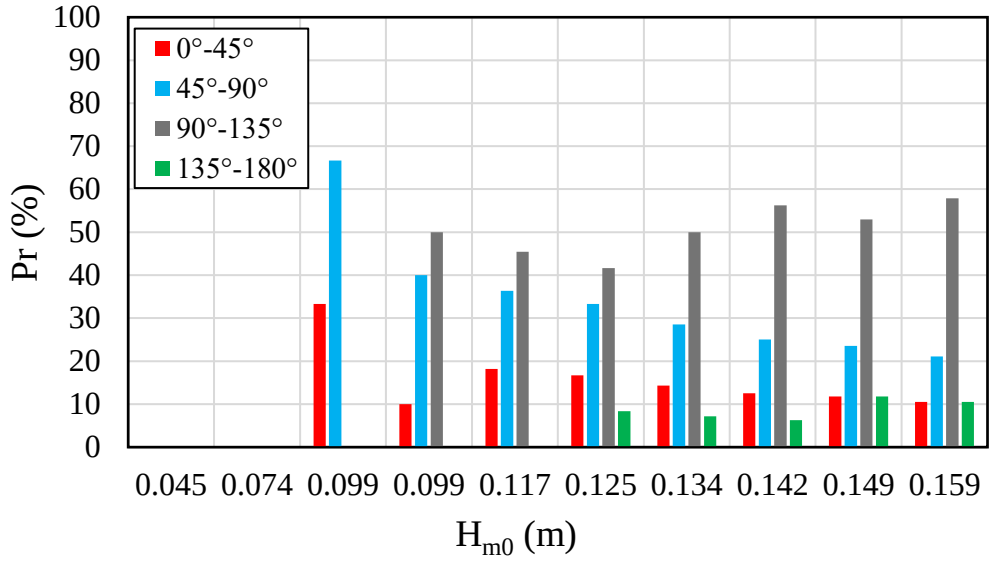

Figure 4.34 Movement percentages of HD cubes in swell waves

For wind wave conditions, in Figure 4.33, it is clear that movement starts at 2nd sector and percentage of movements decreases for the 2nd sector while percentage of movement increases for the 1st sector. After the 7th wave percentage of the

movement shifts to the 2nd sector. As the wave height increases breaking shifts to the rear sectors and movements can be seen at 3rd sector after design wave height.

For swell wave conditions in Figure 4.34, it is clear that swell waves are more effective at rear side of roundhead (3rd and 4th sectors) as the wave height increases movements can be seen at 4th sector. At initial waves, the 2nd sector has moving cubes but as the wave height increases this movement shifts to the rear side, because of the breaking of the waves are now plunging at rear side.

In terms of the movement, for wind wave conditions, frontal sectors are more prone the movements, while for swell wave conditions, the 3rd sector is the most critical and 2nd sector also affected by swells.

5
CONCLUSION

This study examined the stability of high-density (31.5 kN/m³) cube blocks arranged in a single layer on the roundhead section of a breakwater, exposed to both wind and swell waves. Wind wave conditions produced a wave steepness (S_p) ranging from 0.0330 to 0.0375, with an average of 0.035. Swell wave conditions resulted in a wave steepness range of 0.0092 to 0.0179, averaging 0.013. Spectral wave steepness values were 0.033 for wind waves and 0.013 for swell waves. The model head section had a radius (R) of 0.5462 m around SWL, with an R/D_n ratio of 13.66. Under wind waves, R/L_p ranged from 0.118 to 0.379, and R/H_{m0} ranged from 3.64 to 13.00. For swell waves, R/L_p was between 0.051 and 0.118, and R/H_{m0} ranged from 3.44 to 12.11. The slope was 1:1.5.

Under wind wave conditions, the most significant movement occurs in the second and third sectors. As waves approach the head, they begin to turn and steepen, leading to breaking in the second sector, starting from the first. This breaking process continues into the third sector, where waves are further influenced by the plunging jet. As wave energy (height) increases, the third and fourth sectors experience greater movement. Conversely, under swell wave conditions, the influence of the wave period becomes more pronounced. Waves of the same energy exhibit higher run-up behavior in swell conditions. Steepening waves break in the second sector under swell waves, and with increasing wave energy, the third and fourth sectors are affected by breaking process. Consequently, as wavelength increases, the fourth region of the head also becomes susceptible to wave impact.

While swell waves initiate movement earlier than wind waves, the rate and severity of movement are higher in wind waves. Wind waves cause the most movement in the second and third sectors, with the fourth sector experiencing the least movement compared to the first. In contrast, swell waves exhibit no movement in the first sector but increasing movement in the fourth. The second sector experiences the most movement under swell wave conditions, followed by the third and fourth sectors. Notably, movement begins earlier in the fourth sector under swell waves compared to wind waves. Consequently, the fourth region of the head section also undergoes significant movement under swell wave conditions.

An examination of the behavior and damage of high-density blocks in the armor layer revealed very low movement rates. Heavy blocks exhibited no displacement under both wind and swell wave conditions of this experimental conditions. As a result of these physical model studies, a stable breakwater roundhead was obtained by using a high-density cube. Since roundhead stability can be achieved with cubes, it has emerged as an economical alternative and solution.

REFERENCES

Berenguer, J. M., & Baonza, A. (1999). Experimental research on hollowed cubes for breakwater protection. In Proceedings of the International Conference Coastal Structures (Vol. 1).

Burcharth, H. F., & Hughes, S. A. (2002). Coastal Engineering Manual, Part VI, Fundamentals of Design, Chapter V-1, Engineer Manual 1110-2-1100. U.S. Army Corps of Engineers, Washington, DC.

Burcharth, H. F., Andersen, T. L., & Medina, J. R. (2011). Stability of Cubipod armoured roundheads in short crested waves. In 32nd International Conference on Coastal Engineering ICCE 2010 in Shanghai, China. Coastal Engineering Research Council. http://journals.tdl.org/ICCE/issue/view/154

Burcharth, H. F., Haagensen, P. R., & Macineira, E. (2003). Stability of roundheads armoured with cubes. In Coastal Structures 2003, Portland Oregon, United States (pp. 66-77). https://doi.org/10.1061/40733(147)6

Carver, R. D., & Heimbaugh, M. S. (1989). Stability of stone-and dolos-armored rubble-mound breakwater heads subjected to breaking and nonbreaking waves with no overtopping. Technical report (U.S. Army Engineer Waterways Experiment Station); CERC-89-4.

Comola, F., Andersen, T. L., Martinelli, L., Burcharth, H. F., & Ruol, P. (2014). Damage pattern and damage progression on breakwater roundheads under multidirectional waves. Coastal Engineering, (Vol. 83), 24-35.

Frens, A. B. (2007). The impact of placement method on Antifer-block stability. TU Delft Faculty of Civil and Environmental Engineering and Geosciences, Hydraulic Engineering. Delft, Netherlands.

Frens, A. B., VAN GENT, M. R., & OLTHOF, J. (2009). Placement methods for antifer armour units. In Coastal Engineering 2008: (In 5 Volumes) (pp. 3337-3345).

Hudson, R. Y. (1958). Laboratory investigation of rubble-mound breakwaters. Proc. of American Society of Civil Engineers. Journal of the waterways and Harbors division, (Vol. 85, Issue 3), 93-121. https://doi.org/10.1061/JWHEAU.0000142

Hughes, S. A. (1993). Physical Models and Laboratory Techniques in Coastal Engineering. World Scientific.

Ito, M., Iwagaki, Y., Murakami, H., Nemoto, K., Yamamoto, M., & Hanzawa, M. (1994). Stability of high-specific gravity armor blocks. Proceedings of the 24th International Conference on Coastal Engineering, Kobe, Japan.

Jan Verhagen, H., d'Angremond, K., & van der Vliet, K. (2003). Positioning of cubes on a breakwater slope. In Coastal Engineering 2002: Solving Coastal Conundrums (pp. 1550-1560).

Jensen, O. J. (1984). A monograph on rubble mound breakwaters. Danish Hydraulic Institute. Hørsholm.

Juhl, J., Alikhani, A., Sloth, P., & Archetti, R. (1996). Roundhead stability of berm breakwaters. In Coastal Engineering 1996, (pp. 1693-1706). https://doi.org/10.1061/9780784402429.132

Losada, M.A., Dalrymple, R.A., Vidal, C., 1990. Water waves in the vicinity of breakwaters. J. Coast. Res. I, 119–138.

Maciñeira, E. G., & Burcharth, H. F. (2016). Stability of cube armoured roundheads exposed to long crested and short crested waves. Coastal Engineering, (Vol. 112), 99-112. https://doi.org/10.1016/j.coastaleng.2016.03.002

Maciñeira, E., & Burcharth, H. F. (2007). New Formula for Stability of Cube Armoured Roundheads. In L. Franco, P. Ruol, G. R. Tomasicchio, & A. Lamberti (Eds.), Coastal Structures 2007 : Book of Abstracts : International Conference 2-4 July, Venice, Italy (pp. 36). American Society of Civil Engineers. https://doi.org/10.1142/9789814282024_0003

Madrigal, G., Lozano, J., 1992. Stability of accropode and comparison with parallepipedic block. Civ. Eng. Oceans V, 704–717.

Mansard, E. P. D., & Funke, E. R. (1980). The measurement of incident and reflected spectra using a least squares method. In Proceedings of the 17th Coastal Engineering Conference (pp. 154–172). Sydney, Australia.

Matsumi, Y., Kimura, A., Ohno, K., 1996. Velocity field measurements over breakwater heads under 3D waves. Coastal Engineering 1996, 1777–1788.

Matsumi, Y., Kimura, A., Ohno, K., 1998. Wave kinematics on breakwater heads and stability of armour layers under multidirectional waves. Coastal Engineering 1998, 1907–1919.

Matsumi, Y., Kimura, A., Ohno, K., 2000. Stability of armour units on breakwater heads under multidirectional waves. Coastal Engineering 2000, 1946–1958.

Matsumi, Y., Mansard, E.P.D., Rutledge, J., 1994. Influence of wave directionality on stability of breakwater heads. Coast. Eng. 1994, 1397–1411.

Rock Manual (2007). The use of rock in hydraulic engineering. CIRIA-CUR, Publication C683, London.

Sande, J., Peña, E., & Maciñeira, E. (2016). Damage Criteria in Roundheads Armoured with a Single Layer of Cubipod Armor Units. Coastal Engineering Proceedings, (35), 13-13.

Sande, J., Peña, E., & Maciñeira, E. (2016). Damage Criteria in Roundheads Armoured with a Single Layer of Cubipod Armor Units. Coastal Engineering Proceedings, (Vol. 35), 13-13. https://doi.org/10.9753/icce.v35.structures.13

Van der Lem, C., Stive, R., & Van Gent, M. R. A. (2016). Sal Rei breakwaters with single layer cubes. Proceedings of the PIANC-Copedec, Rio de Janeiro, Brazil, 16-21.

Van Gent, M. R. (2014).Oblique wave attack on rubble mound breakwaters. Coastal Engineering, 88, 43-54.

Van Gent, M. R. A. (2003). Recent developments in the conceptual design of rubble mound breakwaters. COPEDEC VI, Colombo, Sri Lanka.

Van Gent, M. R. A., & Luis, L. (2013). Application of cubes in a single layer. In Proceedings of the 6th International Short Course/Conference on Applied Coastal Research (SCACR).

Van Gent, M. R. A., & Spaan, G. B. H. (1998). Breakwaters with a single layer of cubes. Delft Hydraulics Report H3387. Delft Hydraulics, Delft.

Van Gent, M. R. A., D'Angremond, K., & Triemstra. (2001). Rubble mound breakwaters: Single armour layers and high-density concrete units. Proceedings of Coastlines, Structures and Breakwaters 2001, ICE, London, UK.

Van Gent, M. R. A., Plate, S. E., Berendsen, E., Spaan, G. B. H., Van Der Meer, J. W., & d'Angremond, K. (1999). Single-layer rubble mound breakwaters. Proceedings of Coastal Structures 99.

Vidal, C., Losada, M. A., & Medina, R. (1991). Stability of mound breakwater's head and trunk. Journal of waterway, port, coastal, and ocean engineering, (Vol. 117, Issue6),570-587.

Vidal, C., Losada, M.A., Medina, R., 1989. Estabilidad del Morro de los Diques en Talud. Influencia de sua Geometria. Revista de Obras Publicas. 887–907.

Vidal, C., Losada, M.A., Medina, R., 1991. Stability of mound breakwater's head and trunk. J. Waterways Port Coast. Ocean Eng. 117 (6), 570–587

Vieira, F., Taveira-Pinto, F., & Rosa-Santos, P. (2021). Damage evolution in single-layer cube armoured breakwaters with a regular placement pattern. Coastal Engineering, 169, 103943.

Wolters, G., van Gent, M., Allsop, W., Hamm, L., & Muhlestein, D. (2010). HYDRALAB III: Guidelines for physical model testing of rubble mound breakwaters. In Coasts, marine structures and breakwaters: Adapting to change: Proceedings of the 9th international conference organized by the Institution of Civil Engineers and held in Edinburgh on 16 to 18 September 2009 (pp. 559-670). Thomas Telford Ltd.

Yagci, O., & Kapdasli, S. (2003). Alternative placement technique for antifer blocks used on breakwaters. Ocean engineering, 30(11), 1433-1451.

Yuksel, Y., van Gent, M. R., Cevik, E., Kaya, A. H., Guner, H. A. A., Yuksel, Z. T., & Gumuscu, I. (2022). Stability of high density cube armoured breakwaters. Ocean Engineering, 253, 111317.

PUBLICATIONS FROM THE THESIS

Conference Papers

1. Yüksel, Y., Çevik, E., van Gent, M., Şahin, C., Öztürk, M., Güner, A. A., Polat, B., Rehber, M. B., Mustafazade, C., İnal, U., & Oğur, M. U. (2024). *Stability of high density cubes on breakwater roundheads*. Poster presentation at the 38th International Conference on Coastal Engineering (ICCE 2024), Rome, Italy.